INSTITUTO NACIONAL DE TECNICA AEROESPACIAL

"ESTEBAN TERRADAS"

Madrid, Spain

O P E N F I R E S

AND

T R A N S P O R T O F F I R E B R A N D S

Principal Investigator:

C. Sánchez Tarifa

Colaboratora:

P. Pérez del Notario

A. Rodriguez Villa

A. Liñán Martínez

M. Ortega Pérez

MAY 31, 1964 - MAY 31, 1965

OPEN FIRES AND TRANSPORT OF FIREBRANDS

S U M M A R Y

a) Open Fires

The research work on Open Fires has been devoted during the report period to the theoretical and experimental study of the fire model proposed in Third Annual Report.

This work has comprised the theoretical and experimental study of the influence of the overflow on flame characteristics, the study of the influence of vessel size on fire behaviour and the study of the influence on fire properties of the physico-chemical characteristics of the fuel.

b) Transport of Firebrands

The research program on Transport of Firebrands during the report period has been dedicated, in the first place, to the continuation and completion of the experimental studies on firebrands of different geometrical shapes and of several kinds of wood.

In the second place analytical expressions have been derived from these studies, giving all the fundamentals variables of the process.

On the other hand, the studies on the combustion of wood with forced convection have been continued, and results have been represented by means of dimensionless expressions, from which it is possible to derive formulae giving the lifetimes and range of firebrands under given horizontal and convective wind conditions.

Finally, the research facilities have been modified and improved, specially the horizontal wind tunnel in which a mechanism to rotate the firebrands has been fitted.

- - - - - -

I. OPEN FIRES

I - INTRODUCTION

During the report period the research work on Open Fires has been devoted, mainly, to the study of the fire model described in Third Annual Report.

The theoretical and experimental study of this model has been divided into the following three parts:

I.- Theoretical and experimental study of the influence of the overflow on flame characteristics.

II.- Influence of the vessel diameter.

III.- Influence of the type and composition of the fuel.

Theoretical and experimental results corresponding to the first part had been in excellent agreement. These results have been obtained with n-heptane in a vessel of 50 cm in diameter.

Second part has been studied by using n-heptane and dioxane in vessels of 12.5, 25 and 50 cm in diameters.

Third part has been performed by burning mixtures of dioxane and water in a vessel of 50 cm in diameter. By changing the composition of the mixtures the values of the heats of combustion and of the heats of vaporization change considerably, and then flame characteristics change considerably also.

I - OVERFLOW INFLUENCE

a) Theoretical Study

The influence of the overflow $\xi = \dot{m}_b / \dot{m}$, on the burning rate is given by the expression:(*)

$$\dot{m}_b = \frac{1}{q_1} \left[\bar{\varepsilon}_f \sigma T_s^4 \theta_f^4 + \frac{T_s \lambda_v}{Z_{v,min}} (\theta_f - 1) \varphi_v - \frac{T_s \lambda_1}{X_s} (1 - \theta_o) \varphi_{c1} \right] \qquad (I.1)$$

in which

$$\varphi_{c1} = \frac{\nu_1 \, e^{\nu_1}}{e^{\nu_1} - 1} \;, \qquad \nu_1 = \frac{c_1 X_s \dot{m}}{\lambda_1} \qquad (I.2)$$

When $\nu_1 \gg 1$, which is the normal case, equation (1) reduces to:

$$\dot{m}_b = \frac{\bar{\varepsilon}_f \sigma T_s^4 \theta_f^4 + \dfrac{T_s}{Z_{v,min}} (\theta_f - 1) \varphi_v}{q_1 + T_s (1 - \theta_o) \dfrac{c_1}{\xi}} \qquad (I.3)$$

In this equation the upper term represents the heat received by the fuel per unit area; $\bar{\varepsilon}_f \sigma T_s^4 \theta_f^4$ represents the heat received through radiation and $\dfrac{T_s}{Z_{v,min}} (\theta_f - 1) \varphi_v$ the heat received through convection.

This equation gives, within a first-order approximation, the influence of the overflow ξ on burning rate.

It may be seen that the larger is the specific heat c_1 and the smaller the heat of vaporization q_1, the

(*)- See Ref.3 Third Annual Report.

greater is the influence of the overflow.

This influence of ξ is important because the spilled fuel (overflow) absorbs an important percentage of the heat received by the fuel which reduces $\dot{m}_b$ and the flame size, and in turn, the heat transmitted to the fuel.

b) Experimental Results

The influence of ξ has been determined by burning n-heptane in a vessel of 50 cm in diameter. The research facility is the one described in Ref.2 and shown in Fig.30 of Second Annual Report.

The experimental results obtained are shown in Figs. 1 and 2. Each point of these figures is the average value of about 20 measurements, and all these measurements were taken after combustion reaches stationary conditions.

Fig.1 shows that burning rate $\dot{m}_b$ and ratios L/D, A_l/S, $V_f/\pi D^3/12$ and L_h/D increase as the overflow decreases.

Fig.2 shows all the radiant properties of the flame, which depend on ξ indirectly through the size and shape of the flame for a constant value of the diameter.

The results shown in this Fig.2 will be used afterwards. It will be pointed out now that expression $\dot{Q}_{re}/A_l \dot{m}_b$ represents approximately, although with a smaller value, the amount of heat received by the fuel per unit area and per

unit value of the burning rate. The value of that expression remains practically constant for all cases in which $\xi = 1$ as it will be shown furtheron.

c) Comparison of Results

In order to compare the theoretical and experimental results and in order to isolate the influence of ξ, the value of $\dot{q}_s / \dot{m}_b = q_l + T_s (1 - \theta_o)\, c_l / \xi$, obtained from Eq. (3) and the experimental value of $\dot{q}_s / \dot{m}_b$ (*) are compared in Fig.3. Both values are in fairly good agreement. The constant separation between both curves may be produced by the heat lost by the fuel through the vessel walls.

II - INFLUENCE OF THE VESSEL DIAMETER

a) Theoretical Results.

In Eq. (I.1), the influence of the vessel diameter on the burning rate is exerted, essentially, through the radiation term, that is to say, through the mean value of the flame emissivity $\bar{\varepsilon}_f$ and of the average flame temperature T_f.

The second term of that equation is the heat transmitted to the liquid through convection. The possible influence of the vessel size might be due to differences in

---

(*) When these two values are compared, it is eliminated the effect produced by the decreasement of the flame size due to the reduction of the value of ξ. Therefore the heating of the spilled fuel (overflow) is the only effect compared).

shape and size of the mass of fuel vapors existing between the flame and the liquid fuel.

However, the theoretical results show that this term is very small as compared to the radiation term when the values of $\dot{m}_b$ are of the same order of magnitude (or larger) than those utilized in our experiments.

The heat transmitted through convection decreases rapidly as $\dot{m}_b$ augments, mainly due to the coefficient φ_v, which decreases very rapidly also (Eq.(21), Ref.3). This result implies that the convective heat from the flame is mainly used in heating up the fuel vapors, but it does not practically reach the fuel surface.

The convective heat would be a maximum if all the flame would be located at a constant distance Z_v from the fuel surface. For this case,

$$\varphi_v = \frac{\nu_v}{e^{\nu_v} - 1} \quad ,, \quad \nu_v = \frac{c_v Z_v \dot{m}_b}{\lambda_v} \qquad (I.4)$$

For the case of the normal-heptane, a numerical calculation of the different terms of Eq (1) written in the form:

$$1 + \frac{\dot{q}_{cl}}{\dot{m}_b q_l} = \frac{\dot{q}_{rf}}{\dot{m}_b q_l} + \frac{\dot{q}_{cf}}{\dot{m}_b q_l} \qquad (I.4a)$$

in which

$$\dot{q}_{cl} = \frac{\lambda_l T_s (1-\theta_o) \varphi_{cl}}{X_s} \qquad \dot{q}_{cf} = \frac{T_s \lambda_v}{Z_{v,min}} (\theta_f - 1) \varphi_v \qquad \dot{q}_{rf} = \bar{\xi}_f \sigma T_f^4$$

A numerical application has been carried out with the following numerical data:

c_l = 0.51 cal/gr°C ,, $\lambda_l = 0.36 \times 10^{-3}$ cal/cm sec.

q_l = 76.45 cal/gr ,, T_s = 371.43°K ,, X_s = 5 cm.

The terms of left hand side of Eq (4) represent the heat needed for the vaporization of the liquid, and the terms of the right hand side represent the heat received by the fuel surface through radiation and convection respectively. These terms are represented in Fig.4 as functions of $\dot{m}_b$ for T_f = 1000°C. It may be seen that even for a very small value of the distance from the flame to the fuel surface (Z_v=0,1 cm), the heat transmitted through convection tends rapidly towards zero as the burning rate augments.

The values of Z_v required for combustion of a flow $\dot{m}_b$, for the case in which all heat is transferred through convection, are shown in the following table

$\dot{m}_b$, gr/cm^2 sec	0.5×10^{-3}	1×10^{-3}	2.5×10^{-3}	5×10^{-3}	10×10^{-3}
Z_v , cm	0.3	0.15	0.06	0.03	0.015

It has been observed[4,5,6] that the law of variation of burning rate $\dot{m}_b$ as function of vessel diameter has a minimum value, which coincides with the transition of the flame from laminar to turbulent conditions.

For very small values of the vessel diameter, the measured values of $\dot{m}_b$ are of the same order of magnitude than those corresponding to large vessels. For these small vessels, the flame is small and, therefore, the heat transferred through radiation would also be small.

But the mean values of $\dot{q}_{cf}$ are also small, because $\dot{m}_b$ is large and the observed values of Z_v decrease from the center of the flame towards the vessels walls, but keeping values over 0.5 cm. Therefore, it is not easily explained the increasement of $\dot{m}_b$ for very small values of vessel diameter[4,5,6]. Perhaps, this is due to a local effect of heat transfer at the vessel walls, through which some heat might be transferred from the flame into the liquid, since this effect is more noticeable as the vessel becomes smaller.

From that Fig.4, it may be observed that for $Z_v \geq 0.5$ cm. the heat received through radiation $\dot{q}_{rf}/\dot{m}_b q_l$ should be practically the total heat flux, and it is practically constant if overflow does not exist.

The radiation term $\dot{q}_{rf}$ may be written as follows:

$$\dot{q}_{rf} - \sigma \bar{\varepsilon}_f T_f^4 = \sigma (1 - e^{-\alpha L_h}) T_f^4 \qquad \text{I.5)}$$

The value of parameter α depends on the type of fuel, and specially on the existence of solid particles in the flame. L_h depends on the size and shape of the flame and T_f on the heat of combustion and on the air flow

entrained into the flame. An exact determination of this flame temperature is a difficult problem.

b) Experimental Results

The experimental results obtained with n-heptane are shown in Figs. 5 and 6. In Fig.5 it may be observed that burning rate increases as vessel's diameter augments, except in the region of small values in which the value corresponding to D = 3 cm has been also measured and represented.

Another conclusions, derived from that figure is that flame volume is proportional to the third power of vessel's diameter and that L_h is proportional to that diameter.

Total radiant heat $\dot{q}_{rv}$ per unit flame volume, (Fig.6), is constant and it is also constant with vessel diameter the total radiant heat per unit mass of burnt fuel $\dot{q}_{rm}$.

Figs. 7 and 8 show the experimental results obtained with dioxane, whose physical and chemical properties differ appreciably from those of n-heptane.

However, these results are similar to those obtained with n-heptane. It may be pointed out that $\dot{m}_b$ increases more slowly and $\dot{q}_{rv}$ decreases as the diameter augments.

Besides of the aforementioned data, flame tempera-

tures were measured by means of five moving Ni - Ni Cr thermo couples.

Fig.9 shows the measured temperatures, as well as the mean flame shape for n-heptane burning in a vessel of 25 cm in diameter. Each temperature is an average value of six measurements.

The measured temperatures near the flame borders and at its upper region are not actual values, because during part of the time the thermocouples did not remain within the flame region due to the oscillations of the flame. Temperature distribution in the central zone is similar to that found by Fons et al[7].

It can be deduced also from the figure the existence of a fuel vapors zone in the vicinity of the fuel surface because of the low values of the temperature.

Fig.10 shows similar temperature measurements for dioxane, giving values of the same order of magnitude.

Flame temperatures measured by means of thermocouples cannot give very exact values because of soot formation, radiation errors and flame fluctuations. Optics measurements give average values (in time and location) with values somewhat higher than those measured by thermocouples[8]. However, to measure accurately temperatures at a given point in a large turbulent flame is still a problem to be solved.

c) Comparison of Results

From Figs. 6 and 8 it is obtained:

$$\dot{q}_{rm} = \frac{\dot{Q}_r}{S\ \dot{m}_b\ q_r} = 0,25 = K_o \quad \text{(n-heptane)}$$

and.

$$\dot{q}_{rm} = \frac{\dot{Q}_r}{S\ \dot{m}_b\ q_r} = 0.15 = K_o \quad \text{(dioxane)}$$

The amount of heat received through radiation is:

$$S\ \dot{q}_{rf} = \varphi_r\ \dot{Q}_r = \varphi_r\ K_o\ S\ \dot{m}_b\ q_r$$

For the case in which the convective heat is small, it results:

$$\varphi_r\ K_o\ S\ \dot{m}_b\ q_r = S\ \dot{m}_b \left[q_l + c_l\ (T_s - T_o) \right]$$

that is

$$\varphi_r = \frac{q_l + c_l\ (T_s - T_o)}{K_o\ q_r} \qquad \text{(I.6)}$$

from which the conclusion is drawn that φ_r is constant regardless of the vessel diameter.

The following table shows the values of φ_r obtained from the above expression and those calculated by assuming that the flame behaves as a black body

	n-Heptane	Dioxane
$\varphi_r = \dfrac{q_l + c_l (T_s - T_o)}{K_o \, q_r}$	0.045	0.14
$\varphi_r = \dfrac{\frac{\pi D^2}{4}}{\frac{\pi D^2}{4} + A_l}$	0.06	0.18

which shows a fair agreement between both results.

The value of L_h depends on both flame size and flame shape. Flame size depends on $\dot{m}_b$ and this burning rate as a first approximation is a function of q_r / q_l. As a consequence, in Fig. 11 the values of $L_h / D \times q_l / q_r$ have been represented, and it may be observed that they do not depend on vessel's diameter neither on the type of fuel. Its value is approximately given by:

$$\frac{L_h \, q_l}{D \, q_r} = 0.55 \cdot 10^{-2}$$

The value of the absortion coefficient α given by Rasbash[8] is of the order of 0.02. 1/cm.

From these values and disregarding convection, from Eq (4) it is obtained:

$$\dot{m}_b = \frac{\sigma T_f^4}{q_l + c_l (T_s - T_o)} \left[1 - \exp \left(0.55 . 10^{-2} \alpha \frac{q_r}{q_l} D \right) \right] \quad (I.7)$$

which gives the value of $\dot{m}_b$ as a function of both vessel diameter and radiant flame temperature.

The average value of T_f is of the order of 625°C and it has similar values for many types of fuels, as shown by the experimental data of Fons et al [7] as well as in our experimental results. With such values, Eq (7) may be written in the form:

$$\dot{m}_b = \frac{0.9}{q_l + c_l (T_s - T_o)} \left[1 - \exp \left(0.0055 \alpha \frac{q_r}{q_l} D \right) \right] \quad (I.8)$$

in which $\alpha \simeq 0.02$ for flames with carbon particles in suspension (hydrocarbons) and $\alpha \simeq 0.015$ if such particles do not exist (alcohol flames or dioxane, for example).

Fig. 11 also shows the values of $\dot{m}_b$ obtained from that expression and those experimentally obtained.

When the vessel diameter is large, Eq (8) gives the same results as those given by the expression:

$$v_\infty = \frac{0.0076\ q_r}{q_l + c_l (T_s - T_o)} \text{ cm/min.}$$

derived by Grumer et al [9].

For very small values of the vessel diameter the influence of its walls (through convection) is important, radiation does not control the phenomenon and Eq (8) no longer holds.

III - INFLUENCE OF THE FUEL

The influence of the type of fuel has been studied by comparing the results obtained by burning n-heptane, pure dioxane, and mixtures of dioxane and water.

The two more important properties of fuels as far as open fires is concerned, are the heats of vaporization q_l and combustion q_r .

Fig. 12 shows the values of q_l , q_r and q_r / q_l for several mixtures dioxane-water.

It seems that the influence of fuel composition on the burning rate depends on vessel size, because on this size depends the relative importance of the two heat transfer mechanism: radiation and convection.

For large vessels, the value of q_r / q_l influences in the flame size and then, its emissivity. In Fig. 11 it may be observed that the influence of fuel composition is more important as the vessel diameter becomes larger.

For small vessels, in which the relative importance of the radiation heat transfer is small, the influence of fuel composition is less important, resulting similar values of $\dot{m}_b$ for n-heptane and dioxane. This is probably due to the fact that an important percentage of the heat transferred to the fuel is through the vessels walls heat transfer which depends, largely, on the local flame temperature.

Figs. 13 and 14 show the experimental results obtained with several mixtures dioxane-water. It may be observed that $\dot{m}_b$ increases as the proportion of water in the mixture decreases, as it might be expected.

As it is shown in Fig. 10, dioxane flames do not extend over the whole fuel surface. Therefore, for small flames all date in connection with flame size and flame shape present some scattering which is not observed when experimenting with large flames.

II. TRANSPORT OF FIREBRANDS

1.- INTRODUCTION

During the report period the following work has been carried out concerning the problem of transport of firebrands.

a) Continuation of the experimental and theoretical studies on flight paths and burning lifetimes of firebrands.

b) Derivation of a series of analytical expressions for the different parameters affecting flight paths and burning lifetimes of firebrands.

c) Design and construction of new research facilities.

d) Experimental and analytical studies on firebrands combustion under forced convection.

In the first place we have finished those studies on flight paths which were not completed in the Third Annual Report. Moisture content effects are shown in a series of different tests, and a series of experiments with square plates of different thickness ratio and kind of wood have been carried out. We also performed experiments with charcoal and natural firebrands such as pine cones, pine brackets, etc.

In part b) analytical expressions, to calculate and relate the different parameters defining the burning characteristics of the firebrands, has been found as functions of size, shape and mass characteristics of firebrand. The values given by these analytical expressions agree quite well with the values of the parameters experimentally calculated.

In part c) we look over the improvements introduced in the working facilities, making special remark on the new vertical wind tunnel of variable cross-section, which will allow us to test the firebrands in free flight conditions.

Last we have carried out a series of combustion tests at constant velocity with spheres and cylinders of a chosen kind of wood and of different sizes. As before we have found analytical expressions of the parameters affecting the burning characteristics of the firebrand, which give us also values of these parameters which agree very well with those experimentally calculated.

Part a) As before, the vertical wind tunnel was used to make tests at terminal velocity of cylinders of oak ("quercus rubra"), pine wood ("pinus pinaster"), spruce ("picea excelsa"), aspen ("populus tremuloides") and balsa wood ("ochroma lagopus"). The cylinders dimensions were: Do x Lo = 15 x 45 mm, 12 x 36 mm, 10 x 30 mm, 8 x 24 mm and 6 x 18 mm for moisture contents of 2% and 25%.

The way in which tests were carried out need not to be

described as it has already been explained in previous reports. However we want to emphasize the fact that slight errors are introduced by the attachements, and hence the interest for the new vertical wind tunnel of variable cros section, now under construction.

The results are shown in figures 15 through 24 for the case of inclined convection column, using the same parameters already shown in the Third Annual Report. From observing the figures it can be seen that moisture content has not a substancial influence on the behavior of the firebrand, at least, once combustion has started. However, its influence is considerable for ignition time (ignition time is, approximately, 50% longer for a firebrand with M.C. = 25% ; than for one with M.C. = 2%). As it will be shown in part b), it can be considered that an increase in M.C. produces a similar effect as an increase in wood density.

In these figures 15 through 24 the representative parameters of the process are represented as functions of u_y . Only values of u_y larger than the initial terminal velocity of the firebrand have been considered, because for u_y smaller than such velocity, the horizontal range reached is smaller. However, in the Third Annual Report was developed a theoretical method for the case of u_y smaller than the initial terminal velocity and during this year some experiments have been carried out in order to check that method. These experiments show good agreement between both epxerimental

and theoretical values. As experiments are still going on and we do not have definitive conclusions as yet, no graphs are included in this report.

In figures 26 through 30 are represented the flight paths results corresponding to the actual convection column shown in Fig. 25.

Also during this year period tests with square plates were carried out. The same kind of woods were utilized (except spruce as it has practically similar characteristics than pine wood). The effect of M.C. was not taken into account as it was shown to be of little importance. The dimensions of the square plates used were: 32 x 32 x 16 mm , 32 x 32 x 8 mm , 32 x 32 x 4 mm and 32 x 32 x 2 mm. The tests were carried out by placing the square face of the plate perpendicular to the air flow. Results are shown in figures 31 through 34.

As suggested by the Forest Service Division Authorities Charcoal have been included in our experiments during this report period. Tests have been carried out with spheres (Do = 22 mm and 15 mm) cylinders (Do x Lo = 15 x 45 mm, 12 x 36 mm, 10 x 30 mm, 6 x 18 mm) and square plates (28 x 28 x 11 mm. and 26 x 26 x 5 mm). The results are shown in Figs. 35 through 37. As it was to be expected burn out time comes out to be longer than the corresponding ones for the woods we have been testing. For instance out of wood spheres of Do = 22 mm, we have produce specimens of charcoal whose burnt-out times happened to be

about double of the corresponding ones for the original wood spheres. These specimens although keeping their spherical shape pretty well, have their volume decreased.

Last we have tested pine cones and pine brackets with the results showing in Figs. 38 and 39. Generally speaking we observed that the core of the pine-cones behave very much like wood of similar density.

Pine cones start burning in a characteristic way with all its brackets on, but after a while, they (the brackets) separate, and then the way of burning changes approaching the one of woods of similar density. It is interesting to notice than although pine brackets separate quite soon, they are not very dangerous because fire extinguish quite soon on them.

Part b)

As we have shown in former reports, it was necessary for the calculation of the firebrand flight-path, the knowledge of the relation between firebrand terminal velocity w_f and time. Through the experiments we have carried out up to date, we have obtained a series of curves, similar to the ones shown in Fig. 40, which provide us with the above mentioned relation for a wide range of firebrands of different kind of woods, shapes and dimensions. From these curves we know $\nu_f = \frac{w_f}{w_{f_o}}$, and hence the knowledge of the firebrand terminal velocity w_f is inmediate as

w_{f_o} is given by

$$w_{f_o} = \sqrt{\frac{2\, m_o\, g}{\rho\, A_o\, C_{D_o}}} \qquad (II.1)$$

From the way curves in Fig.40 (and in the other graphs not shown here) look like, it seemed possible to get all of them (curves) together if we chose an appropiate dimensionless time coordinate. This was taken $\tau = t / t_b$. With this change in time coordinate Fig.40 changes into Fig. 41. In this figure we have concentrate all curves from Fig. 40 in a mean curve, as we see that the experimental values of different sizes and different moisture content are not at all scattered. On the other hand and thanks to these transformation of the time coordinate, twenty-six figures similar to Fig.40, can be represented in only six (Figs. 42 through 47).

In order to have a simpler handling of these results we have searching for an easy expression which may relate v_f and τ , in such a way that its representation coincides, as much as possible, with the experimental results. Some different kind of expressions have been studied (polinomial forms, Fourier series, etc.) and at last we have found that the most appropiate, both due to its simplicity (it depends on two parameters only)and to its good degree of approximation is the following

$$v_f = \frac{1}{1 + \eta \left(\frac{\tau}{1 - \tau}\right)^{\gamma}} \qquad (II.2)$$

With the experimental results as base, values of the parameters η and γ have been calculated for the different kind of woods and shapes. These values are given in Appendix III and the corresponding values for expression (II.2) are given in Fig.42 through 47.

Now then, what are interested in is w_f, and this terminal velocity can be obtained from expression (II.2) once w_{f_o} and t_b are known. We have already seen that w_{f_o} is given by (II,1). In this expression all parameters are immediately known, except C_{D_o} for which mean values, corresponding to the different shapes of the firebrand tested, have been calculate from experimental results, and are given in Appendix IV . On the other hand, t_b is well known due to the experiments, and has been represented v.s. wood density ρ_w in Fig.48 through 50 . Also for t_b v.s. ρ_w we have looked for analytical expressions which allow us to approach the problem of firebrand more easily. The expressions which seem to approach quite well the experimental values are the following ones:

Cylinders $L_o/D_o = 3$

$$t_b = \lambda^2 \rho_w \qquad (II.3)$$

where

t_b = burn-out time in seconds

λ = $\sqrt{2}$ x D_o in mm.

ρ_w = wood density in gr/cc.

Spheres

$$t_b = 20\ \lambda\ \rho_w \qquad \text{(II.4)}$$

where

$$\lambda = D_o$$

Thick plates ($\alpha \leq 4$)

$$t_b = \lambda^2\ \rho_w{}^{.3} \qquad \text{(II.5a)}$$

Medium plates ($4 \leq \alpha \leq 8$)

$$t_b = \lambda^2\ \rho_w{}^{.5} \qquad \text{(II.5b)}$$

Thin plates ($\alpha \geq 8$)

$$t_b = \lambda^2\ \rho_w{}^{.8} \qquad \text{(II.5c)}$$

In these expressions (II.5) the value of λ is given by

$$\lambda = \sqrt{\frac{\log 2}{\log 2\alpha}}\ \text{x side length.}$$

All these expressions (II,3) through (II.5) are represented in Fig. 48 through 50 together with the experimental values.

As we have been observing that moisture content has a similar effects, on wood characteristics, as an increase in density, we can use expressions (II.3) through (II.5), no matter how much moisture content is,whenever we use the actual

wood density.

One integral we have to know to be able to calculate flight-paths is the following

$$\int_o^t w_f \, dt = w_{f_o} \, t_b \int_o^\tau \nu_f \, d\tau \qquad (II.6)$$

We have already got an analytical expression for ν_f, see expression (II.2), but its integration does not give results close enough to the values we obtain by numerically integration of experimental results. This is why we have preferred to adjust these values obtained by numerical integration with a simple function such as

$$\chi = \int_o^\tau \nu_f \, d\tau \simeq \delta \left[1 - (1 - \tau)^{1/\delta} \right] \qquad (II.7)$$

in which the values of δ are given in Appendix V. Expression (II.7) has been represented in Fig. 51 through 53, where experimental values have been omitted because they practically coincide with the ones given by (II.7).

Next we are going to calculate values of $\frac{L}{u_x}$, Y_m and t_b, for a chosen firebrand by making use of the analytical expressions we have developed, and we will compare them with the ones calculated by making use of the experimental values.

The firebrand chosen is an oak cylinder of Do x Lo = 15 x 45 mm.

Data

$$\begin{cases} \rho_{w_o} = .8 \text{ gr/cm}^3 \\ \rho_o = \frac{1}{8}\, 10^{-3} \text{ gr/cm}^3 \\ T = 288^\circ \text{ K} \\ A_o = 6.75 \text{ cm}^2 \\ C_{D_o} = .85 \text{ (from Appendix IV)} \end{cases}$$

Inclined convection column.

Solution

From expression (II.1) we have

$$w_{f_o} = 13 \text{ m/seg.}$$

and from expression (II.3)

$$t_b = 360 \text{ sec.} \qquad \text{(II.8)}$$

The equations for the flight path are:

$$X = \int_o^t u_x \, dt = w_{f_o} \, t_b \int_o^\tau \frac{u_x}{w_{f_o}} \, d\tau$$

$$Y = \int_o^t (u_y - w_f) \, dt = w_{f_o} \, t_b \int_o^\tau \left(\frac{u_y}{w_{f_o}} - \nu_f \right) d\tau$$

$$(0 < \tau < \tau_v)$$

and

$$Y = Y_m - \int_{t_v}^{t} w_f \, dt = Y_m - w_{f_o} \, t_b \int_{\tau_v}^{\tau} \nu_f \, d\tau$$

$$(\tau_v < \tau < 1)$$

For the calculation of τ_v we have

$$\int_o^{\tau_v} \frac{u_y}{w_{f_o}} \, d\tau = \int_o^1 \nu_f \, d\tau = \delta$$

But $\delta = .378$ (see Appendix V), and as u_y is a parameter independent of τ we have

$$\tau_v = \frac{w_{f_o}}{u_y} \cdot 378 = \frac{5.07}{u_y}$$

and

$$t_v = 360 \cdot \frac{5.07}{u_y} = \frac{1,824}{u_y}$$

but as $t_v = \frac{L}{u_x}$ we have

$$\frac{L}{u_x} = \frac{1,824}{u_y} \qquad \text{(II.9)}$$

we have also

$$Y_m = 13.4 \times 360 \int_o^{\tau_v} \left(\frac{u_y}{13} - \nu_f \right) d\tau$$

and by substitution and after operating we get:

$$Y_m = 1,824 \left(1 - \frac{5.07}{u_y}\right)^{\frac{1}{.378}} \qquad (II.10)$$

Expressions (II.8) through (II.10) have been represented in Fig.54 and comparison with experiments is made. We see that error is, at most, inferior to a 5%.

In order to be able to know which kind of convection column gives maximun value for X_m, for a given average value of u_x, we have also studied this problem for a given u_m (average velocity).

The values of X_m is given by

$$X_m = \int_o^{t_f} u_x \, dt$$

on the other hand

$$\frac{1}{t_f} \int_o^{t_f} u_x \, dt = u_m$$

them

$$X_m = u_m \, t_f$$

is independent of the variation of u_x v.s. time. This is why we have used in our calculations an inclined convection column with u_x = constant.

Part c)

We have tried to improve the equipment in order to have better working conditions and to minimize errors. For instance, we have designed a device to measure terminal velocities, by making use of the horizontal wind tunnel, as was already designed for the small wind tunnel (Fig.55). Without specimen the compensating weight keeps the supporting arm in indifferent equilibrium. When we hang the specimen, it breaks the equilibrium and the arm rotates down. On the other hand, if we have an air flow whose velocity keeps the angle of rotation fixed at 45^{o}, this is the terminal velocity we were looking for. Although not represented in Fig.55, there is a cowling covering practically the whole device.

In Fig. 56 we have represented a system designed to rotate the specimen in order to have a more homogeneous combustion. Rotations of 3 , 9 , 27 and 81 r.p.m. can be selected.

As we have already informed in our advance Report, a new wind tunnel of variables cross section has been designed, Fig.57, whose characteristics were already given in the above mentioned Report. Some difficulties arisen during its manufacturing made it impossible to finish it in the foreseen time, and therefore no tests have been yet carried out in it.

Part d)

A series of tests with firebrands exposed to a constant relative wind velocity have been carried out during this period time. Oak spheres of dimensions (Do = 22 mm, 15 mm, 10 mm) and oak cylinders (Do x Lo = 15 x 45 mm, 12 x 36 mm, 10 x 30 mm, 8 x 24 mm) have been the specimens we have worked with. Variation of weight, surface area, and volume v.s. time have been the measured parameters. Tests have taken place in the horizontal wind tunnel. A range of relative wind velocity, from 2 m/sec. up to firebrand initial terminal velocity w_{f_o} has been used.

For measuring the weights we have made use of the ring type balance described in Third Annual Report, which has been improved with the device showed in Fig.56. As an example in Fig. 58 some of these values are shown.

For measuring the surface area and the volume, a number of photographs from two different angles have been taken during each test. The variation of surface area and volume have been represented in the way shown in Figs. 59 and 60.

Representing the above mentioned parameters as function of dimensionless time:

$$\tau = \frac{t}{t_b}$$

we have obtained only a curve represented in Figs. 61, 62 and 63 (Experimental results). From these curves we have

also calculated the variation of density and characteristic radius v.s. time. This have been represented in Figs. 64 and 65.

In order to simplify calculations in which the above mentioned parameters might be involved, we have adapted to all these experimental curves, the following very simple analytical expressions.

For the variation of mass v.s. time

$$\mu = \frac{1}{1 + \beta_1 \left(\frac{\tau}{1-\tau}\right)^{\varphi_1}} \qquad \text{(II.11)}$$

For the variation of volume v.s. time

$$\frac{V}{V_o} = \frac{1}{1 + \beta_2 \left(\frac{\tau}{1-\tau}\right)^{\varphi_2}} \qquad \text{(II.12)}$$

For the variation of surface area v.s. time

$$\frac{S}{S_o} = (1 - \tau^{\theta}) \qquad \text{(II.13)}$$

The values of the parameters are given in Appendix VI, and expressions (II.11) , (II.12) and (II.13) are respectively represented in Figs. 61 , 62 and 63 (theoretical curves).

We have also for the density the following expression, derived from (II.11) and (II.12)

$$\frac{\rho_w}{\rho_{w_o}} = \frac{1 + \beta_2 \left(\frac{\tau}{1-\tau}\right)^{\varphi_2}}{1 + \beta_1 \left(\frac{\tau}{1-\tau}\right)^{\varphi_1}} \qquad \text{(II.14)}$$

and for the characteristic radius, derived from (II.12) and (II.13)

$$\frac{R}{R_o} = \frac{1}{\left[1 + \beta_2 \left(\frac{\tau}{1-\tau}\right)^{\varphi_2}\right](1 - \tau^{\theta})} \qquad \text{(II.15)}$$

Expressions (II.14) and (II.15) are represented in Figs. 64 and 65 (theoretical curves).

To define the problem completely we have obtained experimentally the burn-out times (Fig.66). An analytical expression to approximate these experimental results is the following:

$$t_b = \frac{\lambda^2}{1 + A\, w^B} \qquad \text{(II.16)}$$

where:

t_b = time in sec.

λ = Do (for spheres) in mm.

λ = $\sqrt{2}$ Do (for cylinders) in mm.

w = relative wind velocity in m/sec.

A and B are parameters depending on the wood which in this case have the following values:

$$A = .1 \qquad : \qquad B = 1.5 \qquad\qquad (II.17)$$

Expression (II.16) with values (II.17) is also represented in Fig.66.

C O N C L U S I O N S

The principal conclusions which have been obtained during the report period are as follows:

OPEN FIRES

1) The influence of the overflow on the burning rate is important. The value of $\dot{m}_b$ may be reduced by a factor higher than two.

2) The values of the overflow $\xi = \frac{\dot{m}_b}{\dot{m}}$ does influence all flame properties (size, shape, radiation, etc.)

3) The influence of ξ is more important for great values of c_1 and small values of q_1 .

4) The heat received through convection by the fuel decreases rapidly as $\dot{m}_b$ augments.

5) Total energy radiated by the flame per unit of $\dot{m}_b$ does not depend on vessel diameter.

6) A semi-empirical expression has been obtained for the burning rate $\dot{m}_b$, as function of vessel diameter and as function of the properties.

7) The influence of the fuel properties on the burning rate depends on vessel diameter. For large diameter that influence is more noticeable.

TRANSPORT OF FIREBRANDS

8) The critical height Y_m giving maximum horizontal range is approximately proportional to wood density, for firebrands of equal initial size and shape.

9) The maximum horizontal range X_m is approximately proportional to wood density, for firebrands of equal initial size and shape.

10) Wood density of firebrands appears to be the most important parameter as far as potential danger of fire spread is concerned.

11) From comparison among firebrands of different initial shape it has been deduced, that shape is not a critical parameter as far as maximum range is concerned. However, spherical firebrands appear to be the most dangerous.

12) Charcoal firebrands have very long lifetimes and they can reach very large distances while still burning. Charcoal ignites easely, therefore, charcoal firebrands are, by far, the most dangerous type.

13) Natural firebrands tested have shown no remarkable differences with geometrical shaped firebrands of similar size.

14) From the experimental results it is possible to derive analytical expressions giving all the fundamental variables for any possible firebrand within a certain

range of shape, size and density.

15) It is possible to represent the laws of combustion of wood under forced convection by means of dimensionless expressions.

16) By means of such dimensionless expressions it is also possible to derive formulae giving the lifetimes and range of firebrands under given convective and horizontal wind conditions.

17) The variation of dimensionless volume and dimensionless surface with dimensionless time during combustion of wood under forced convection do not depend, roughly, on the initial shape of the firebrand.

- - - - - -

REFERENCES

1. SANCHEZ TARIFA,C.- et al: OPEN FIRES AND TRANSPORT OF FIRE-BRANDS. First Annual Report. INTA, Madrid, 1962.

2. SANCHEZ TARIFA,C.- et al: OPEN FIRES AND TRANSPORT OF FIREBRANDS. Second Annual Report. INTA, Madrid, 1963.

3. SANCHEZ TARIFA,C.- et al: OPEN FIRES AND TRANSPORT OF FIRE BRANDS. Third Annual Report. INTA Madrid 1964.

4. HOTTEL, H.C. : FIRE RESEARCH ABSTRACT AND REVIEWS 1959, 1 No 2.

5. FONS, W.L. : RATE OF COMBUSTION FROM FREE SURFACES OF LIQUID HYDROCARBONS. Pacific Southwest Forest and Range Exporiment Station, Forest Service, U.S. Department of Agriculture, Berkeley. California.

6. BURGESS, D.S. GRUMER, J. and WOLFHARD, H.G. : BURNING RATES OF LIQUID FUELS IN LARGE AND SMALL OPEN TRAYS U.S. Bureau of Mines, Pittsburgh, Penn.

7. FONS, W.L., BRUCE, H.D. and PONG, W.Y. : A STEADY-STATE TECHNIQUE FOR STUDING THE PROPERTIES OF FREE-BURNING WOOD FIRES. Pacific Southwest Forest and Range Experiment Station Forest Service, Berkeley, California.

8. RASBASH, D.T., ROGOWSKI, Z.W. and STARK G.W.V. : PROPERTIES OF FIRES OF LIQUIDS. Fuel, Vol XXXV No 1 January 1956.

9. GRUMER, J., STRASSER, A., KUBALA, T.A. and BURGESS, D.S. : UNCONTROLLED DIFFUSIVE BURNING OF SOME NEW LIQUID PROPELLANTS. Fire Research Abstracts and Reviews Vol 3, nº 3, 1961.

A P P E N D I X I.

NOTATION

I. O P E N F I R E S

c . . Specific heats at constant pressure

c_l . . Specific heat of the liquid fuel

c_v . . Specific heat of the vapor fuel

D . . Diameter of the burner

L . . Flame height

L_h . . Mean beam length

$\dot{m}$ . . Fuel flow within the vessel

$\dot{m}_b$ . . Fuel flow burned

$\dot{q}_{cl}$ . . Heat transferred through conduction throughout the liquid per unit area and per unit time.

$\dot{q}_{cf}$ . . Heat transferred through conduction to the liquid surface per unit area and per unit time.

q_l . . Latent heat of evaporation.

q_r . . Heat of the reaction.

$\dot{Q}_r$ . . Total heat radiated.

$\dot{Q}_{ro}$ . . Heat radiated to the surroundings per unit time.

$\dot{Q}_{rf}$ . . Total heat radiated to the fuel per unit time.

$\dot{q}_{rf}$ . . Heat radiated to the fuel per unit area and per unit time

$\dot{q}_{rv}$ . . Total heat radiated per unit flame volume.

$\dot{q}_{rm}$ . . Total heat radiated per unit burning rate.

$\dot{q}_s$ . . Heat received by the fuel per unit area and per unit time.

T_f . . Flame temperature

T_s . . Surface temperature

V_f . . Flame volumen

X_s . . Vessel (fuel) depth.

z_v . . Vertical coordinate in the vapor zone.

α . . Emission coefficient.

ϵ_f . . Flame emissivity

ξ . . Overflow ratio defined by $\dot{m}_b / \dot{m}$

λ . . Thermal conductivity

φ_{cl} . . Dimensionless parameter defined by (I.2)

φ_v . . Dimensionless parameter defined by (I.4)

φ_r . . Dimensionless parameter defined by $\dot{Q}_{rf} / \dot{Q}_r$

ν . . Dimensionless parameter defined by (I-2) and (I-4)

ρ . . Fuel density

σ . . Stefan-Boltzmann constant

ϑ . . Dimensionless temperature defined by T/T_s

- - - - - - - - -

A P P E N D I X II .

TRANSPORT OF FIREBRANDS

NOTATION

λ . . . . Firebrand characteristics lineal dimension (as defined in the text).

D . . . . Firebrand diameter.

A . . . . Firebrand cross-section area.

S . . . . Firebrand surface area.

V . . . . Firebrand volume.

R . . . . Firebrand characteristic radius = volume/surface area = V/S .

C_D . . . . Firebrand aerodynamic drag coefficient.

g . . . . Acceleration of gravity

m . . . . Firebrand mass

μ . . . . Firebrand dimensionless mass = m/m_o

ρ_w . . . . Wood density

ρ . . . . Air density

t . . . . Time

t_b . . . . Firebrand burnt-out time

$t_{y=o}$ . . . . Time at which the firebrand reaches the ground.

t_f . . . . Final time, equal to t_b or to $t_{y=o}$

t_v . . . . Flight time within the convection column.

τ . . . . Dimensionless time = t / t_b

w . . . . Wind relative velocity with respect to the firebrand.

w_f . . . . Firebrand terminal velocity.

u . . . . Wind absolute velocity.

ν . . . . Dimensionless velocity.

ν_f . . . . Firebrand dimensionless terminal velocity = $\frac{w_f}{w_{f_o}}$

X . . . . Horizontal distance.

X_m . . . . Maximum range or horizontal distance reached by a firebrand while still burning.

L . . . . Horizontal distance within the convection column and cylinder longitudinal dimension.

Y . . . . Vertical distance or height.

Y_m . . . . Critical height.

χ . . . . Dimensionless distance = $\int_o^\tau \nu_f \, d\tau$

$\alpha = \frac{1}{\varepsilon}$. Square plate side length / thickness ratio

δ, η, γ . . Dimensionless parameters, (terminal velocity).

β_i, φ_i . . Dimensionless parameters (constant velocity).

Subscripts

o . . . Indicates initial values

x , y . . Indicate X and Y directions.

- - - - - - - -

A P P E N D I X III .

VALUES OF THE PARAMETERS η AND γ IN EXPRESSION (II.2)

a) Cylinders with length/diameter ratio equal 3.

Wood	Oak	Pine	Spruce	Aspen	Balsa	Charcoal
η	2.00	2.33	1.63	3.00	3.17	1.00
γ	1.75	1.85	1.75	1.75	1.55	1.00

b) Spheres

Wood	Oak	Pine	Spruce	Aspen	Balsa	Charcoal
η	4.40	4.88	3.35	7.33	6.14	1.00
γ	1.50	1.50	1.50	1.50	1.50	1.00

c) Square plates

32 x 32 x 16 mm

Wood	Oak	Pine	Aspen	Balsa
η	0.92	2.03	4.56	2.23
γ	1.4	1.4	1.4	1.4

32 x 32 x 8 mm.

Wood	Oak	Pine	Aspen	Balsa
η	1.31	2.23	7.62	2.57
γ	1.4	1.4	1.4	1.4

32 x 32 x 4 mm

Wood	Oak	Pine	Aspen	Balsa
η	1.78	3.35	11.5	3.55
γ	1.4	1.4	1.4	1.4

32 x 32 x 2 mm

Wood	Oak	Pine	Aspen	Balsa
η	3.76	6.69	11.5	4.00
γ	1.4	1.4	1.4	1.4

A P P E N D I X IV.

Experimental firebrand drag coefficients

Shape	Cylinders	Spheres	Square Plates
C_{D_o}	.85	.70	1.25

A P P E N D I X V.

VALUES OF PARAMETER δ IN EXPRESSION (II.7)

Cylinders with length / diameter ratio equal 3

Wood	Oak	Pine	Spruce	Aspen	Balsa
δ	.378	.375	.394	.340	.334

Spheres

Wood	Oak	Pine	Spruce	Aspen	Balsa
δ	.288	.276	.317	.233	.251

Plates

32 x 32 x 16 mm

Wood	Oak	Pine	Aspen	Balsa
δ	.488	.371	.277	.379

32 x 32 x 8 mm

Wood	Oak	Pine	Aspen	Balsa
δ	.473	.378	.237	.360

32 x 32 x 4 mm.

Wood	Oak	Pine	Aspen	Balsa
δ	.405	.307	.219	.296

32 x 32 x 2 mm.

Wood	Oak	Pine	Aspen	Balsa
δ	.297	.237	.238	.286

A P P E N D I X VI .

VALUES OF PARAMETERS β_1 , φ_1 , β_2 , φ_2 , θ EN EXPRESSIONS (II.11) through (II.15)

	β_1	φ_1	β_2	φ_2	θ
Spheres	2.3	1.3	.4	1.6	2.3
Cylinders	2.5	1.5	.7	1.6	2

FIG. 1

INFLUENCE OF ξ - HEPTANE

D = 50 cm

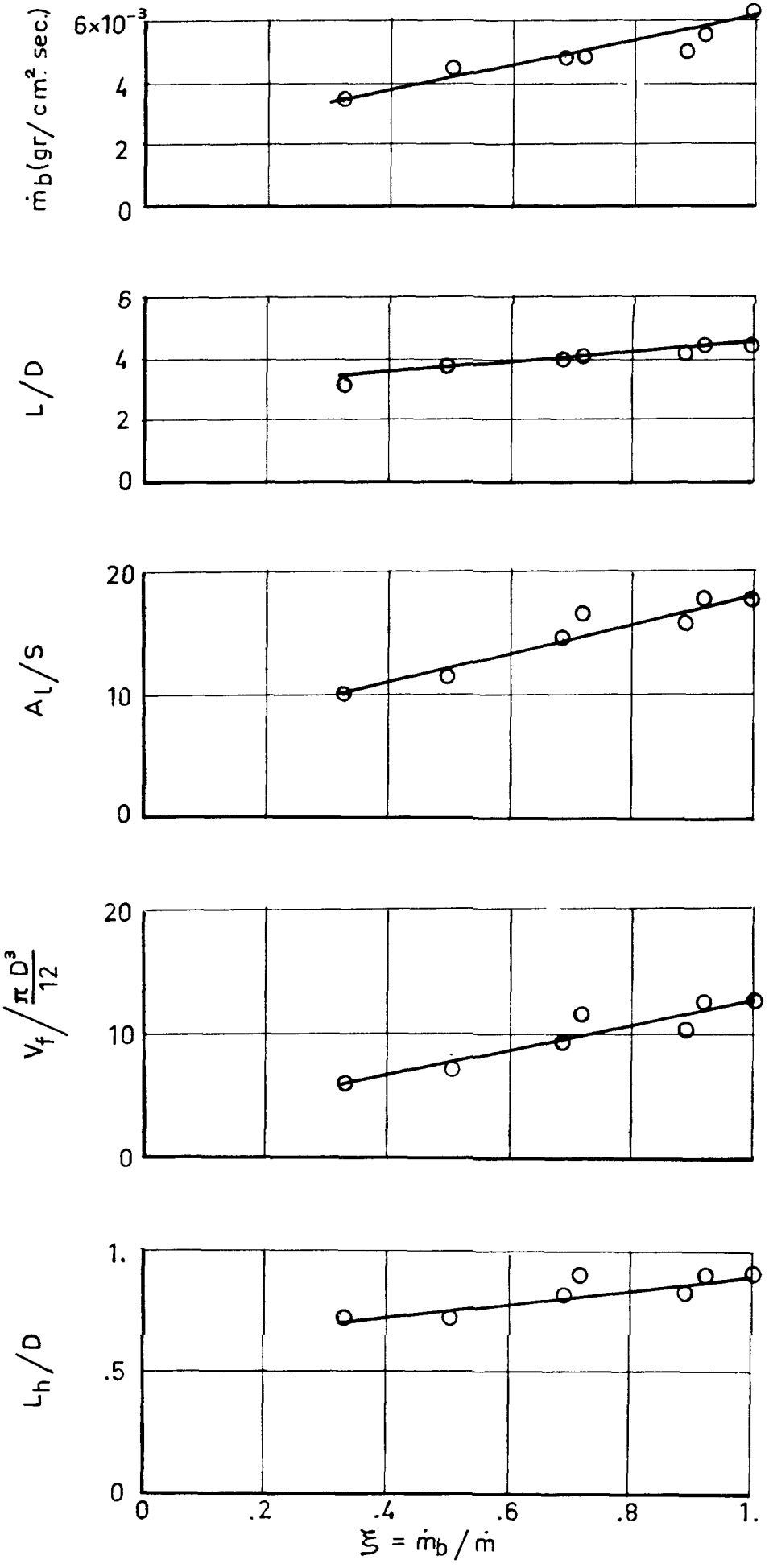

FIG. 2

INFLUENCE OF ξ - HEPTANE

D = 50 cm

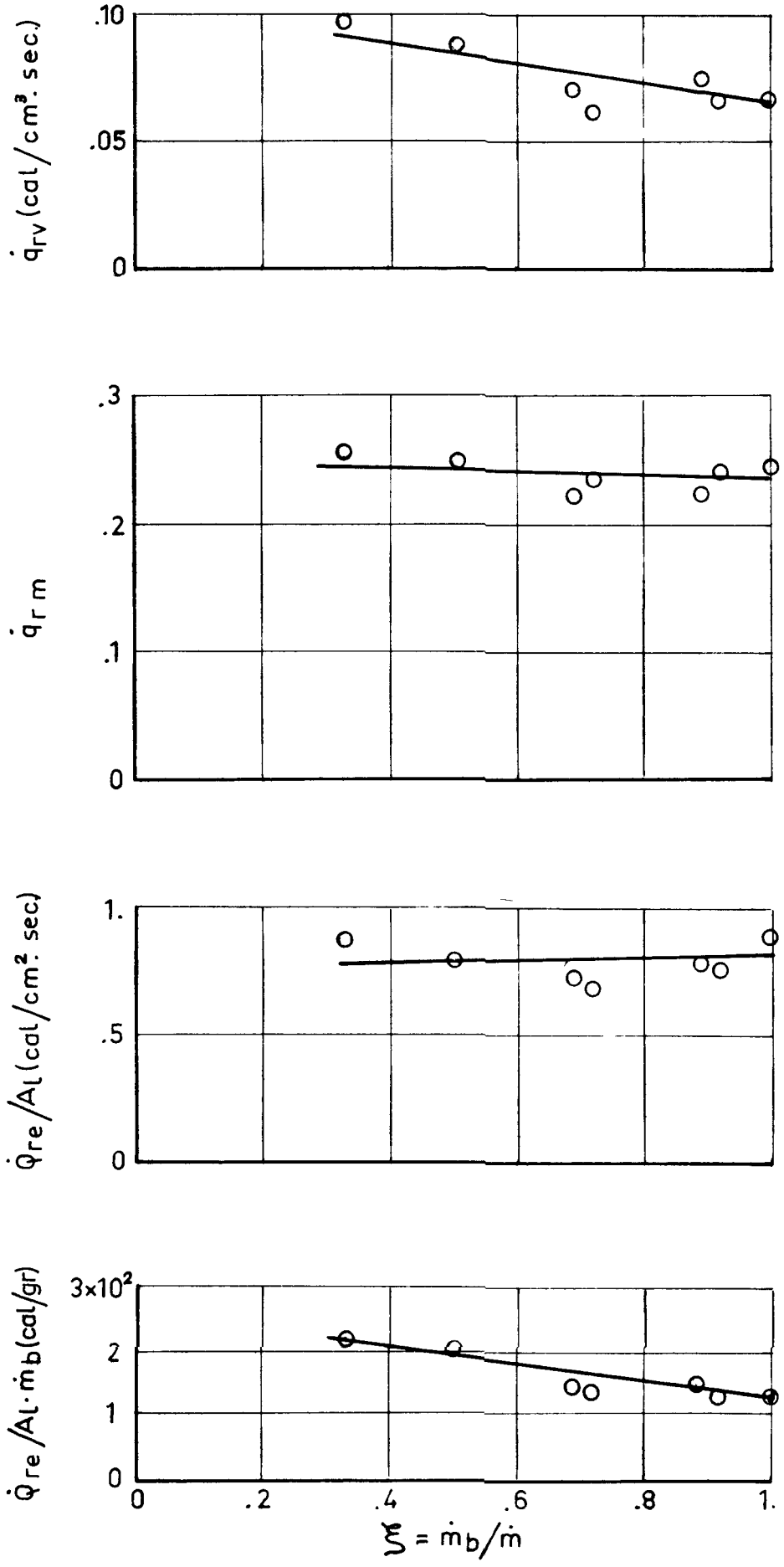

FIG. 3

INFLUENCE OF THE OVER-FLOW

HEPTANE

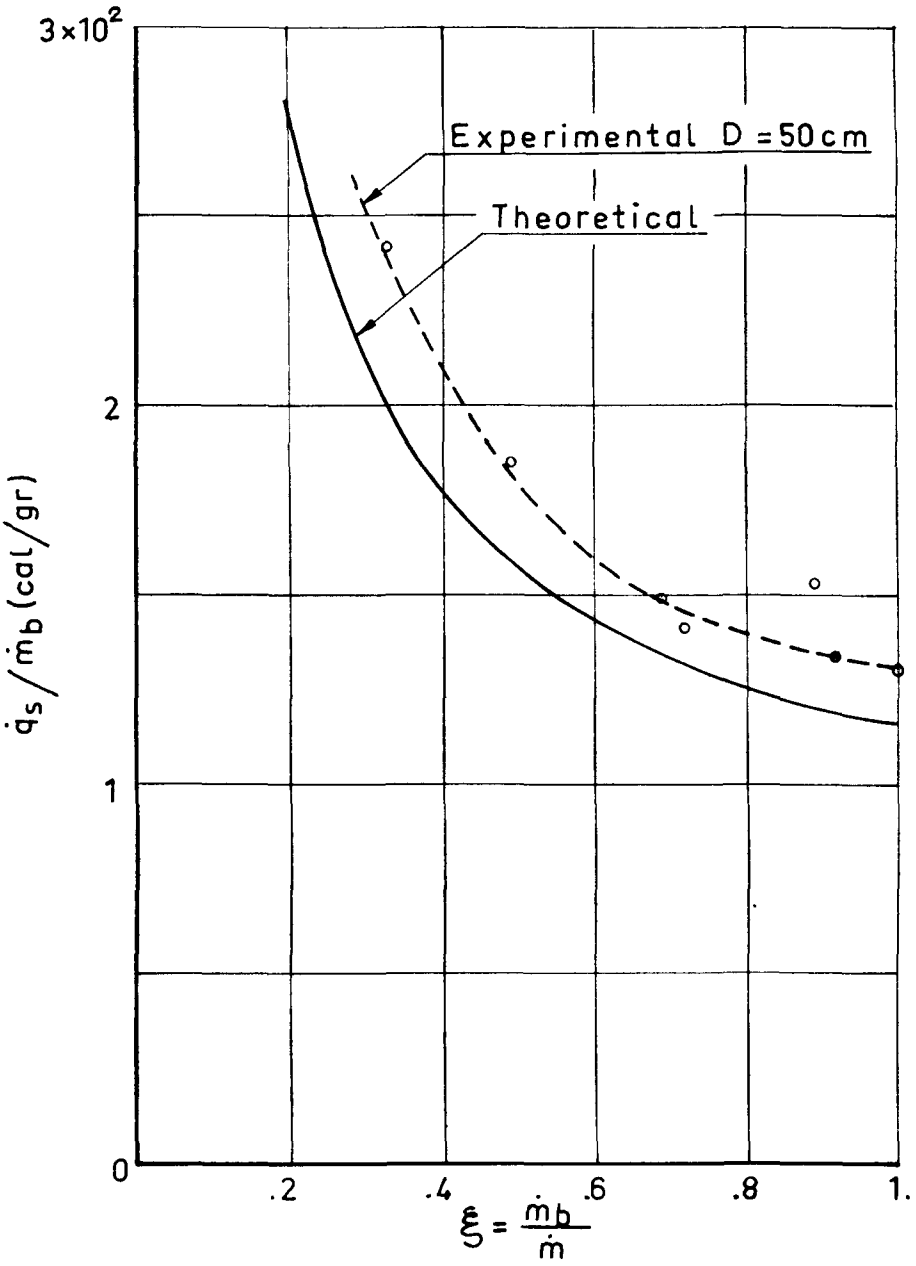

FIG. 4

THEORETICAL RESULTS – Heptane

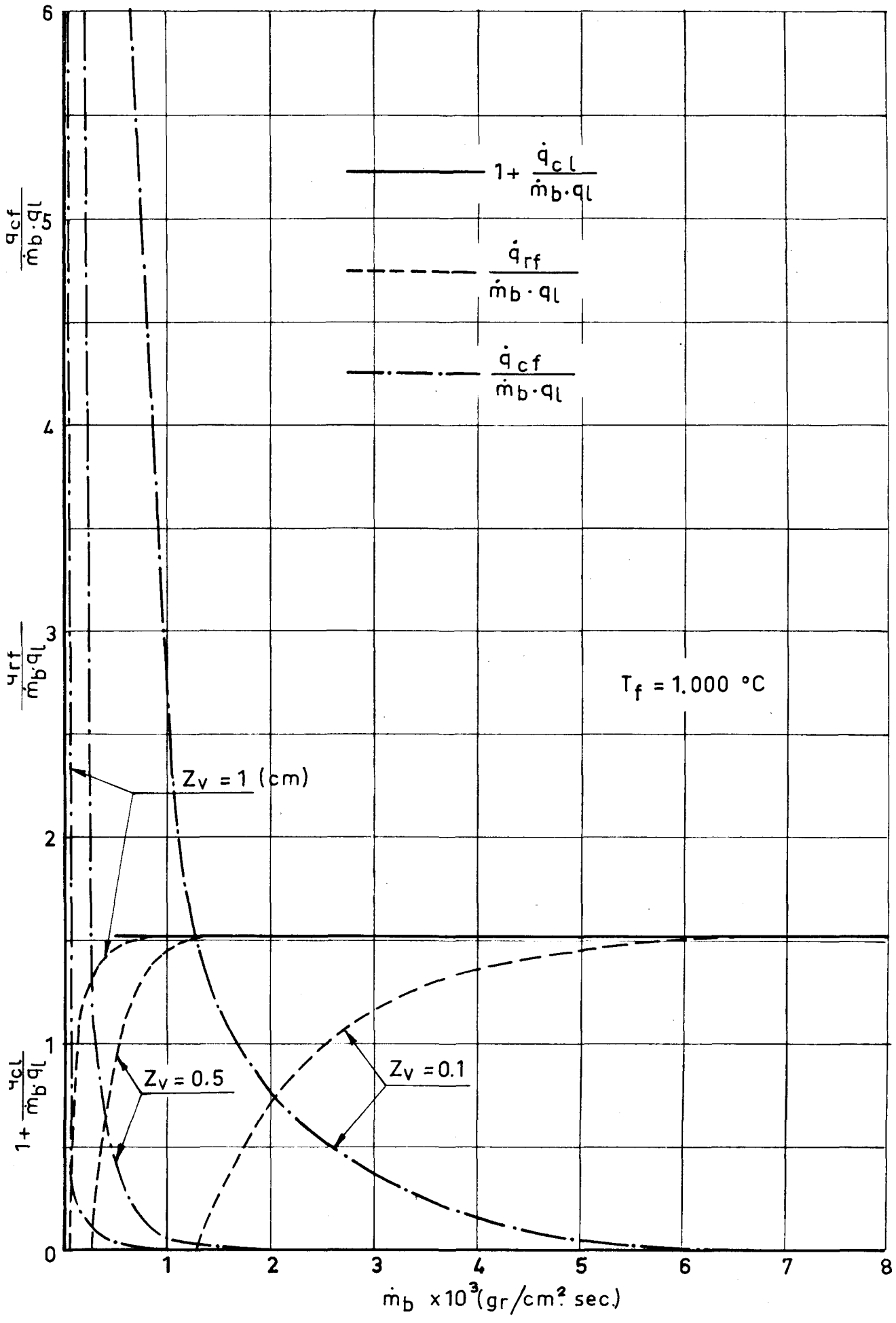

FIG. 5

INFLUENCE OF DIAMETER - HEPTANE

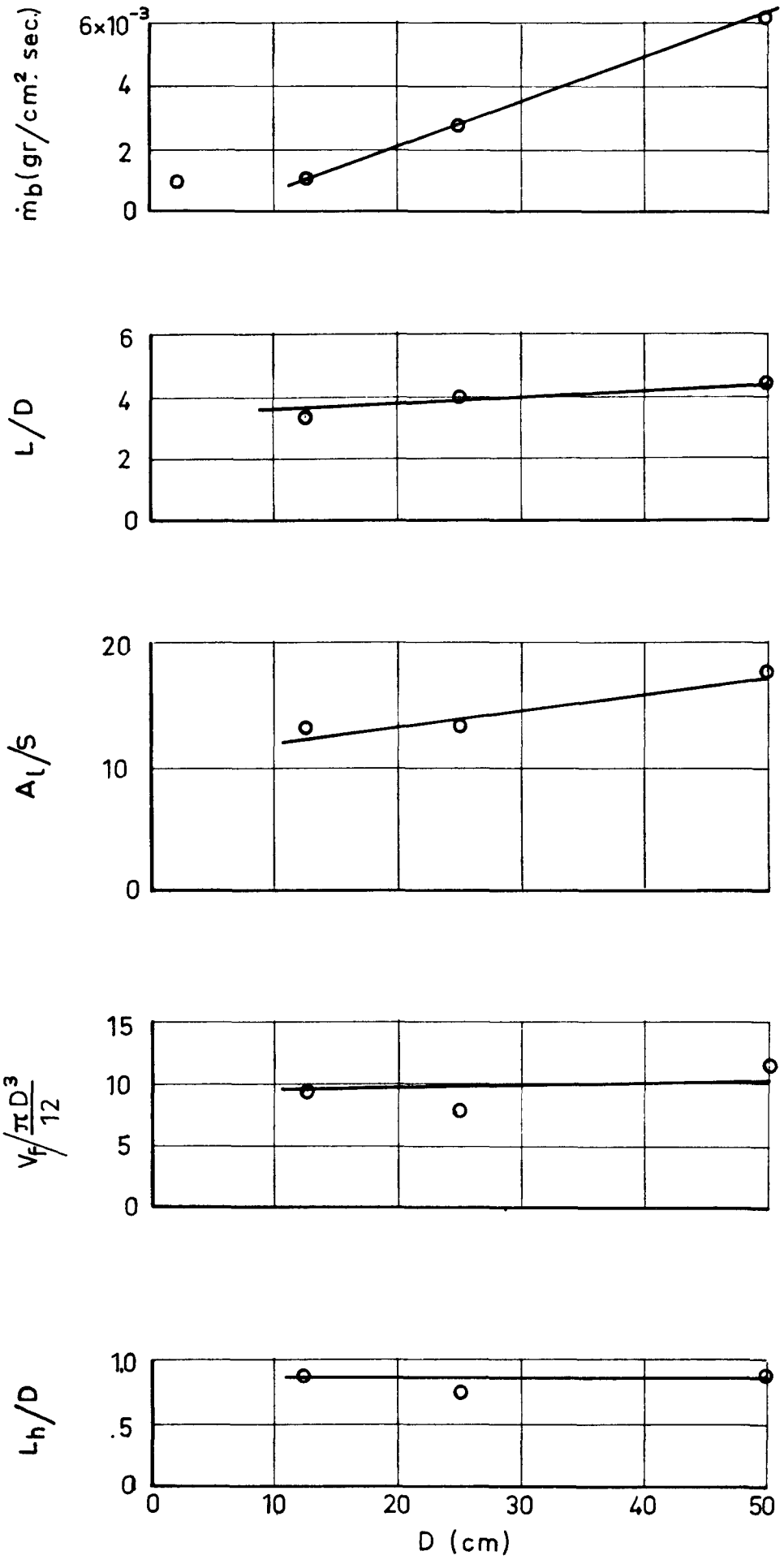

FIG. 6

INFLUENCE OF DIAMETER - HEPTANE

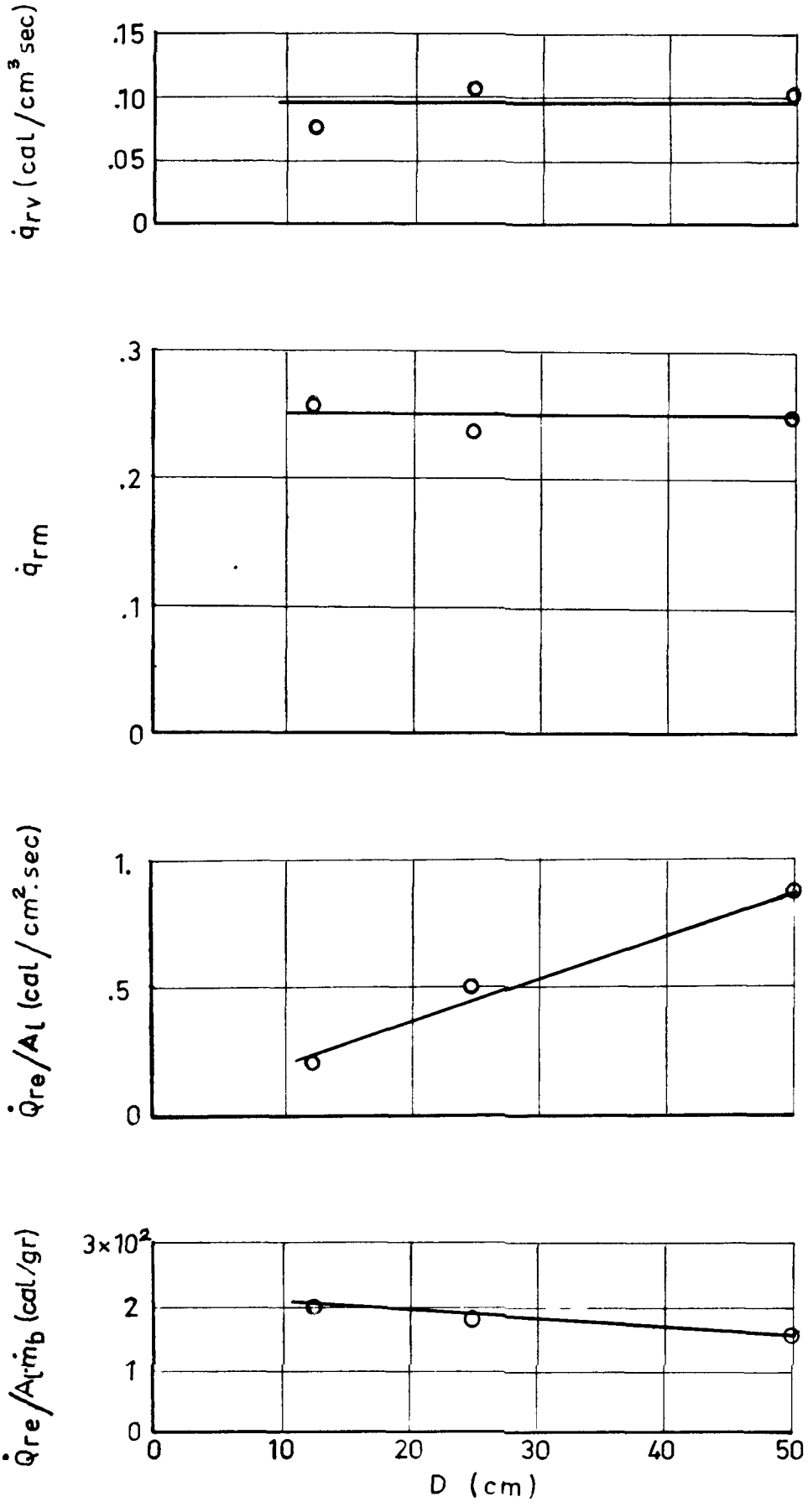

FIG. 7

INFLUENCE OF DIAMETER – DIOXANE

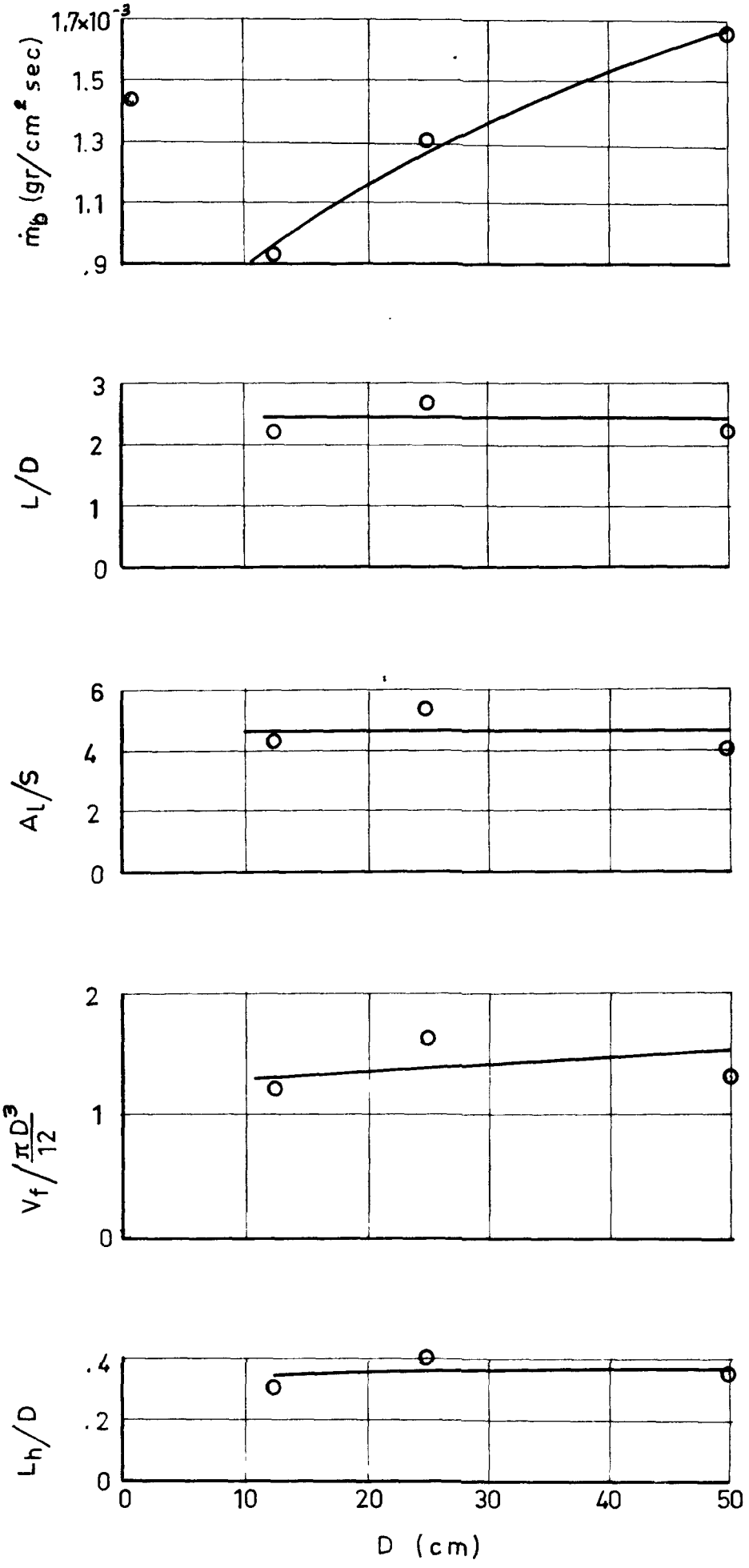

FIG. 8

INFLUENCE OF DIAMETER - DIOXANE

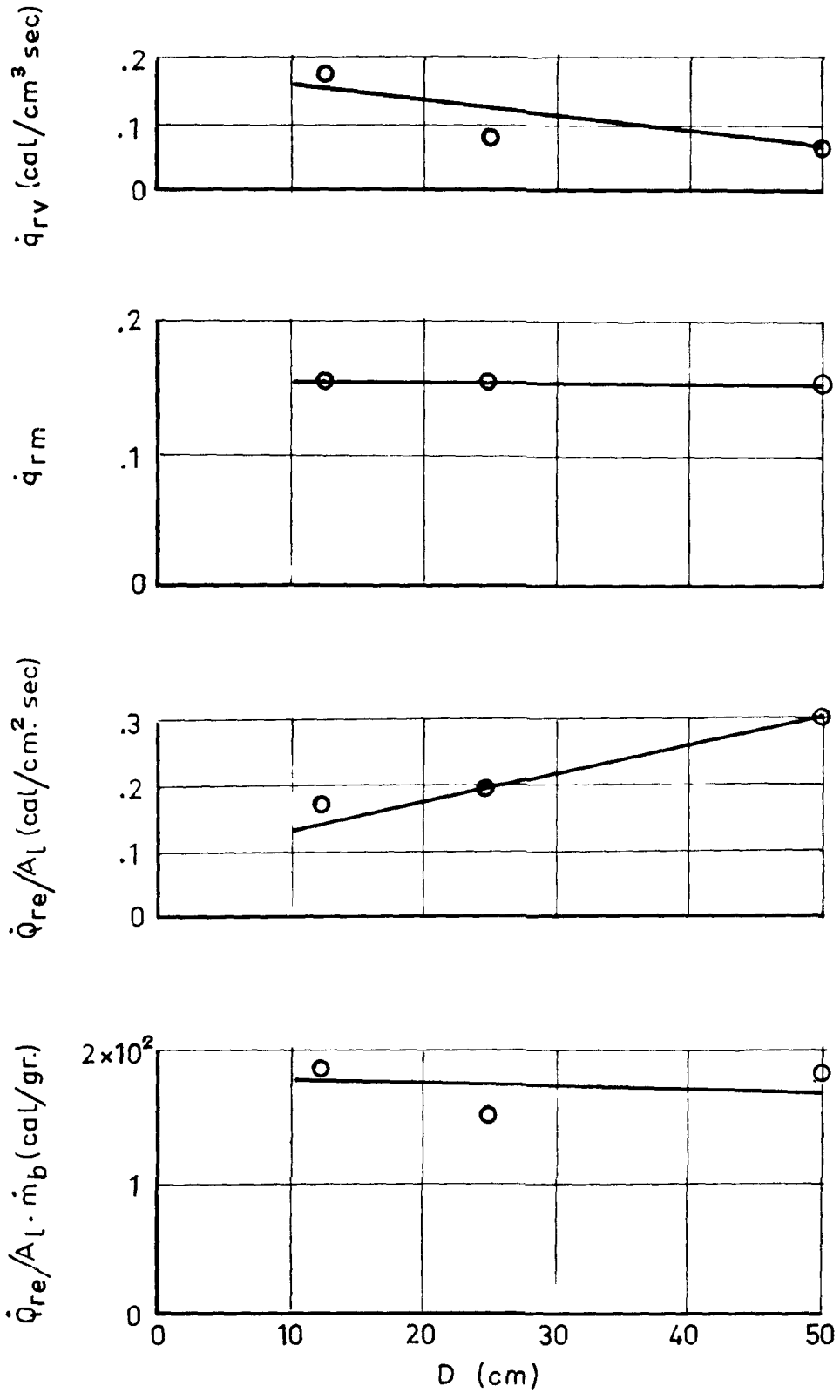

FIG. 9

TEMPERATURE DISTRIBUTION T °C

HEPTANE

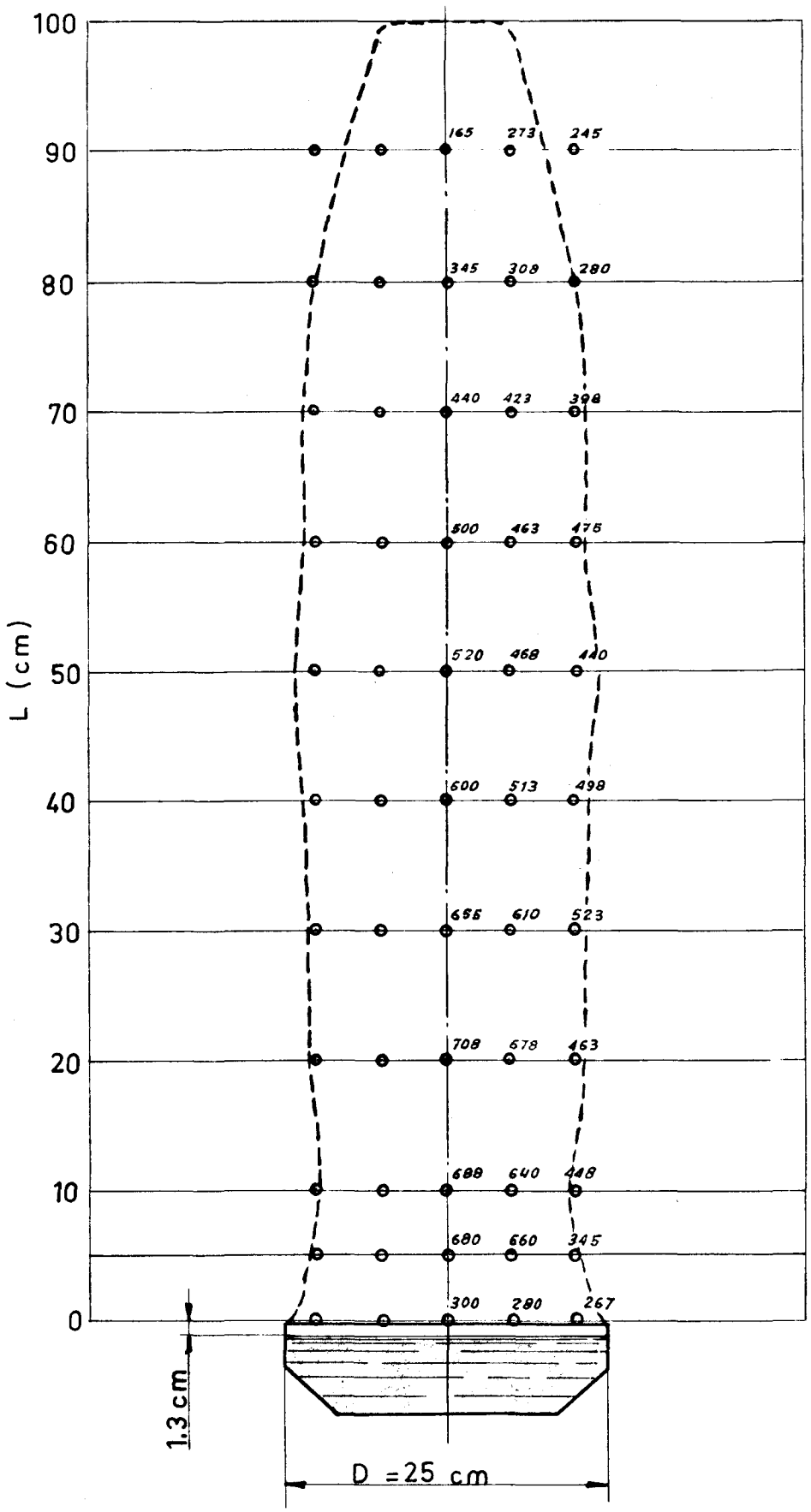

FIG. 10

TEMPERATURE DISTRIBUTION T °C

DIOXANE

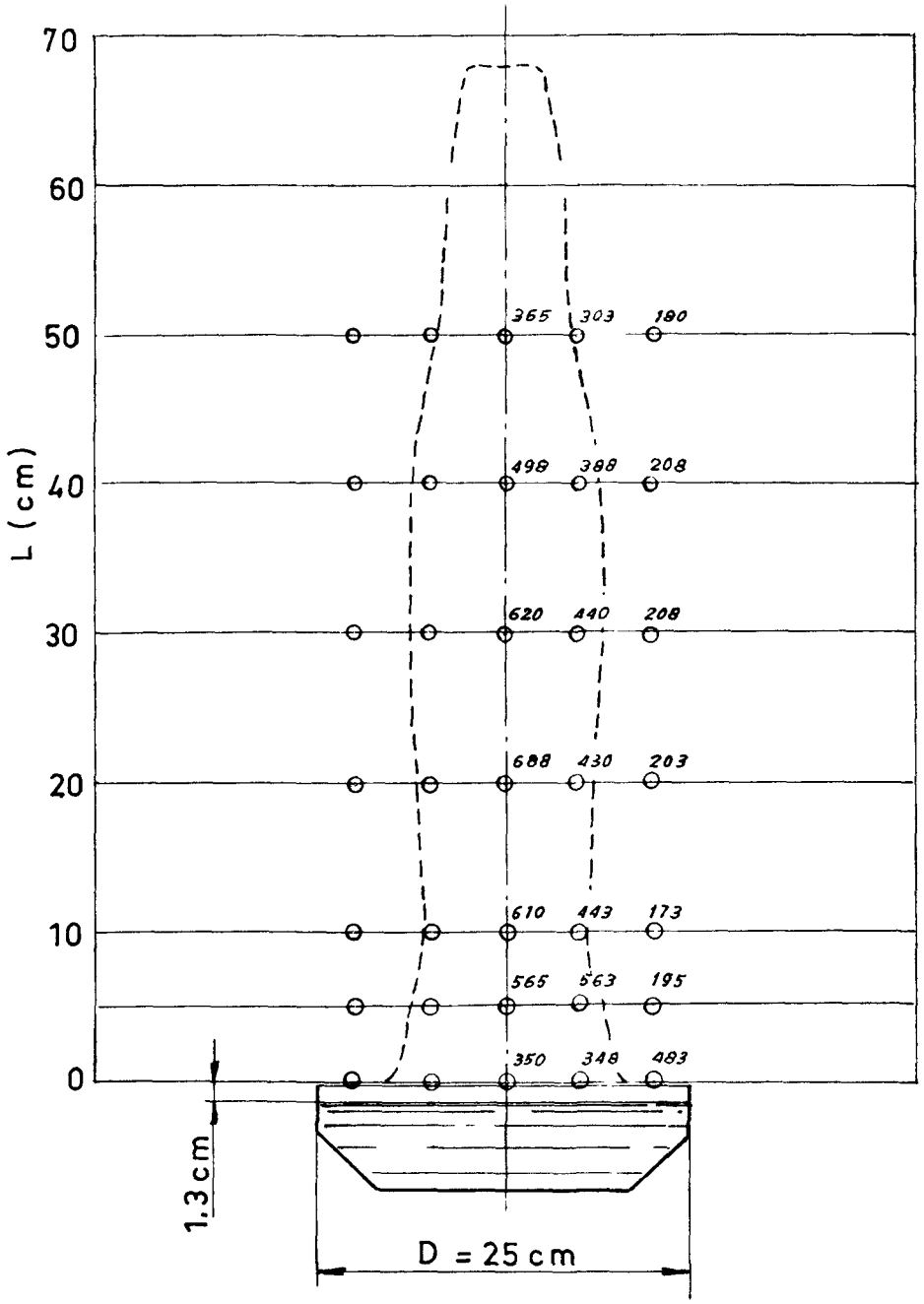

FIG. 11

INFLUENCE OF THE DIAMETER

Theoretical and Experimental results

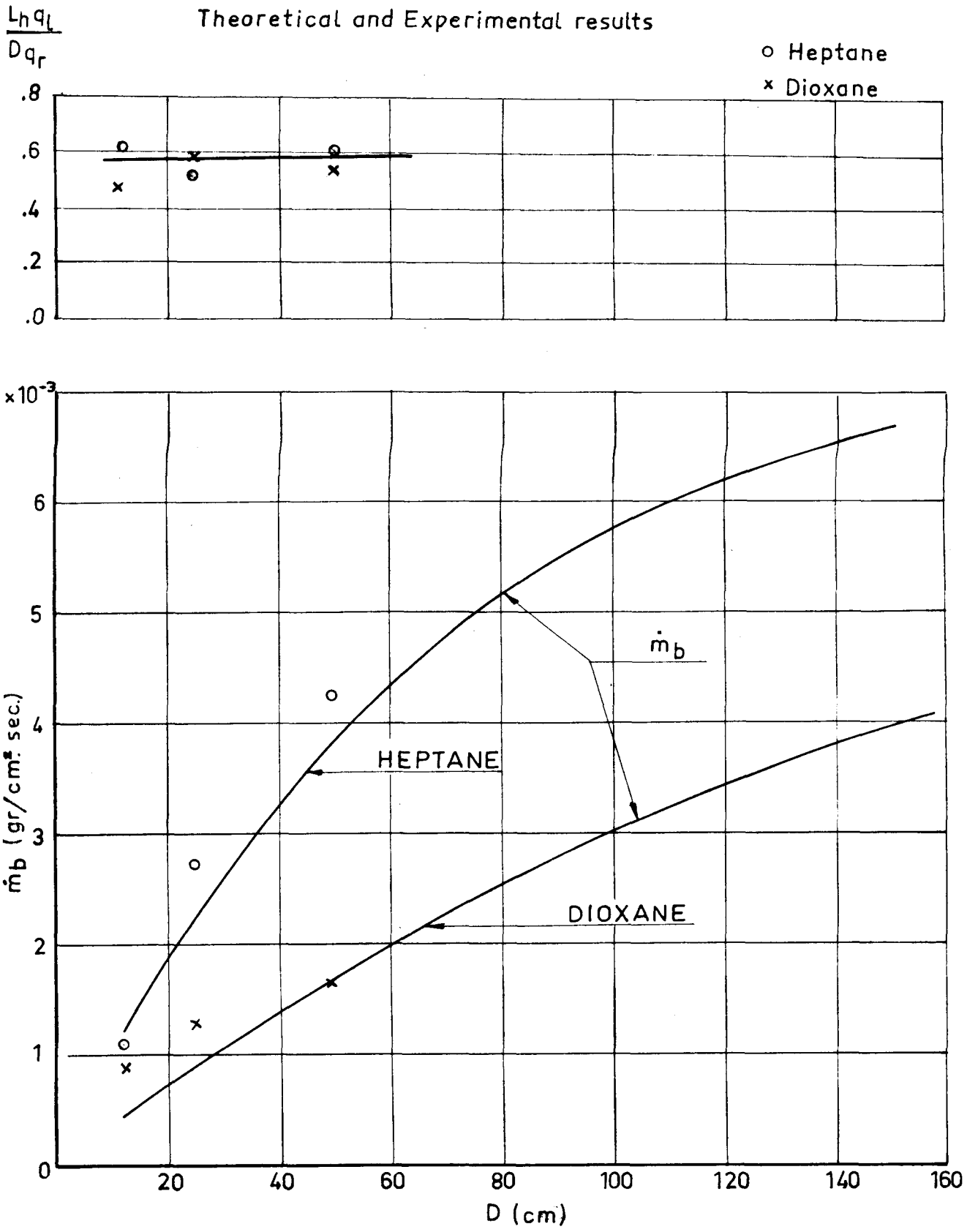

FIG. 12

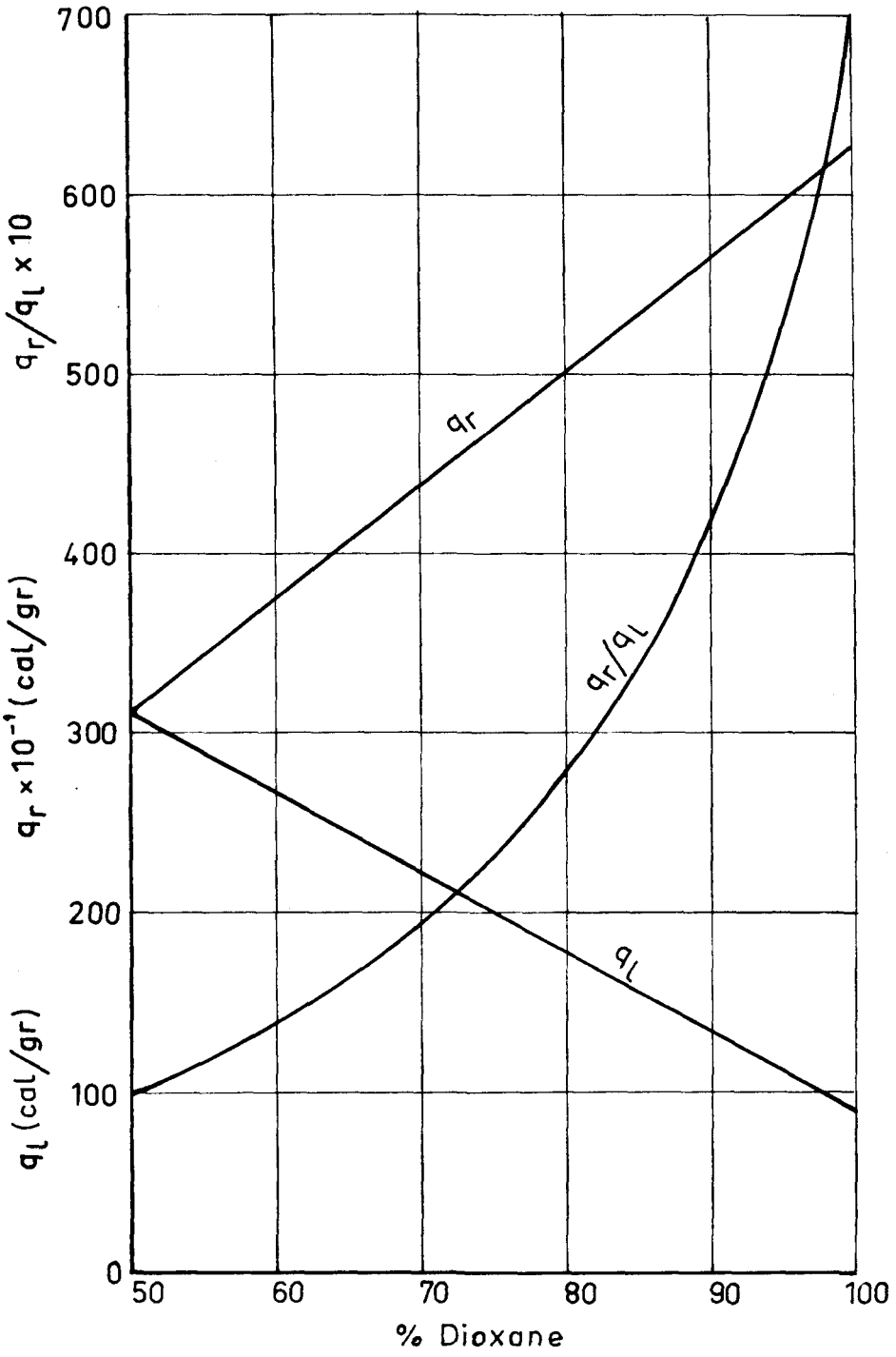
700
600
500
400
300
200
100
0
$q_r/q_l \times 10$
$q_r \times 10^{-1}$ (cal/gr)
q_l (cal/gr)
q_r
q_r/q_l
q_l
50
60
70
80
90
100
% Dioxane

FIG. 13

INFLUENCE OF THE COMPOSITION - DIOXANE

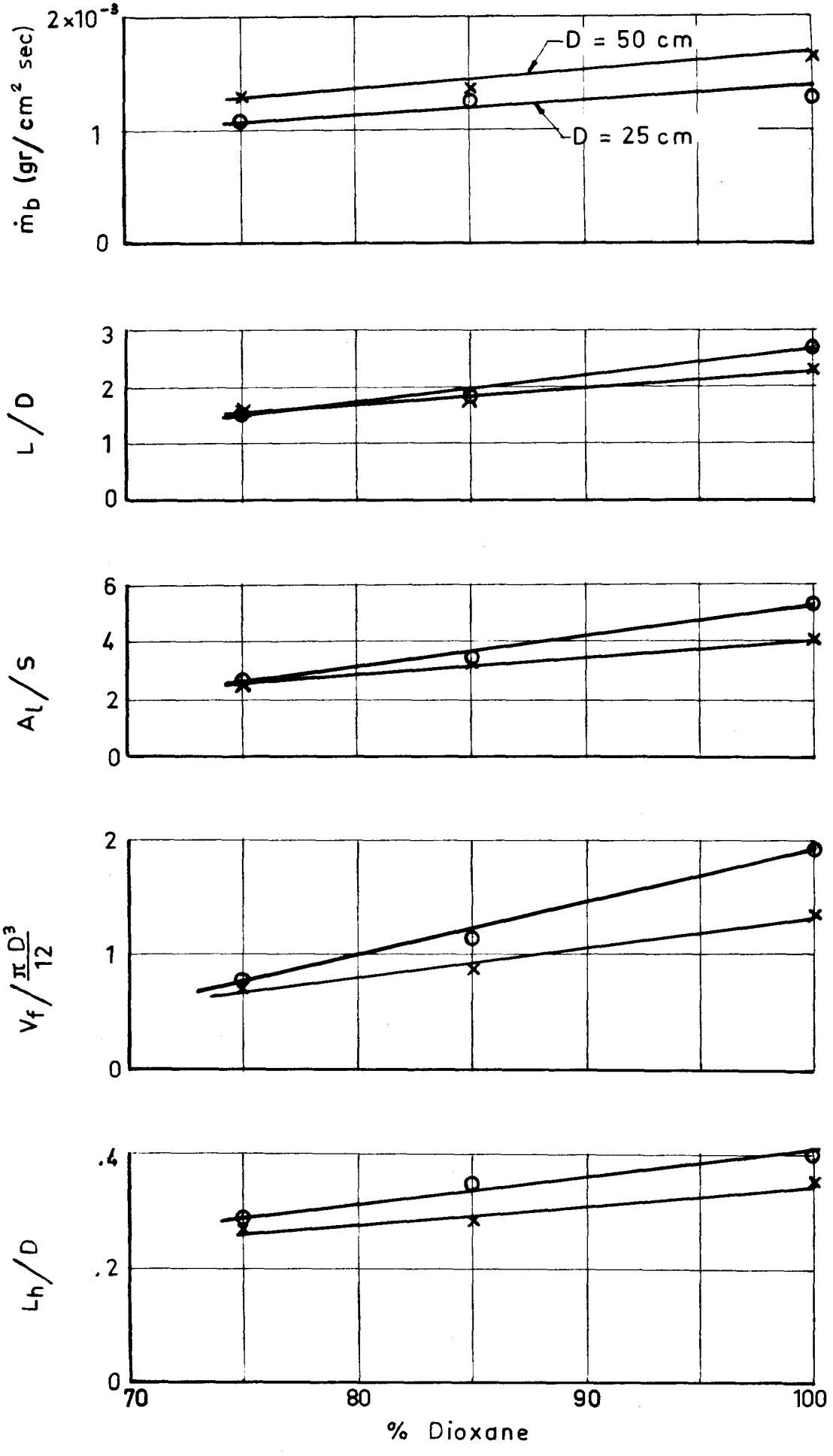

FIG. 14

INFLUENCE OF THE COMPOSITION - DIOXANE

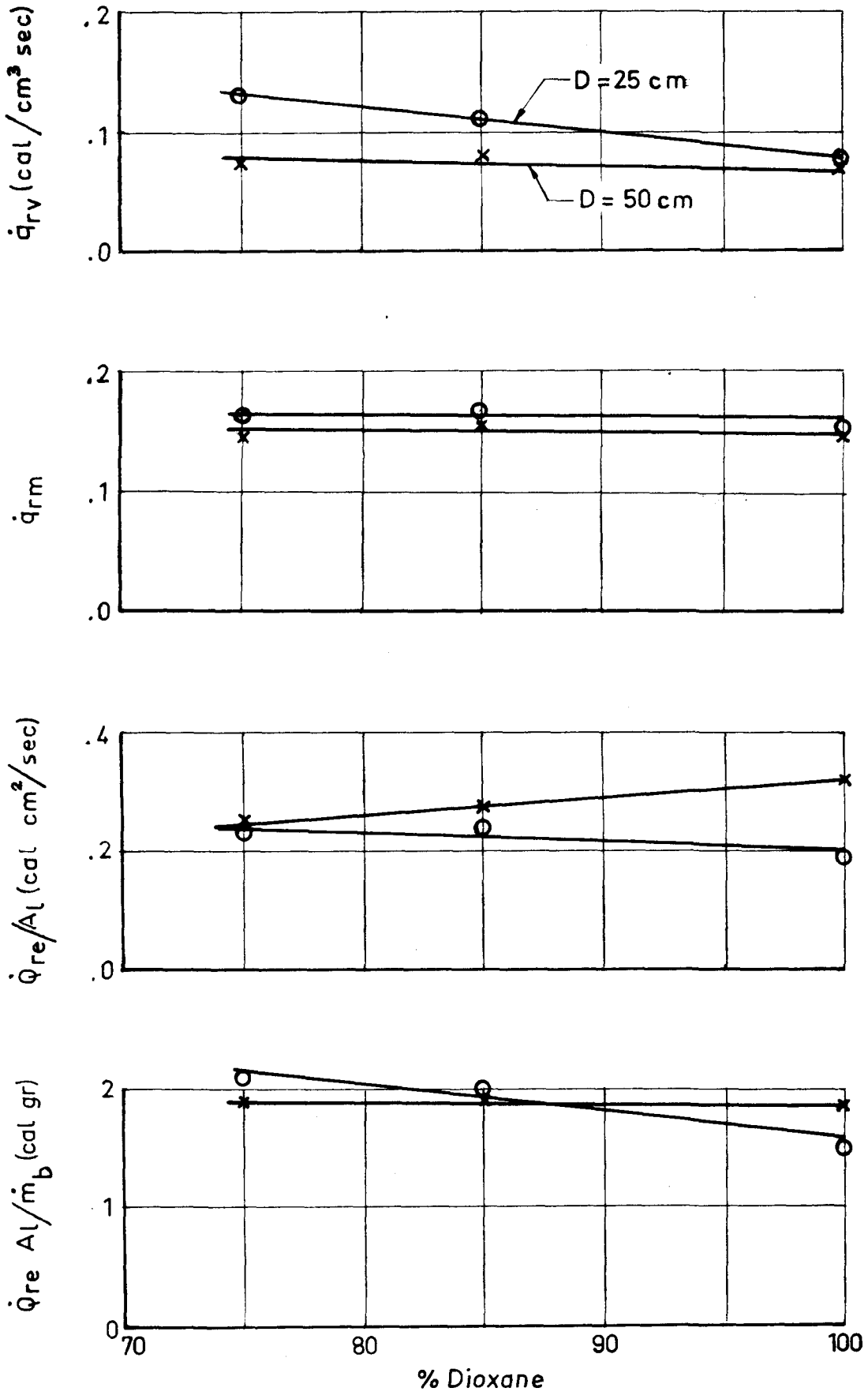

INCLINED CONVECTION COLUMN
CYLINDERS

OAK

FIG. 15

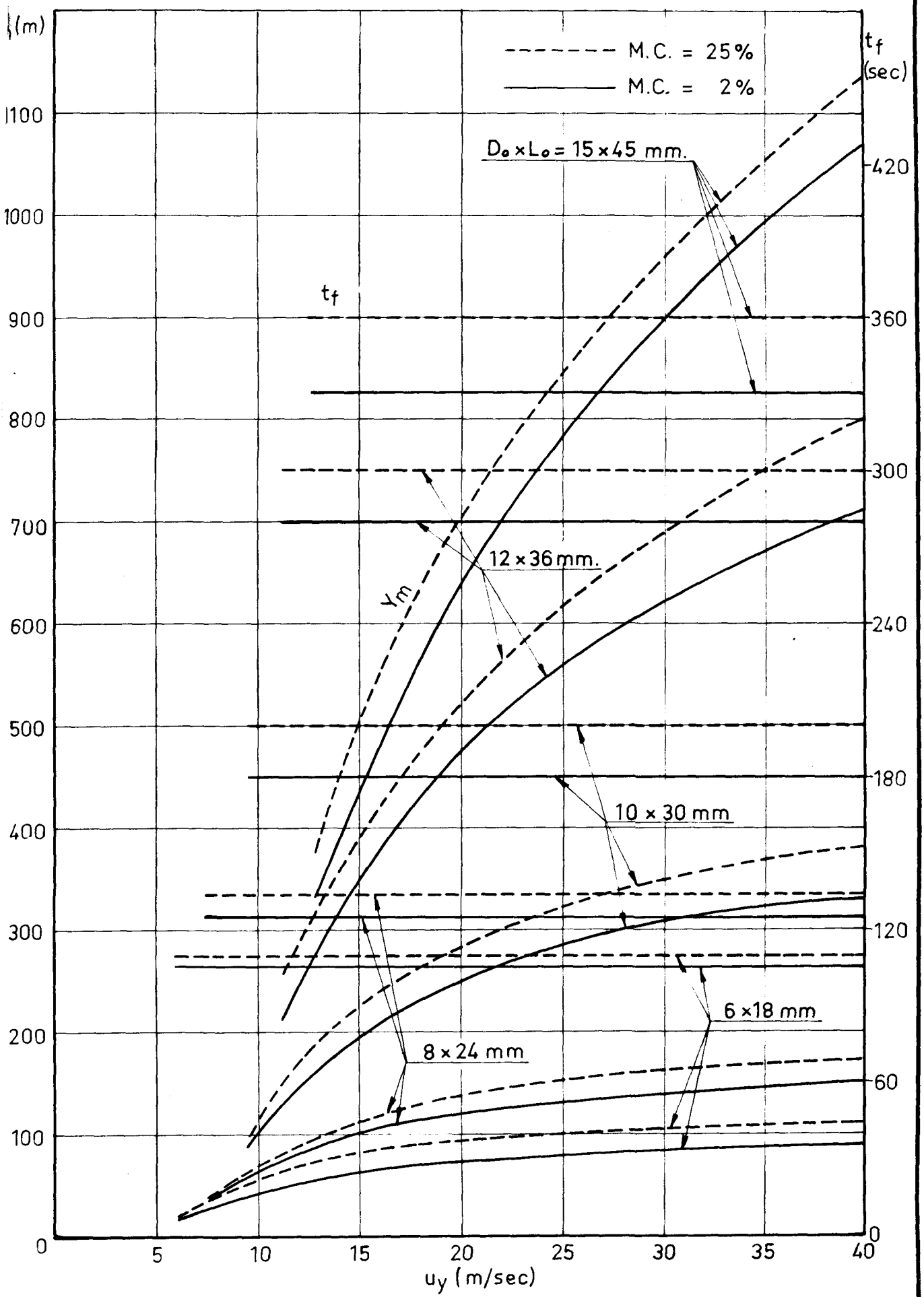

FIG. 16

INCLINED CONVECTION COLUMN

CYLINDERS

PINE

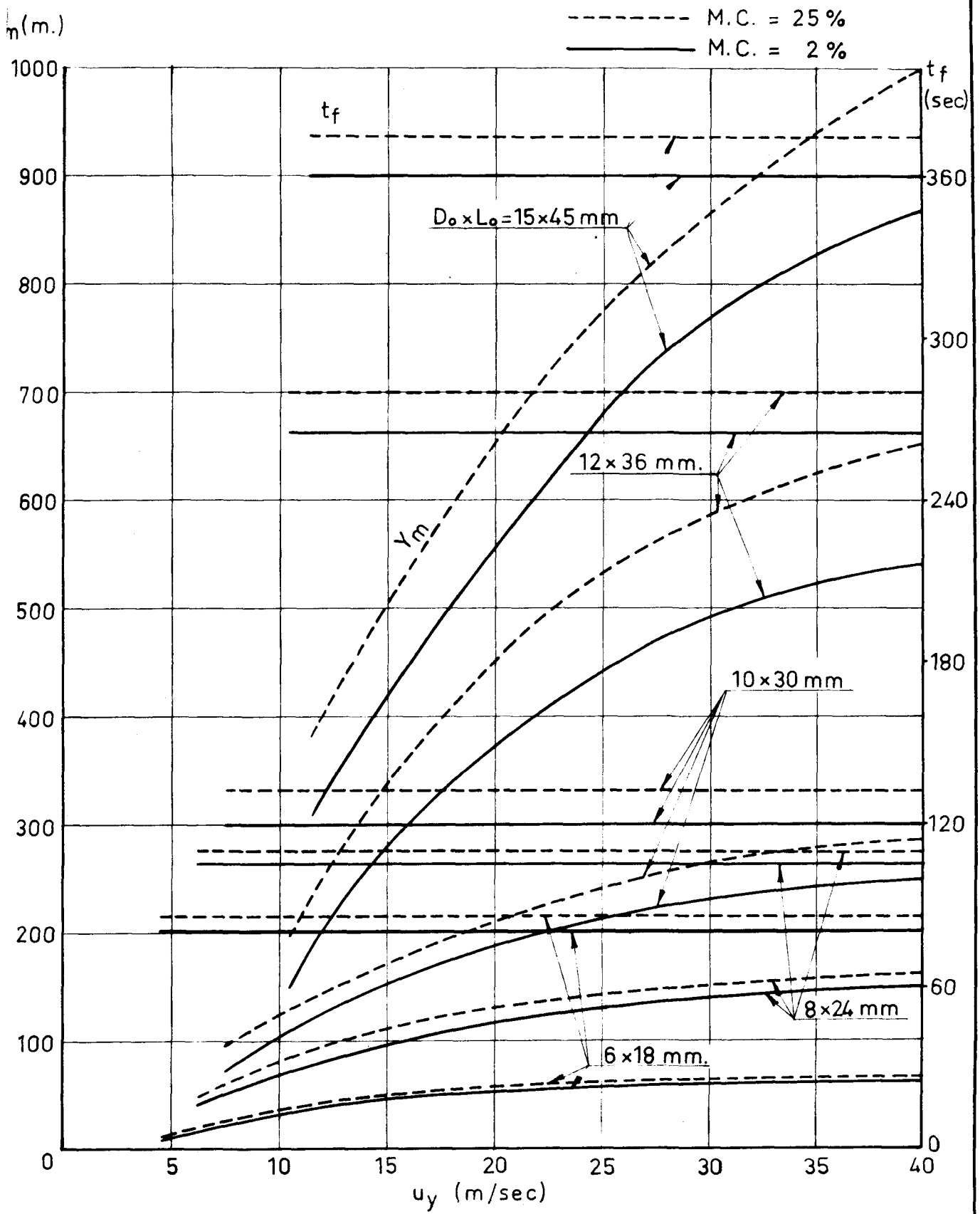

FIG. 17

INCLINED CONVECTION COLUMN

CYLINDERS

SPRUCE

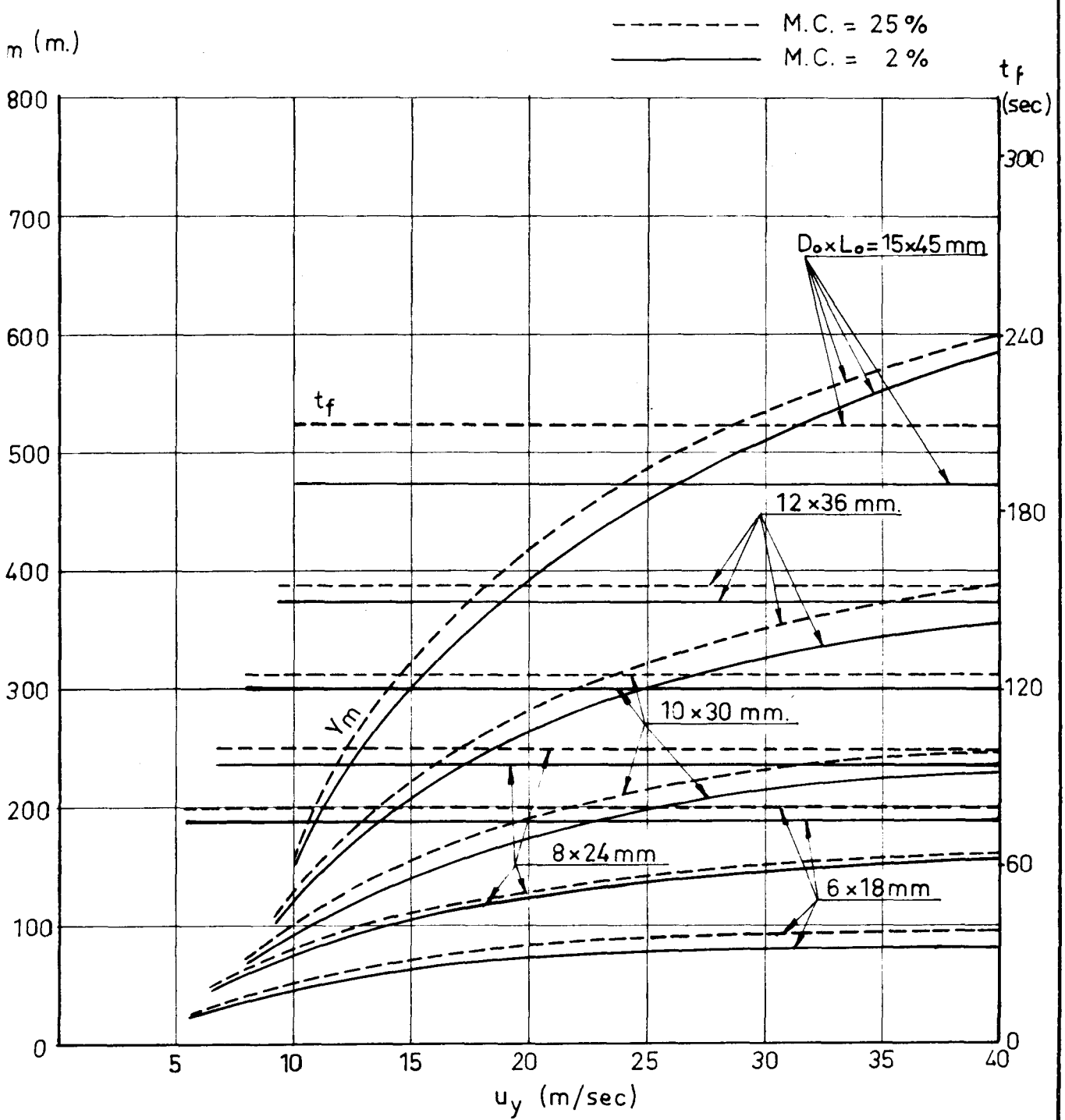

FIG. 18

INCLINED CONVECTION COLUMN
CYLINDERS

ASPEN

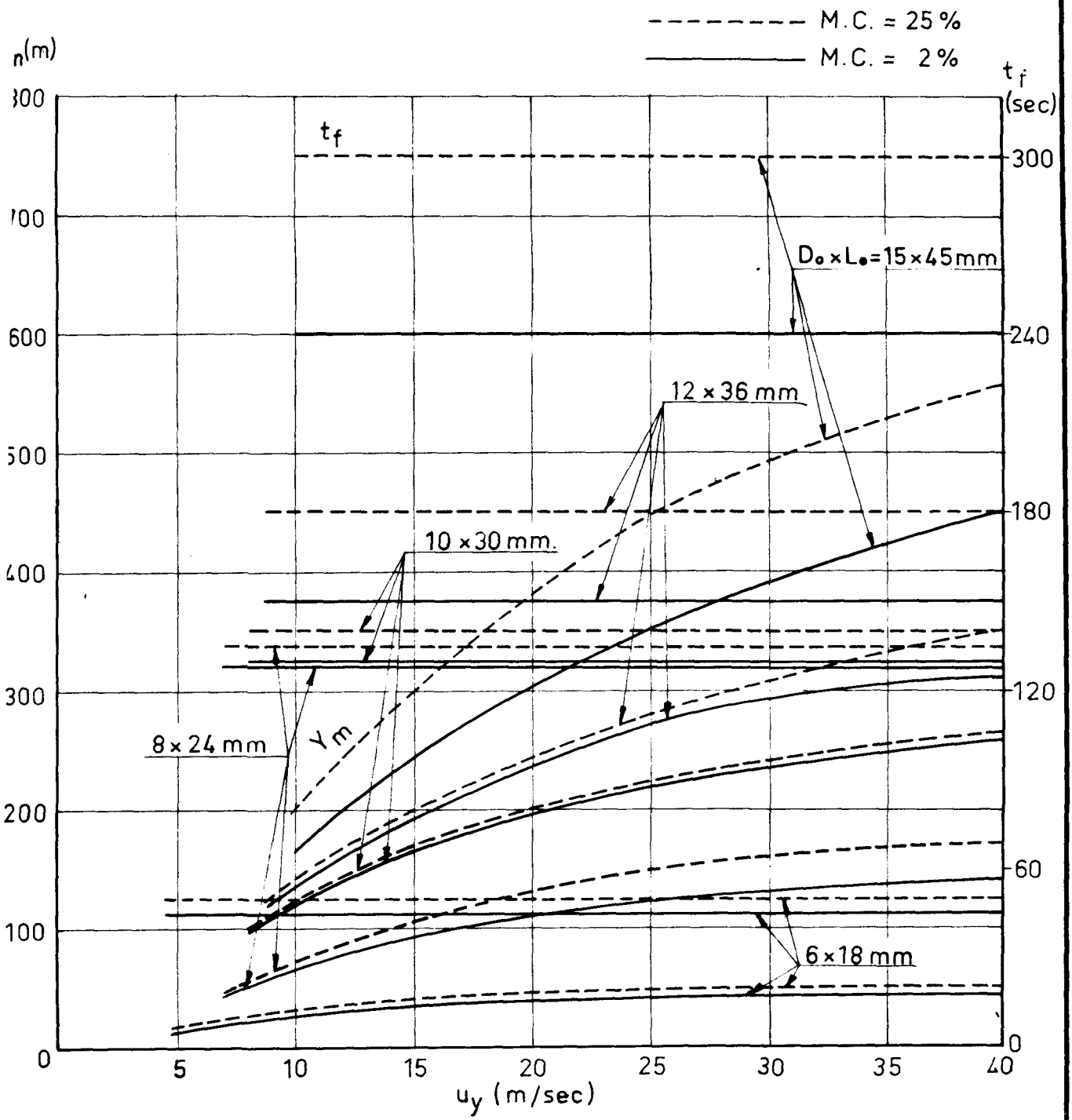

FIG. 19

INCLINED CONVECTION COLUMN
CYLINDERS

BALSA

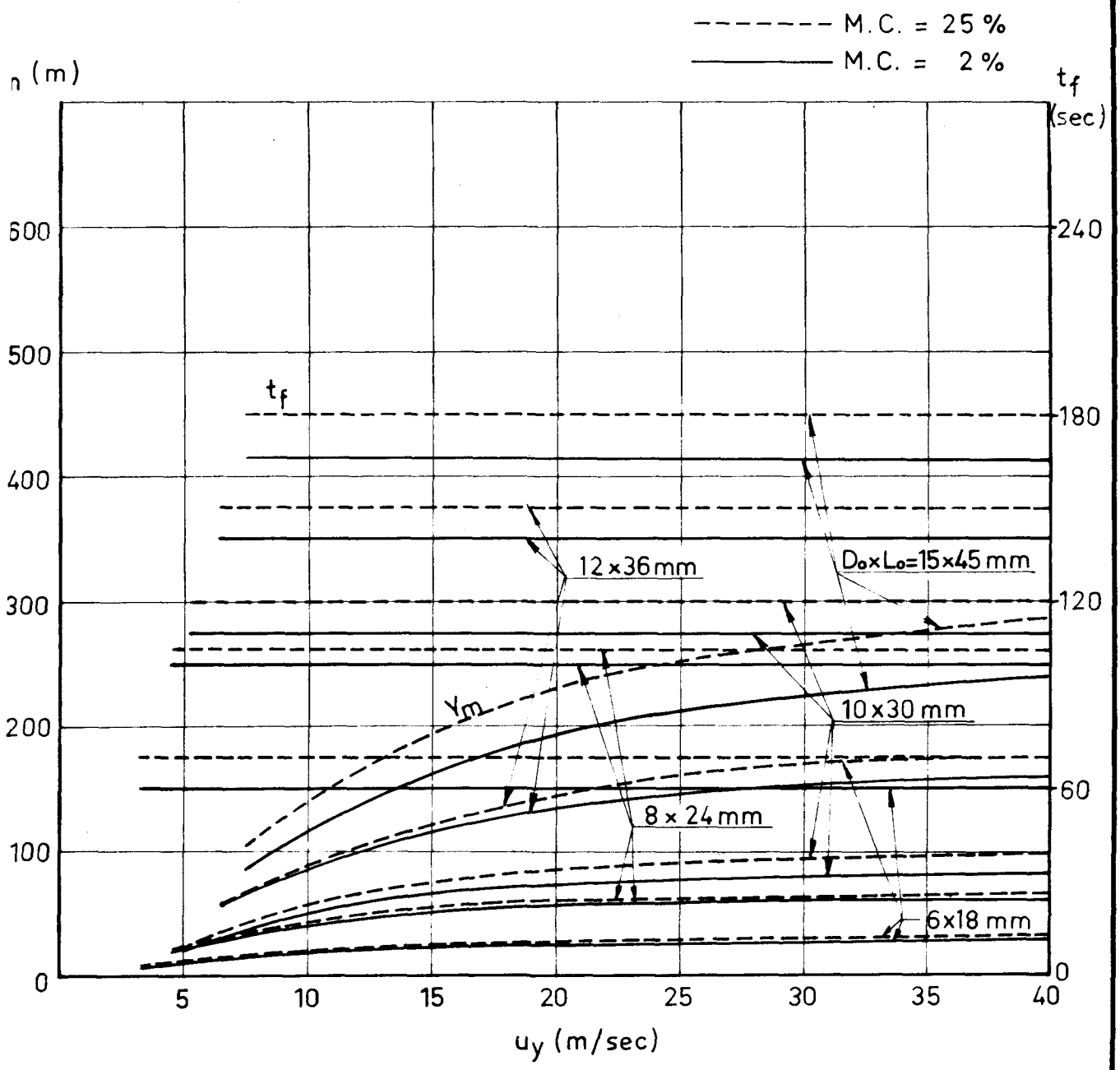

FIG. 20

INCLINED CONVECTION COLUMN
CYLINDERS

OAK

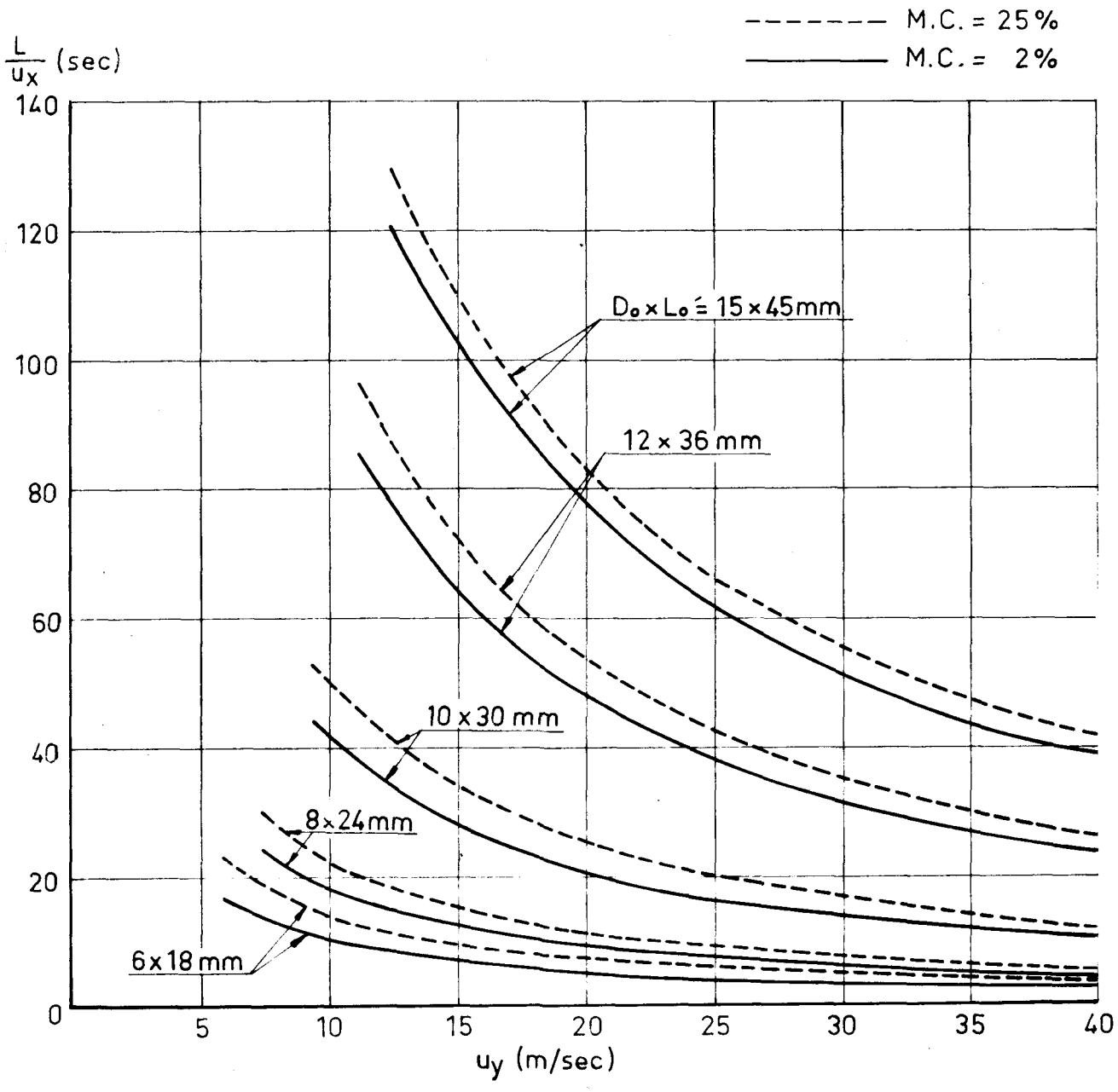

FIG. 21

INCLINED CONVECTION COLUMN
CYLINDERS

PINE

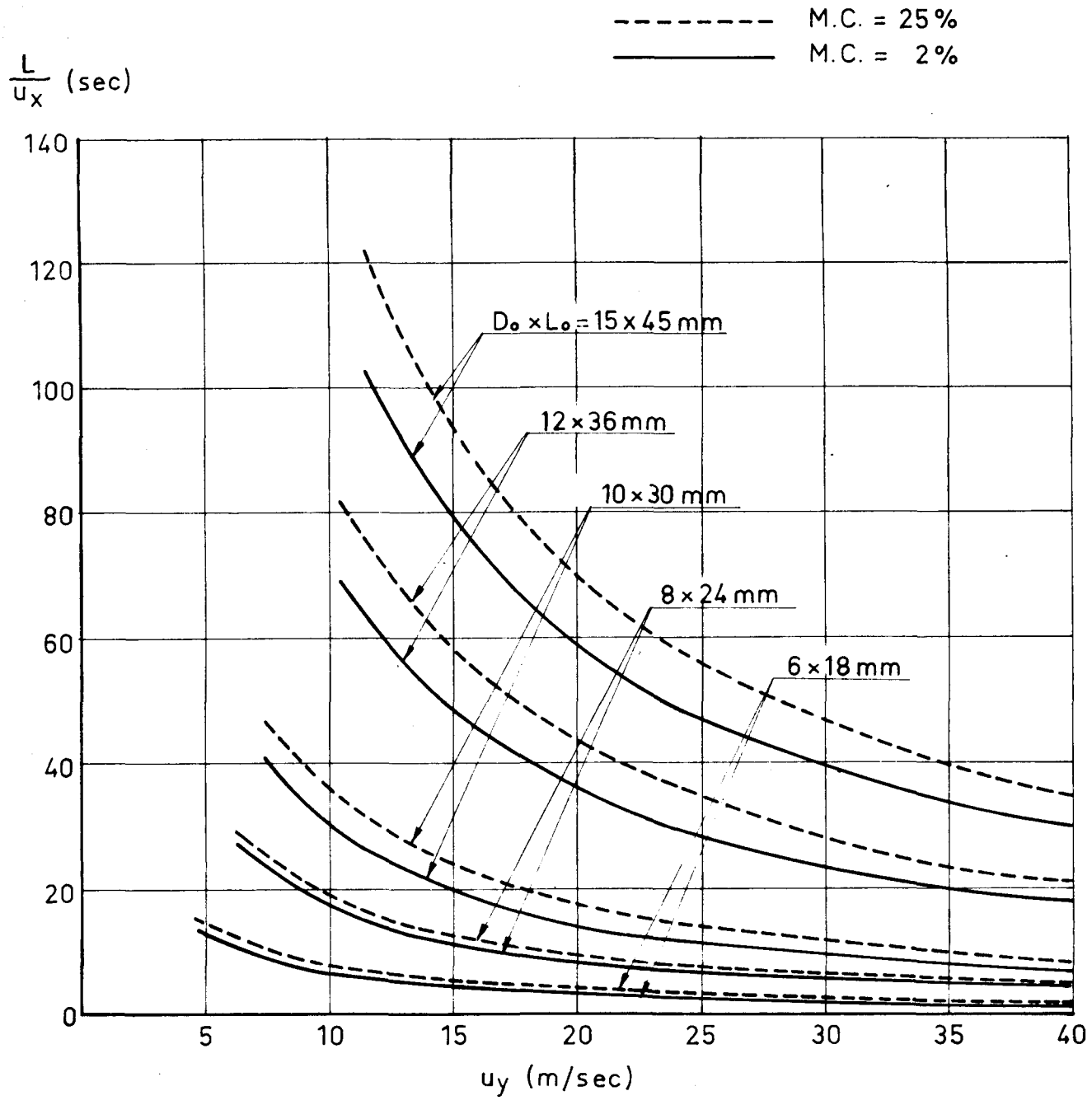

FIG. 22

INCLINED CONVECTION COLUMN
CYLINDERS

SPRUCE

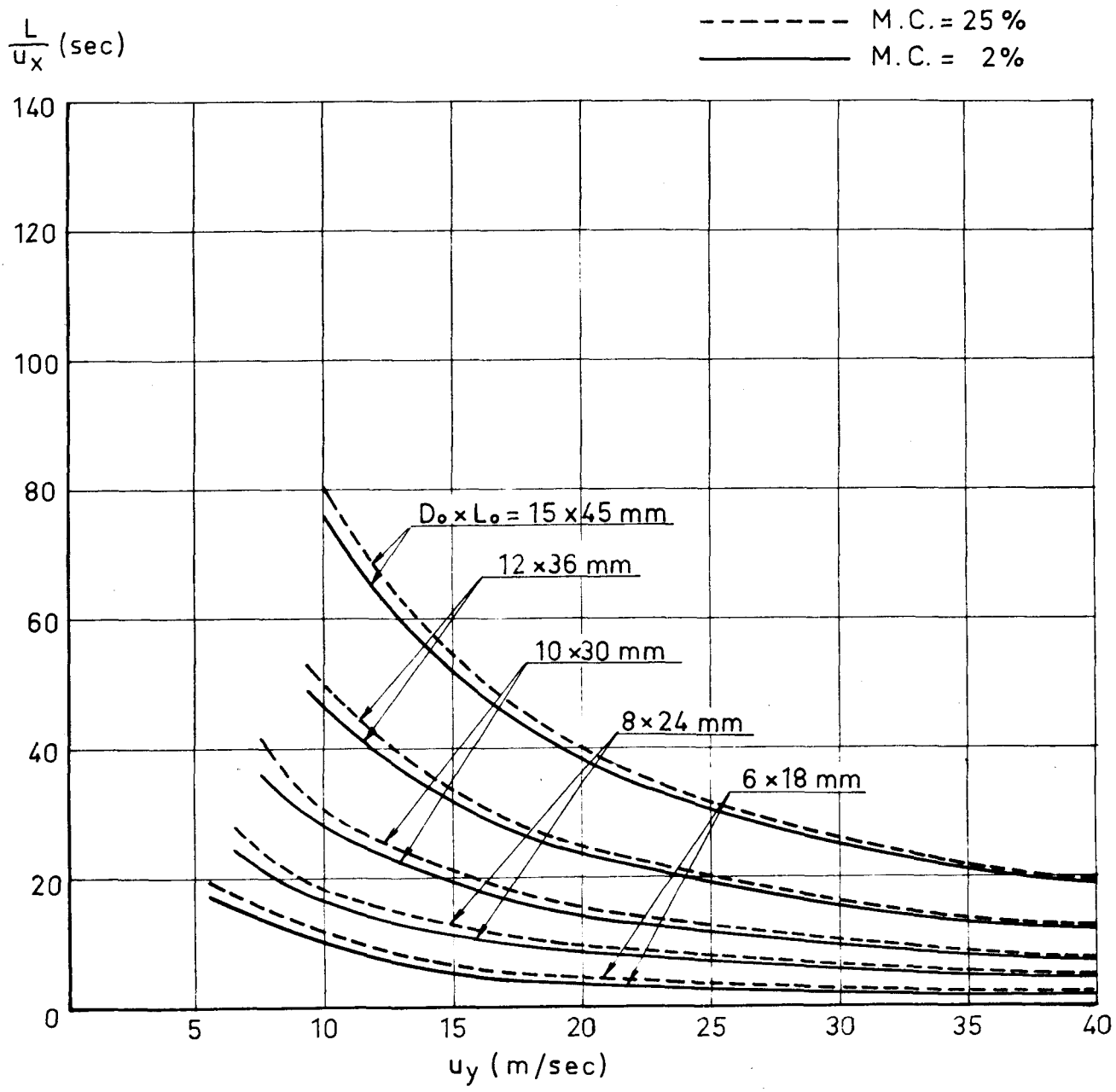

FIG. 23

INCLINED CONVECTION COLUMN
CYLINDERS
ASPEN

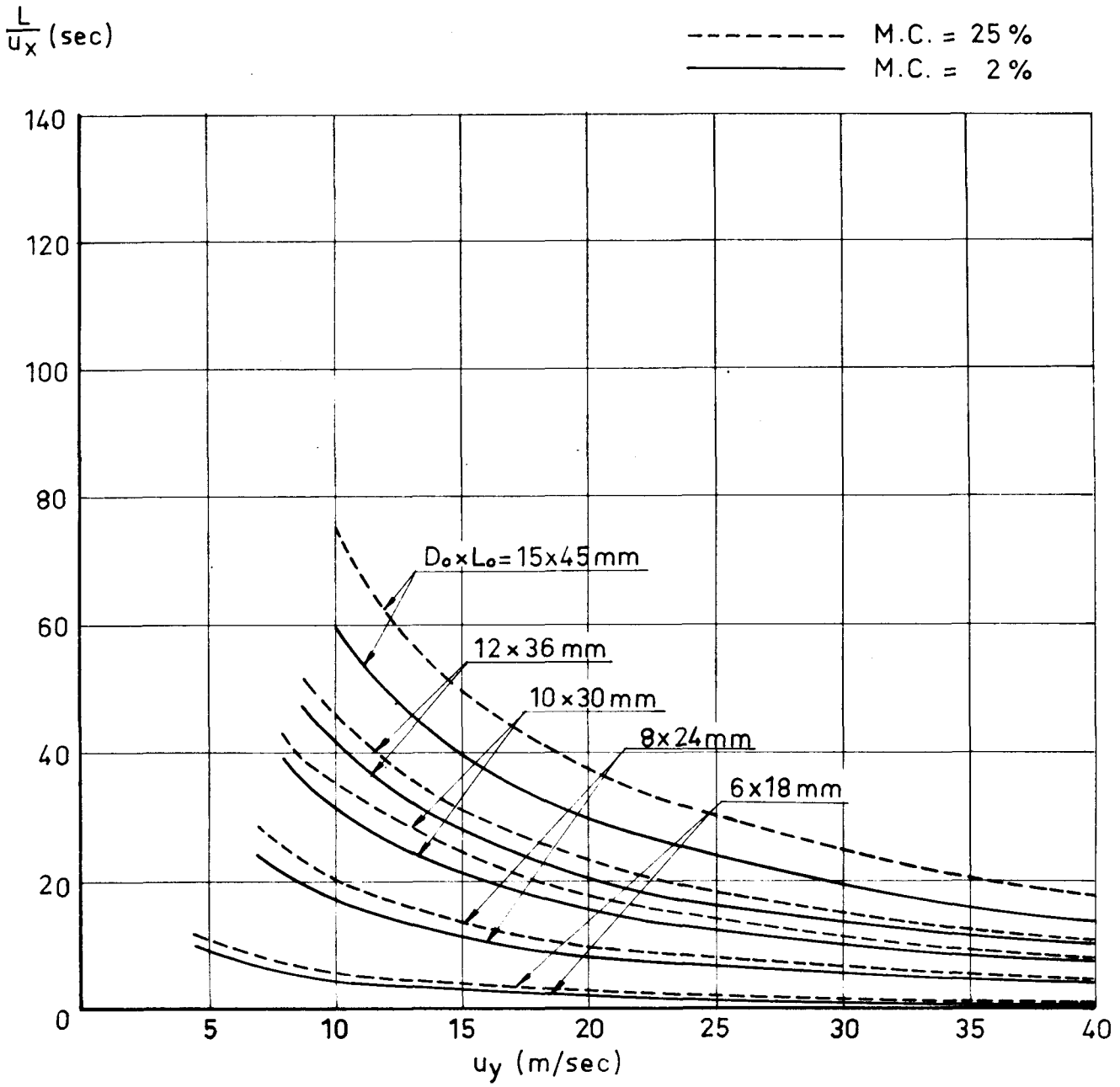

FIG. 24

INCLINED CONVECTION COLUMN
CYLINDERS

BALSA

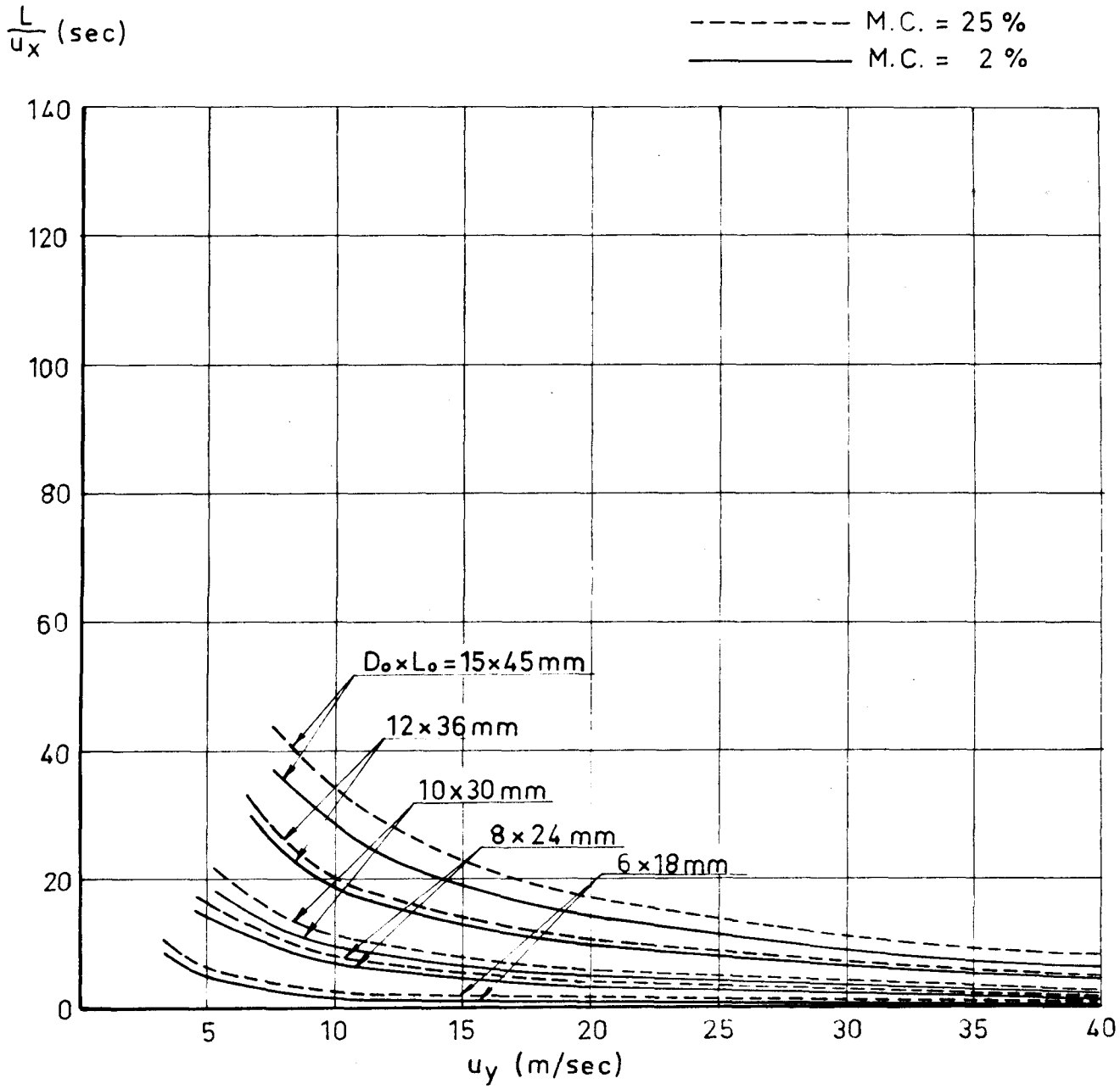

FIG. 25

VELOCITY PROFILES AND RESULTING CONVECTION ZONE

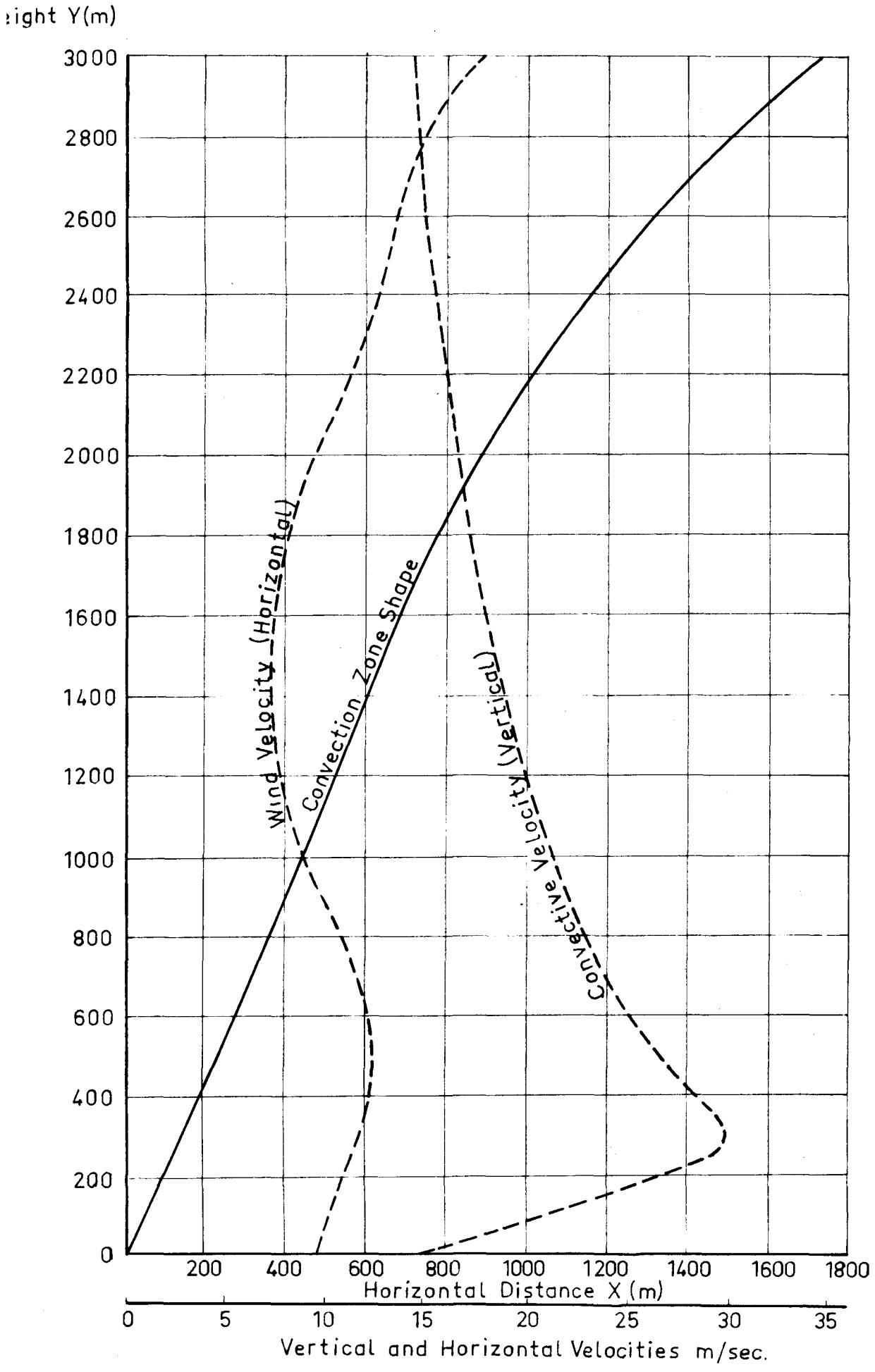

FLIGHT PATHS OF BURNING CYLINDERS

OAK

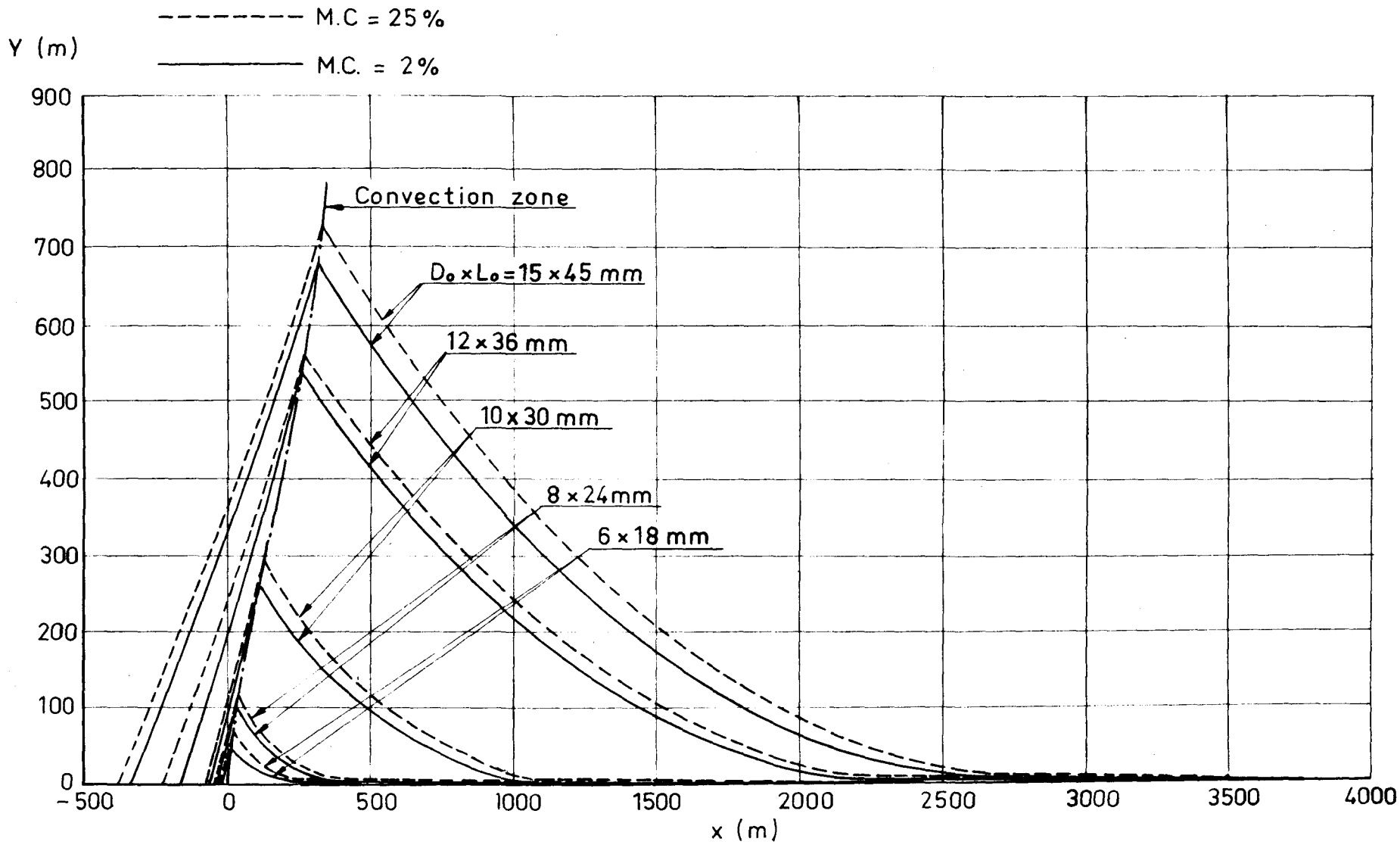

FIG. 26

FLIGHT PATHS OF BURNING CYLINDERS
PINE

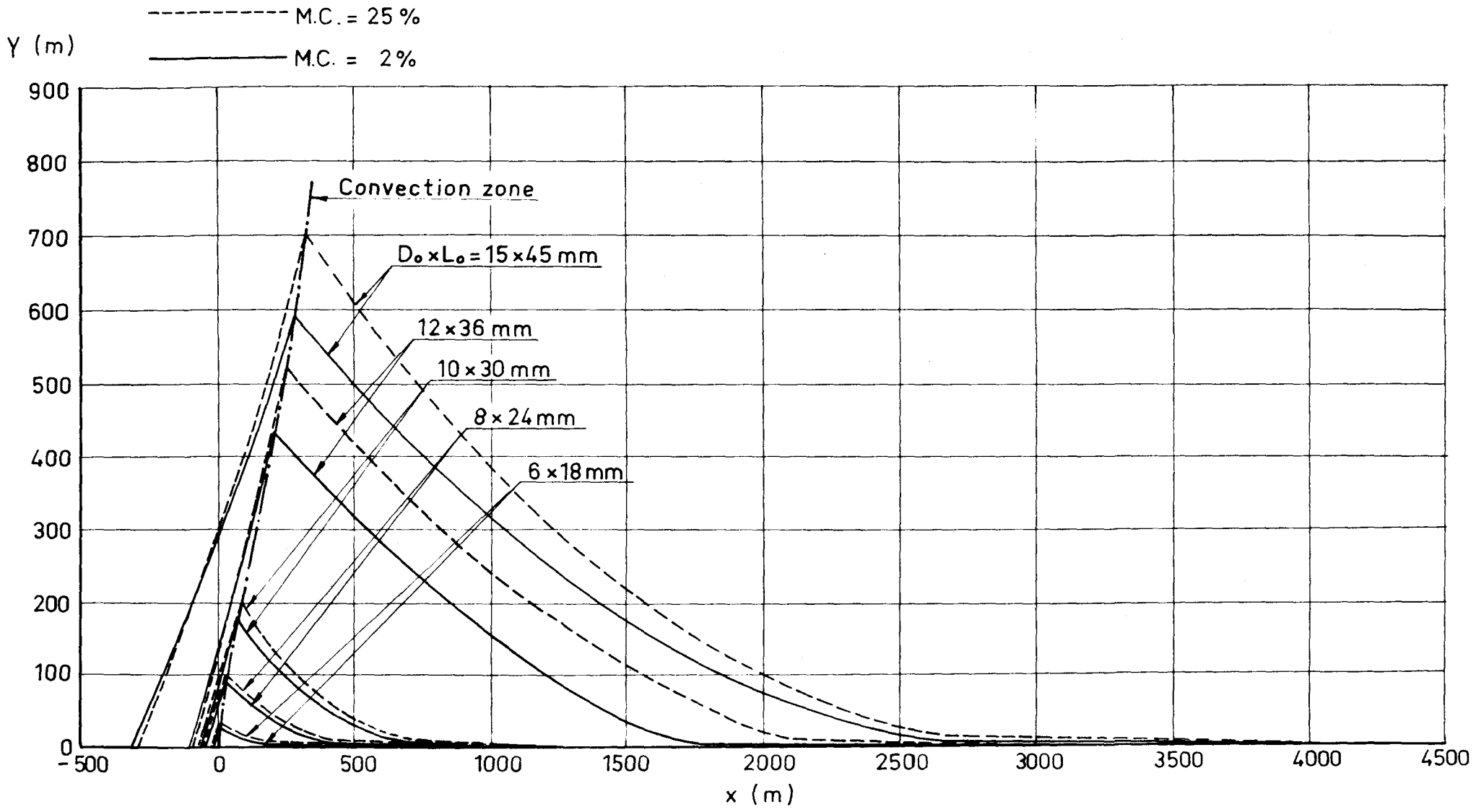

FIG. 27

FLIGHT PATHS OF BURNING CYLINDERS

SPRUCE

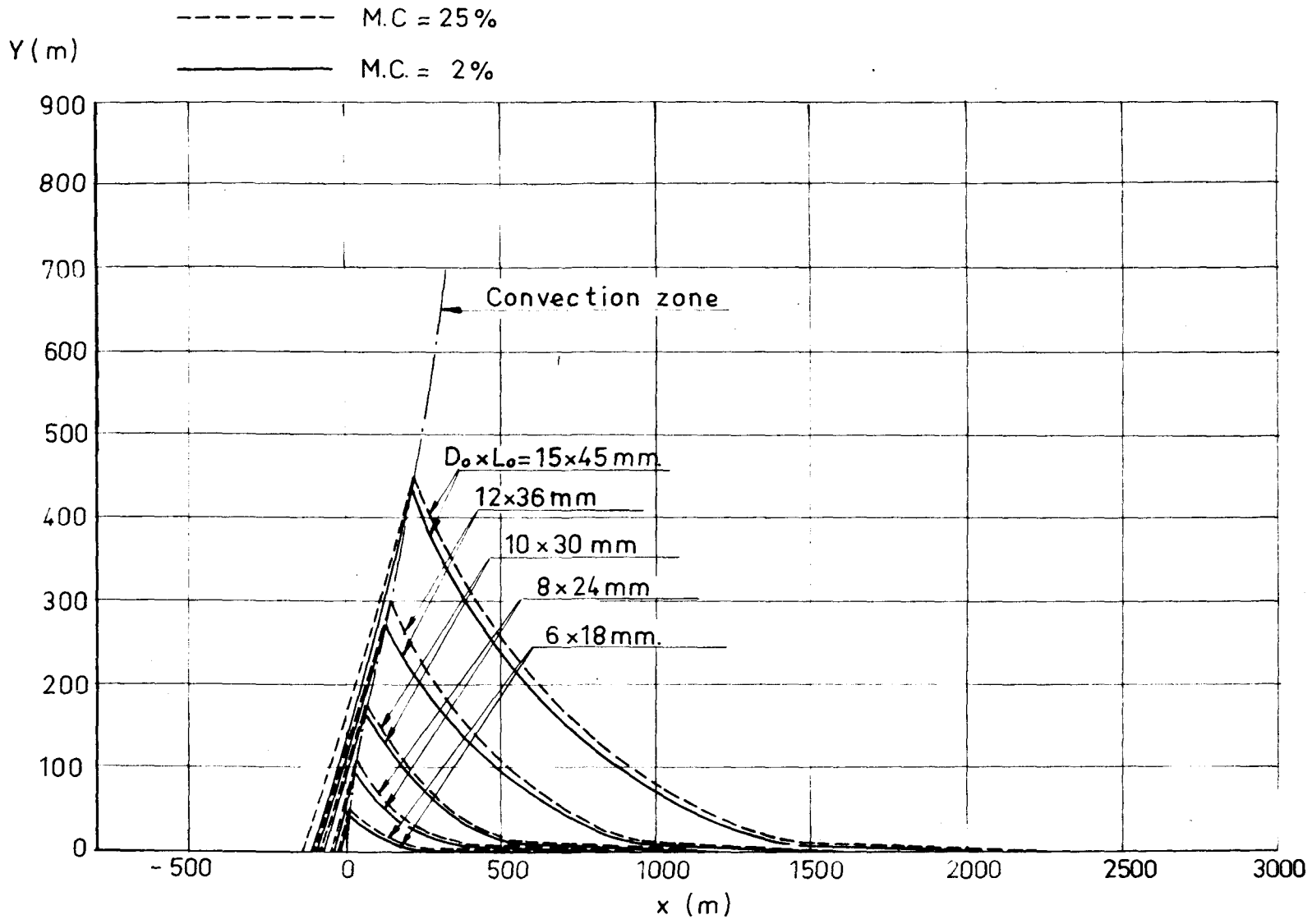

FIG. 28

FLIGHT PATHS OF BURNING CYLINDERS

ASPEN

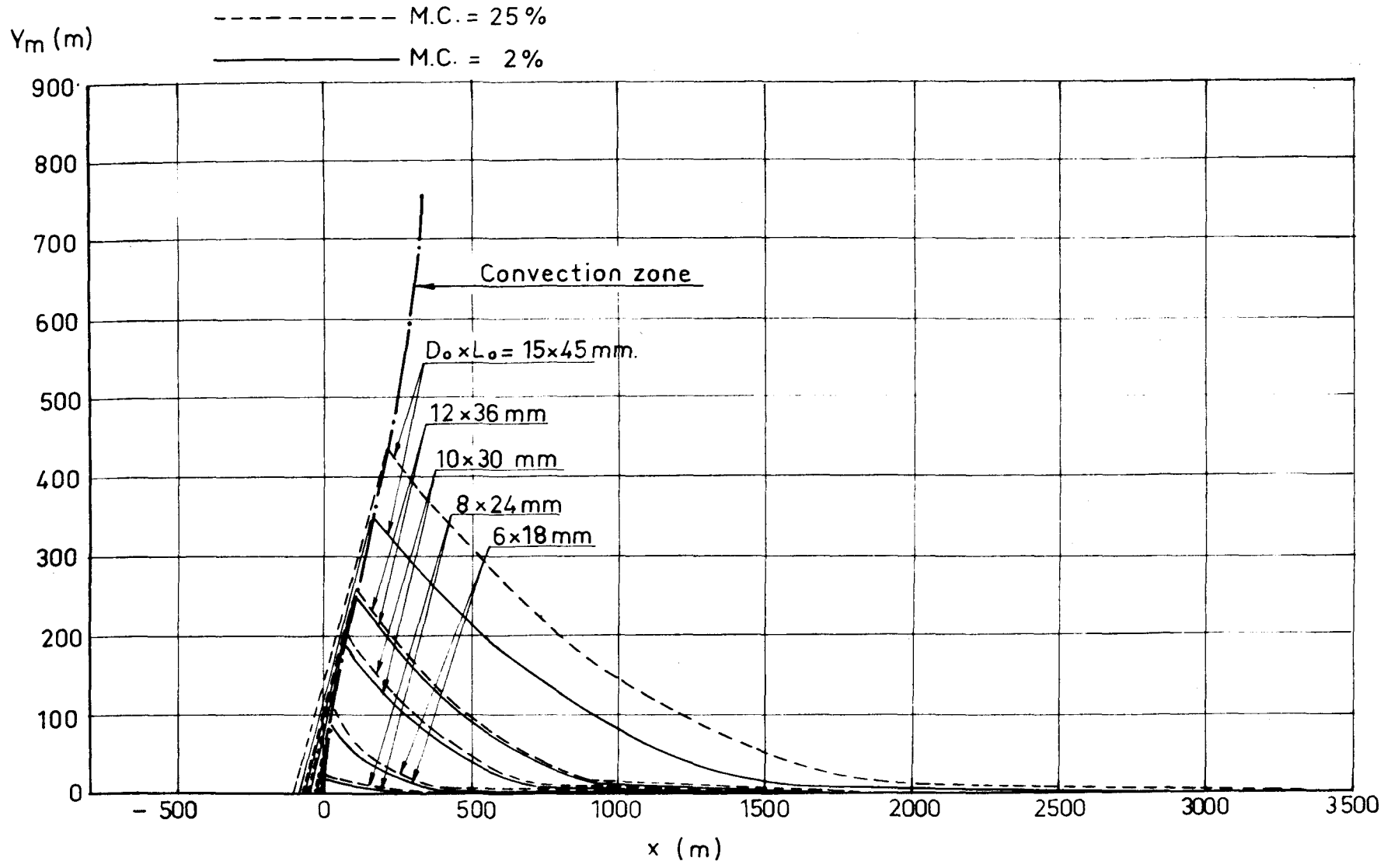

FIG. 29

FIG. 30

FLIGHT PATHS OF BURNING CYLINDERS
BALSA

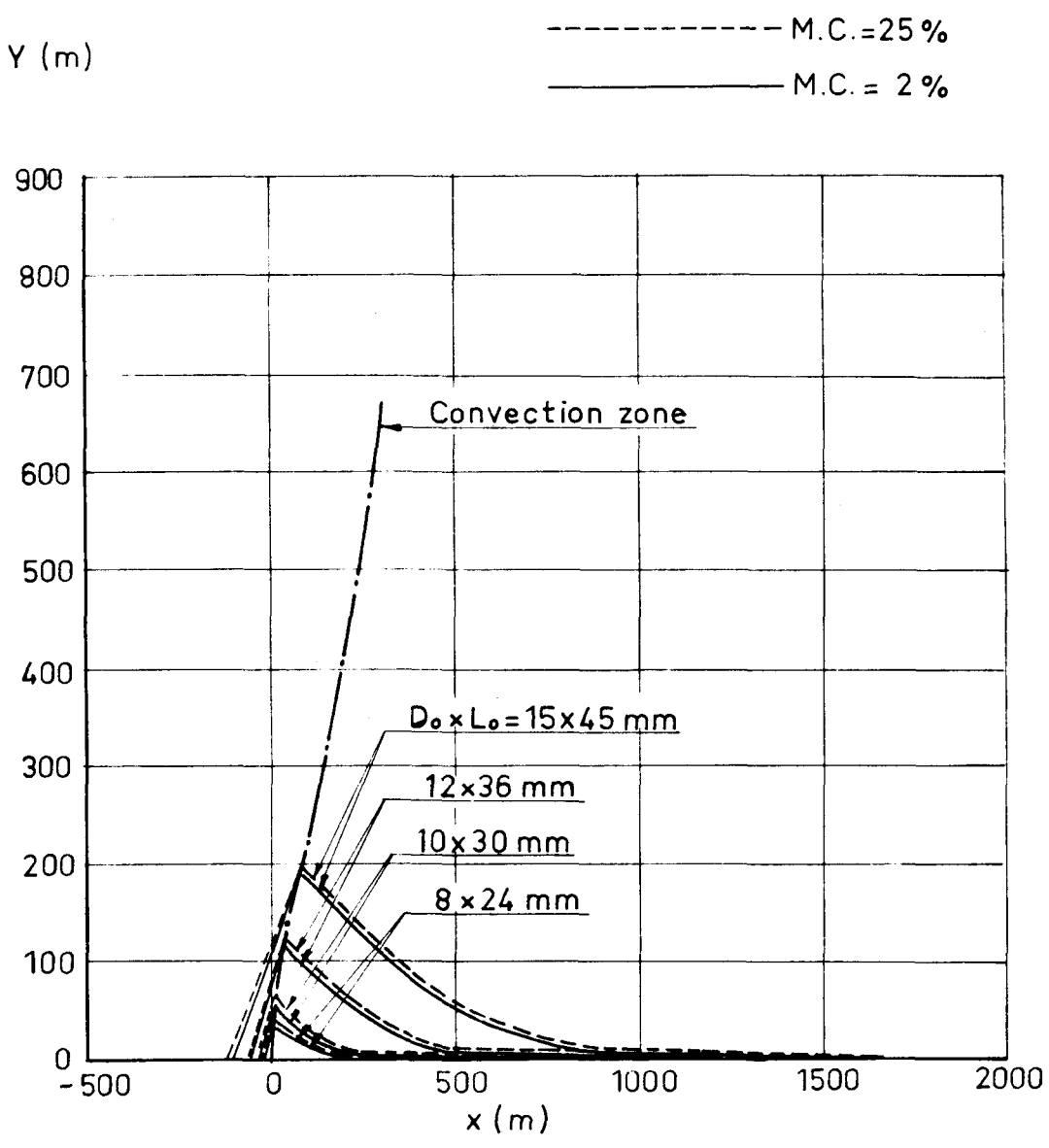

FIG. 31

INCLINED CONVECTION COLUMN
SQUARE PLATES

OAK

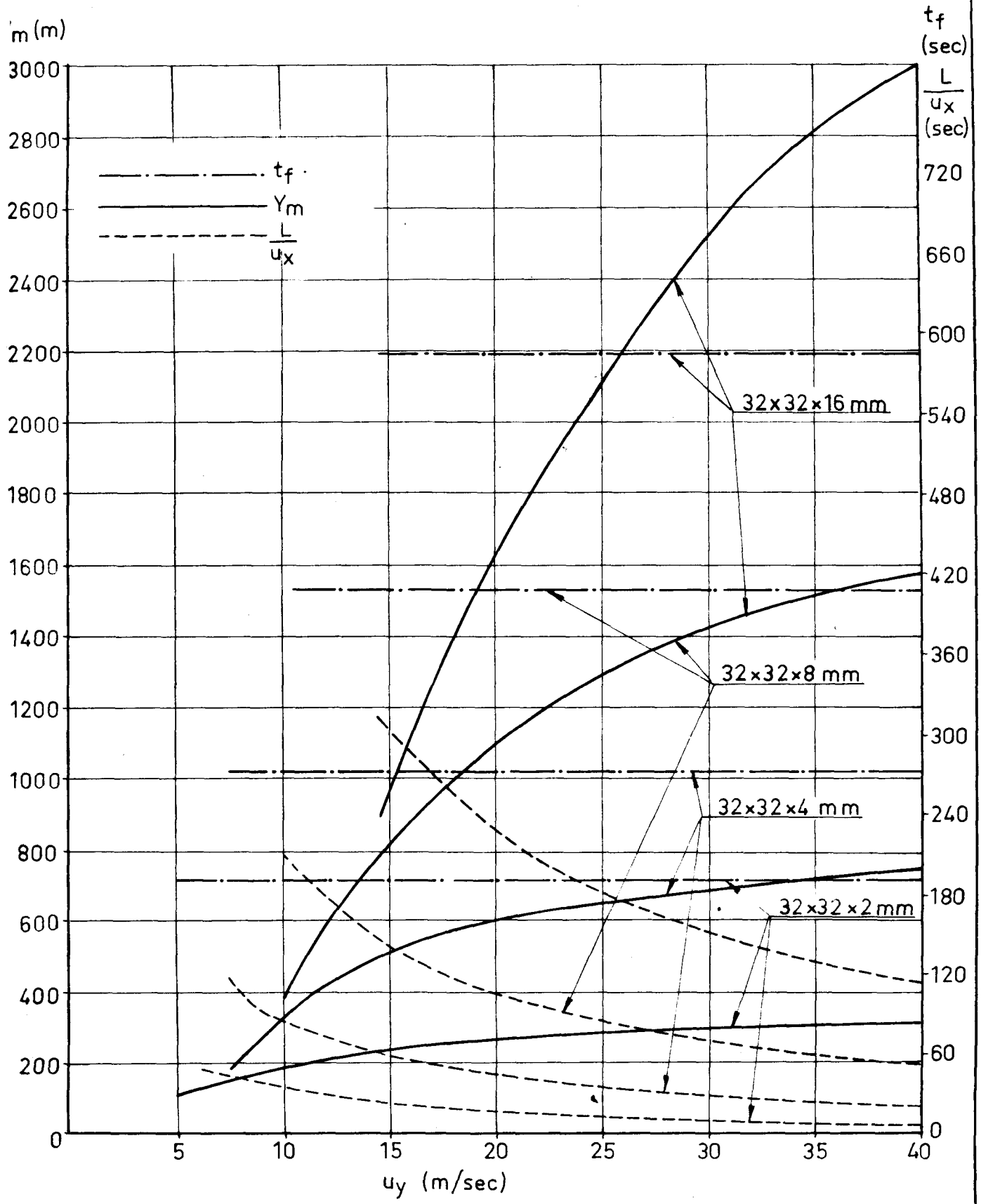

FIG. 32

INCLINED CONVECTION COLUMN
SQUARE PLATES

PINE

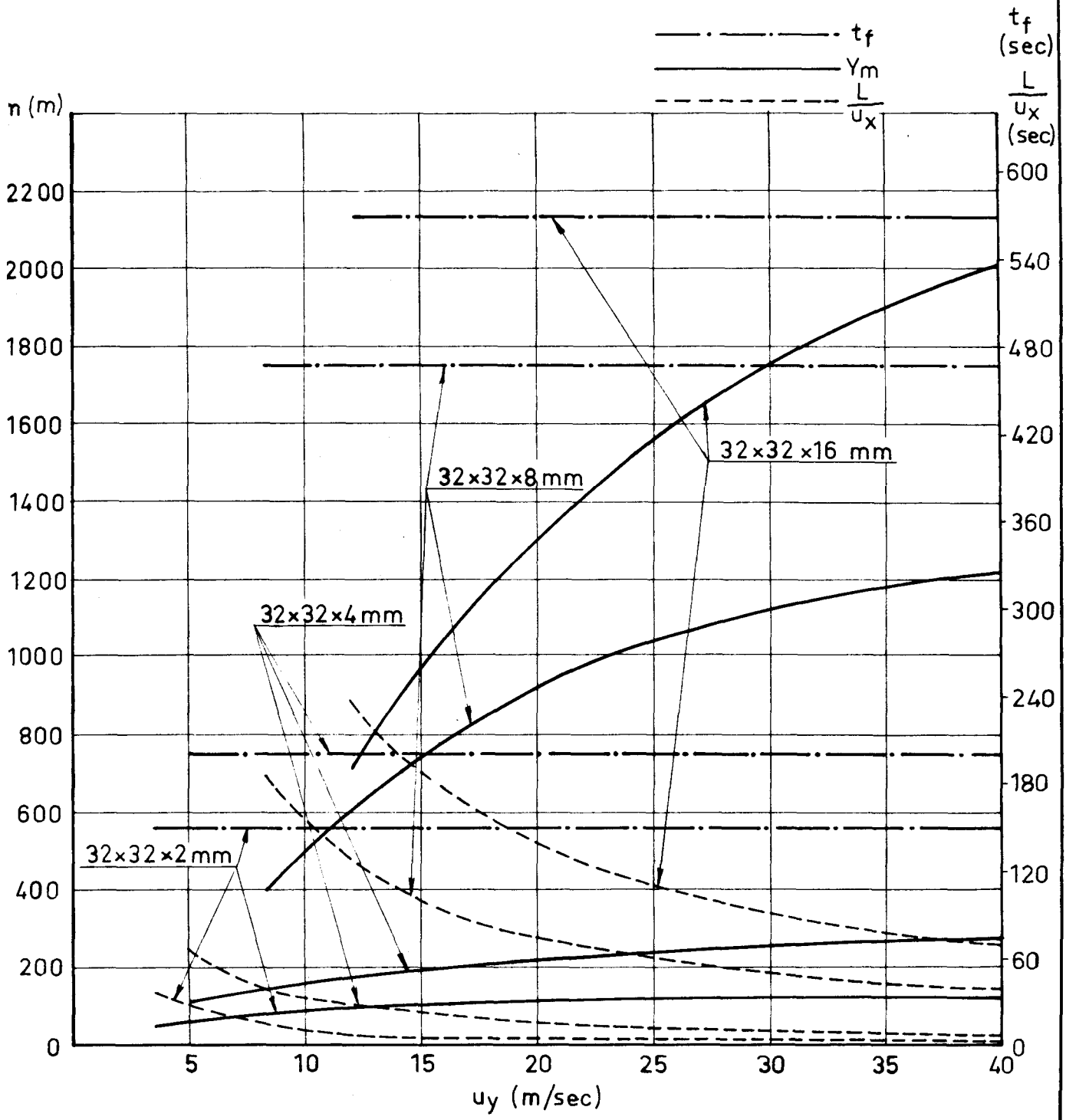

FIG. 33

INCLINED CONVECTION COLUMN
SQUARE PLATES

ASPEN

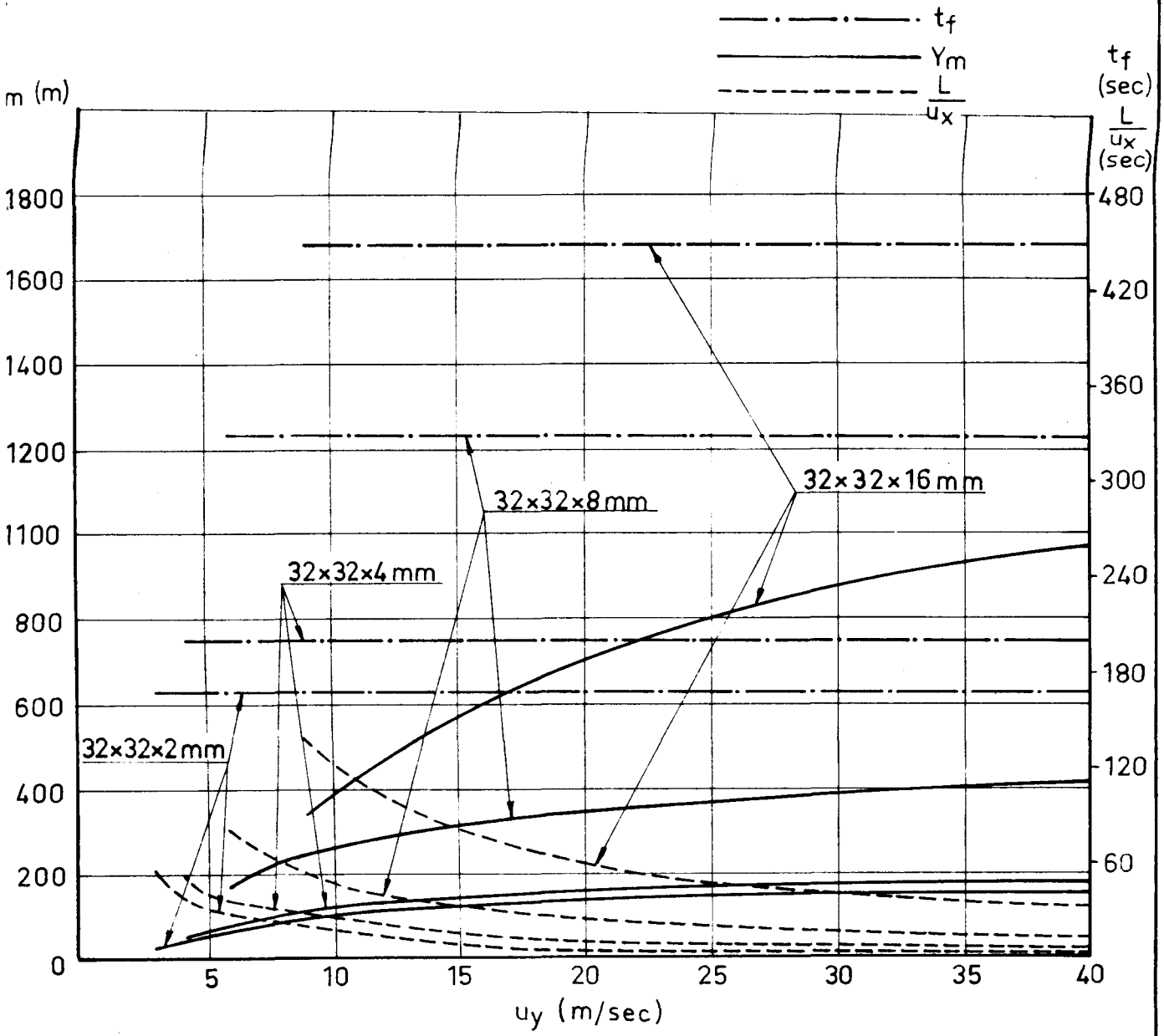

FIG. 34

INCLINED CONVECTION COLUMN
JARE PLATES

BALSA

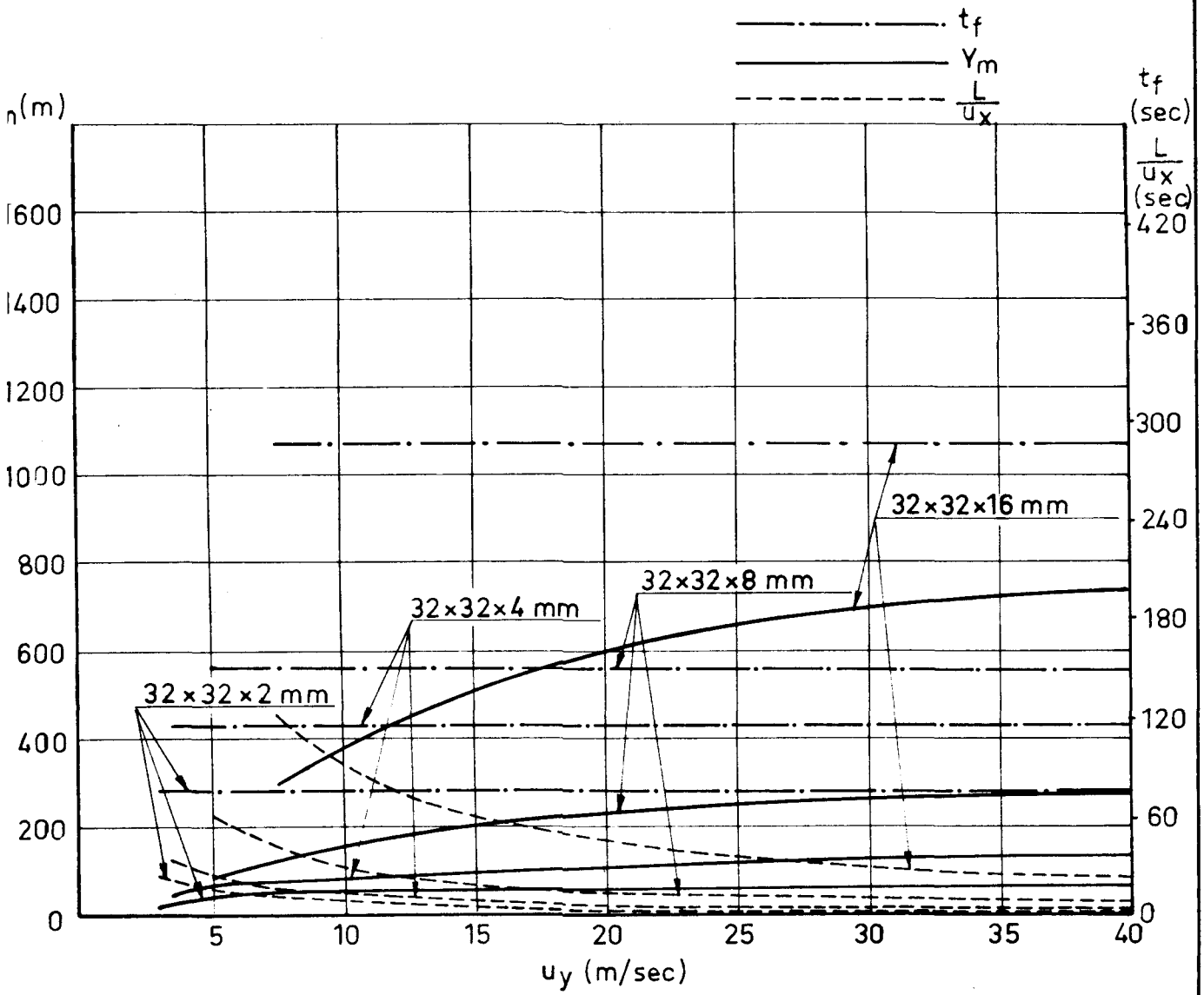

FIG. 35

INCLINED CONVECTION COLUMN
SPHERES

CHARCOAL

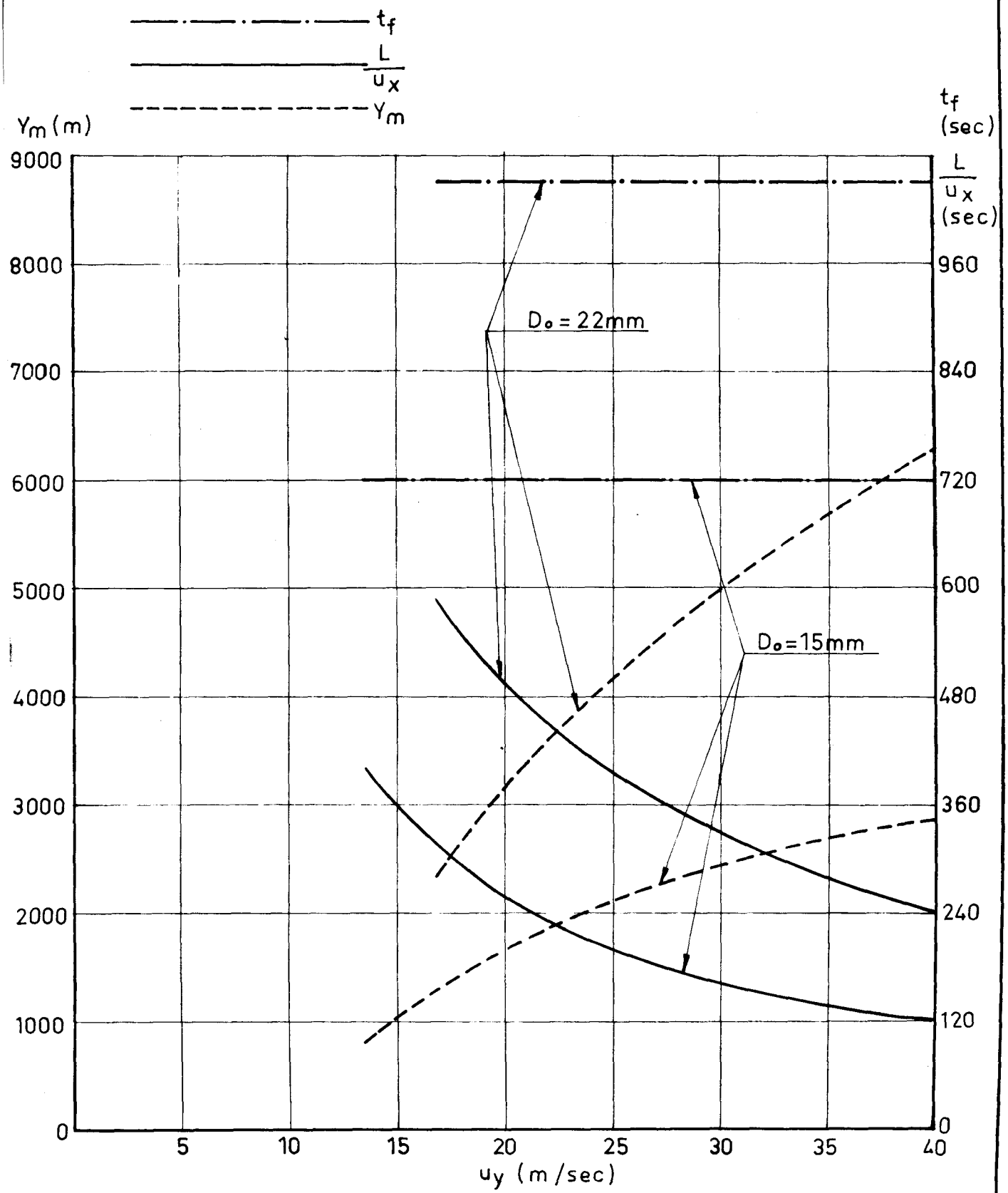

FIG. 36

INCLINED CONVECTION COLUMN
CYLINDERS

CHARCOAL

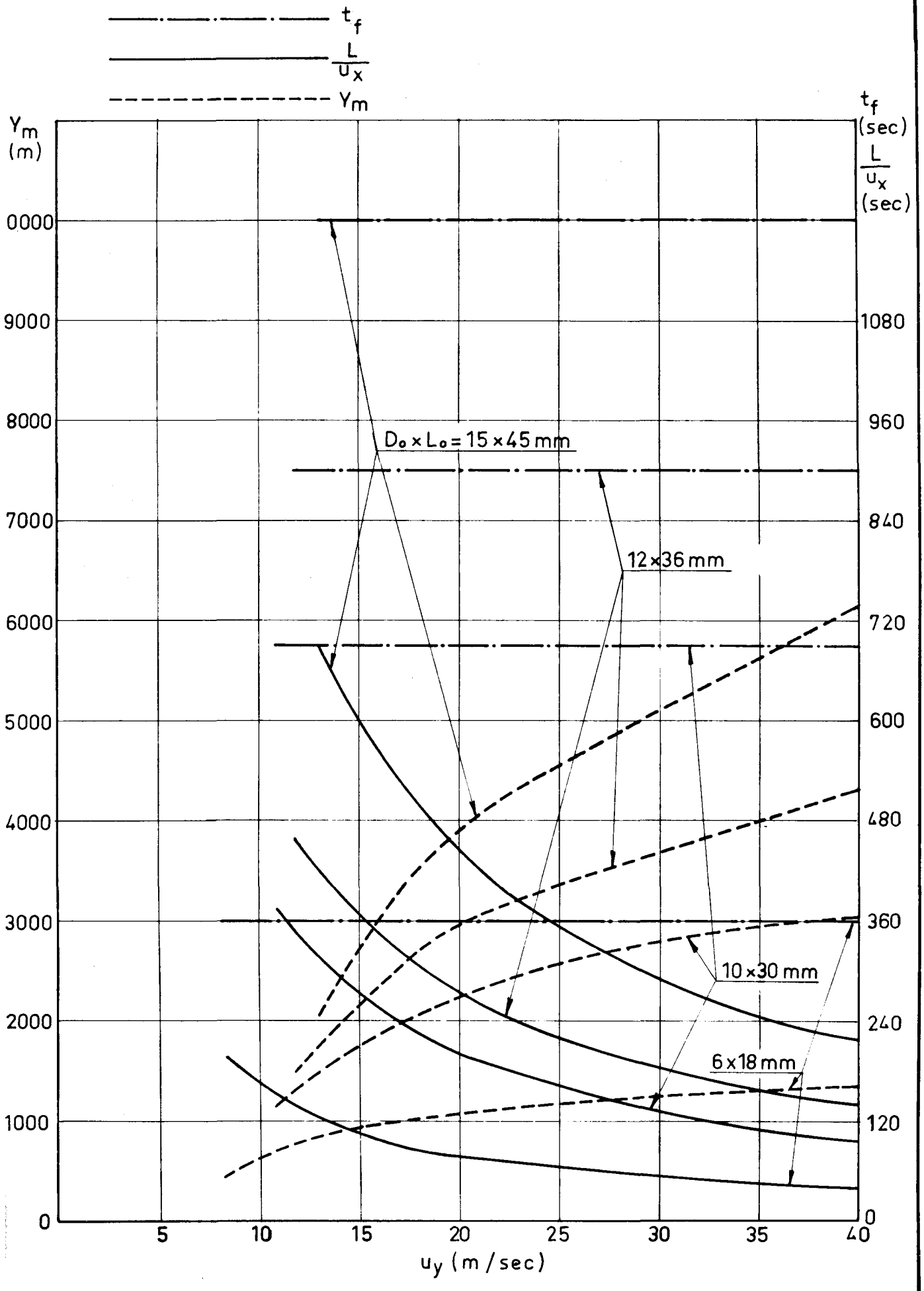

FIG. 37

INCLINED CONVECTION COLUMN
SQUARE PLATES

CHARCOAL

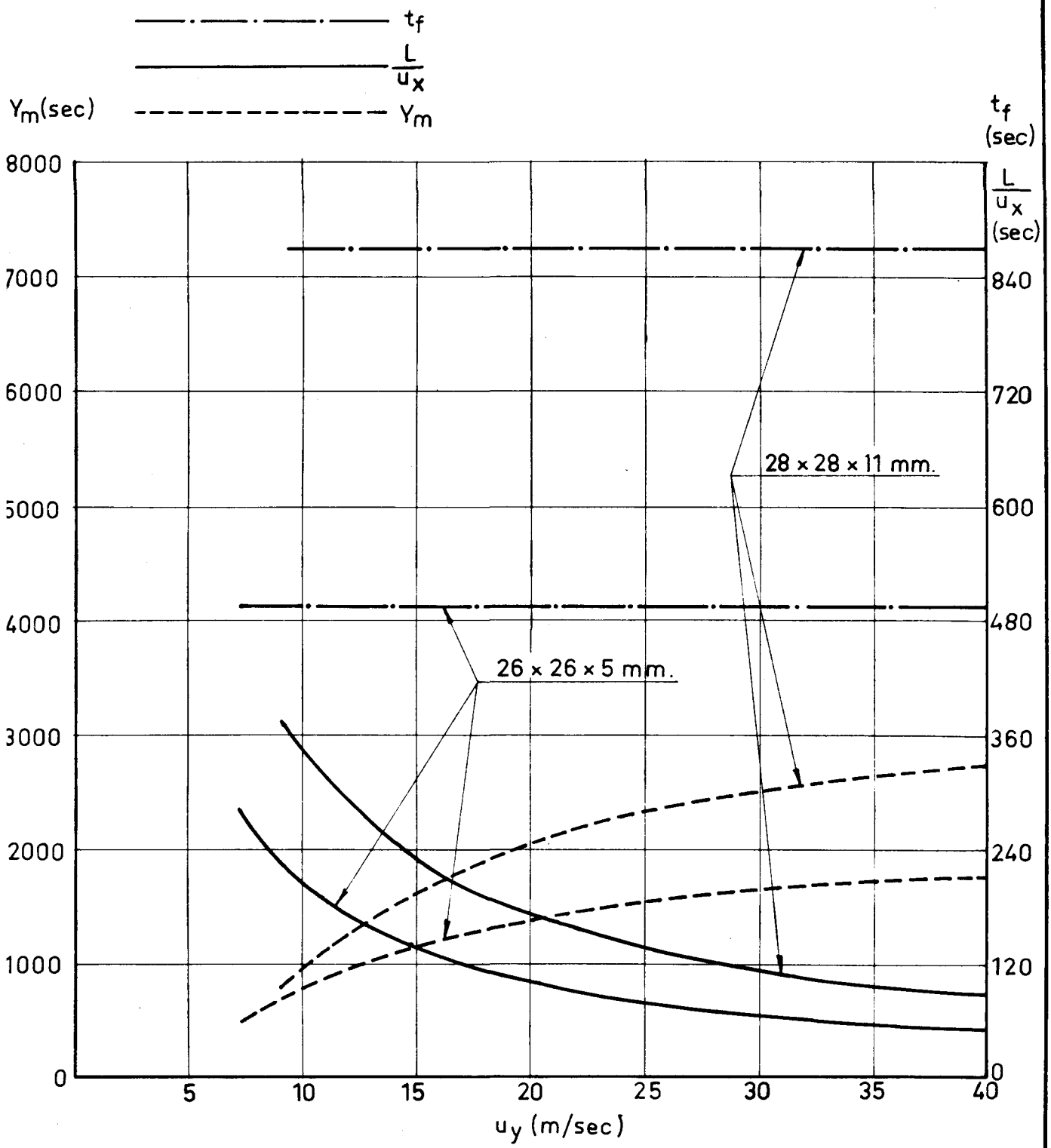

FIG. 38

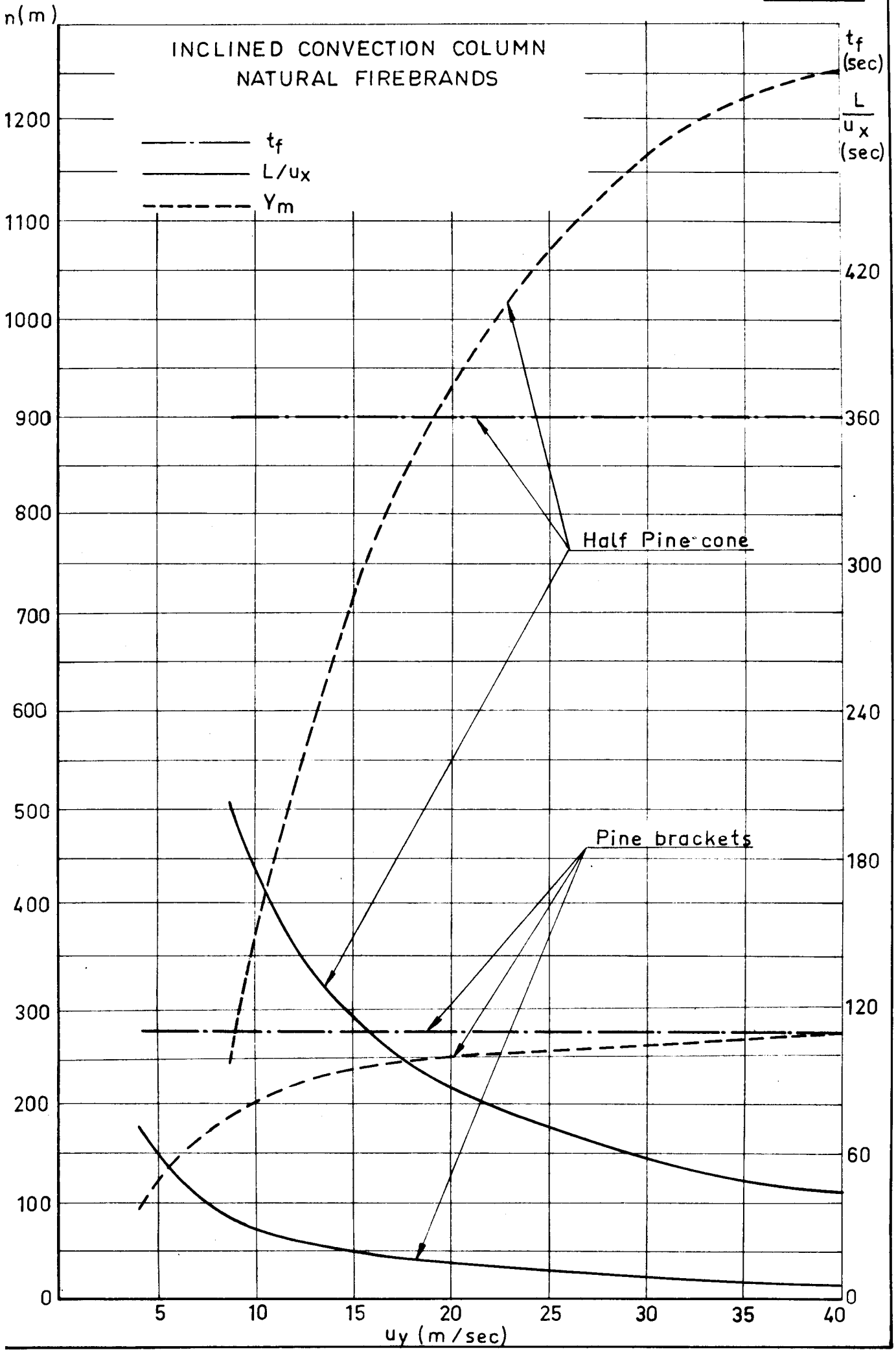
n(m)
INCLINED CONVECTION COLUMN
NATURAL FIREBRANDS
t_f
L/u_x
Y_m
t_f (sec)
$\frac{L}{u_x}$ (sec)
Half Pine cone
Pine brackets
1200
1100
1000
900
800
700
600
500
400
300
200
100
0
420
360
300
240
180
120
60
0
5
10
15
20
25
30
35
40
uy (m/sec)

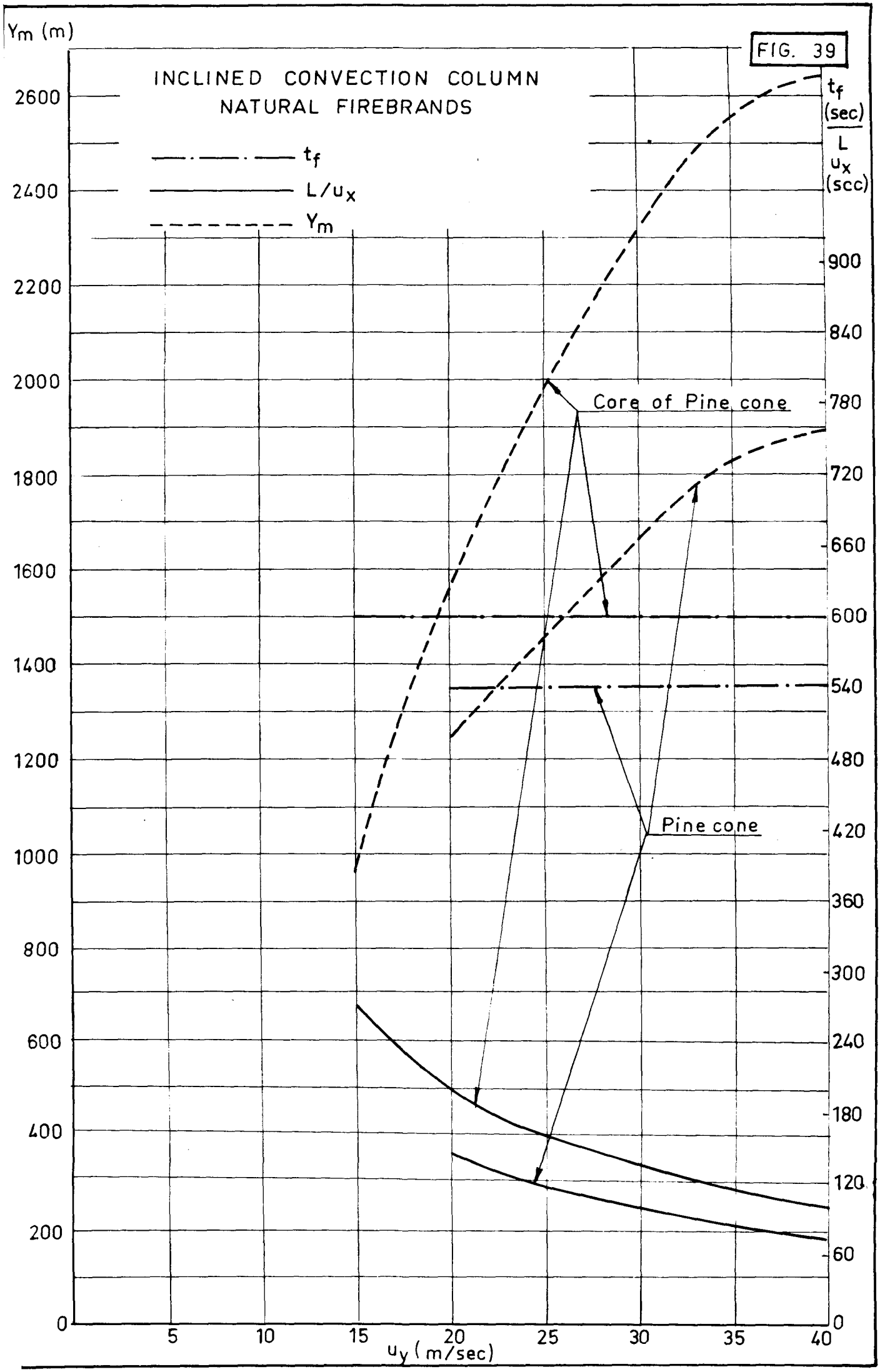
FIG. 39
INCLINED CONVECTION COLUMN
NATURAL FIREBRANDS
t_f
L/u_x
Y_m
Y_m (m)
t_f (sec)
$\frac{L}{u_x}$ (scc)
Core of Pine cone
Pine cone
u_y (m/sec)
0
200
400
600
800
1000
1200
1400
1600
1800
2000
2200
2400
2600
60
120
180
240
300
360
420
480
540
600
660
720
780
840
900
5
10
15
20
25
30
35
40

DIMENSIONLESS TERMINAL VELOCITY V.S. TIME

CYLINDERS

OAK

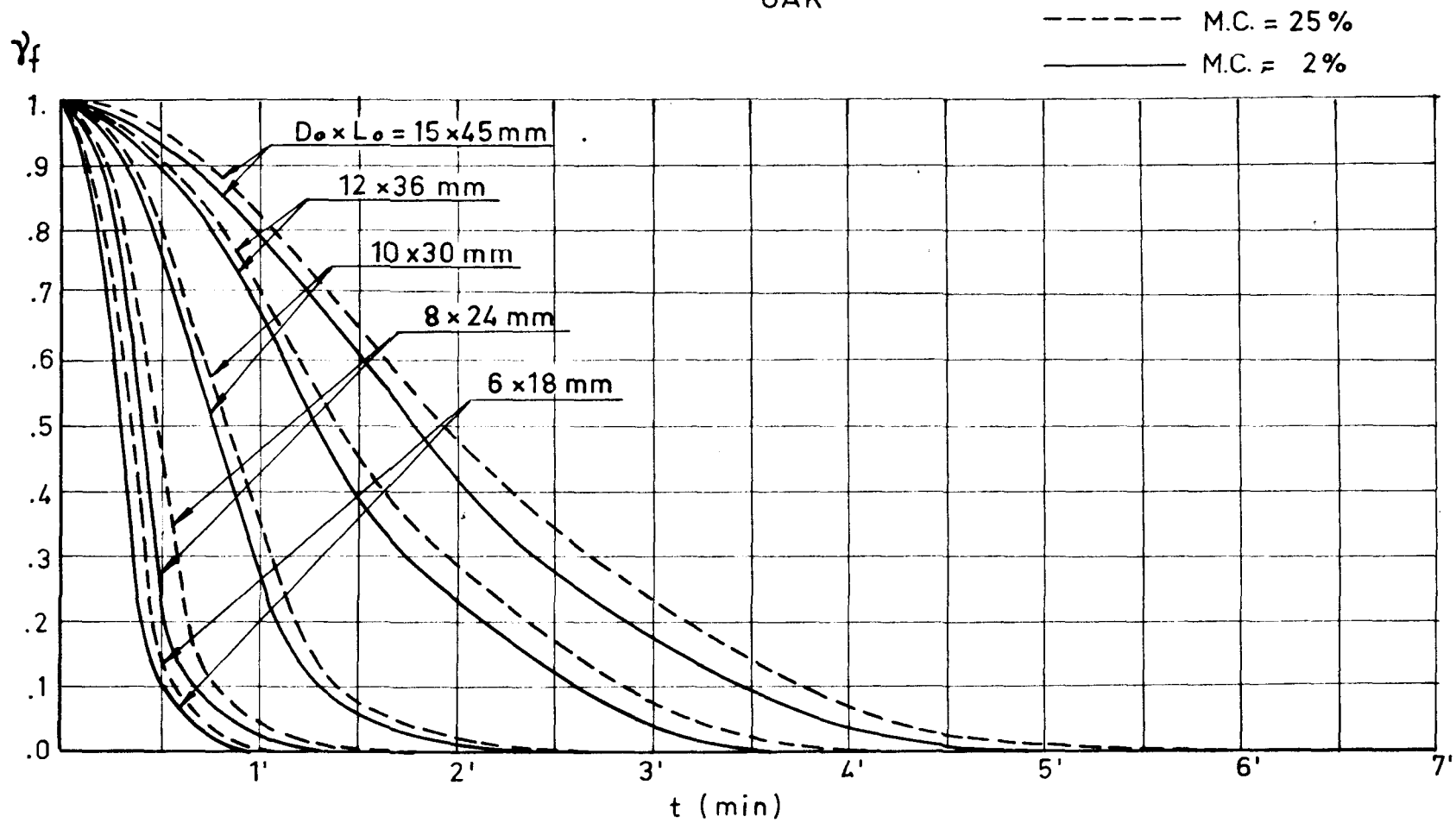

FIG. 40

FIG. 41

DIMENSIONLESS TERMINAL VELOCITY V.S. DIMENSIONLESS TIME

CYLINDERS

OAK

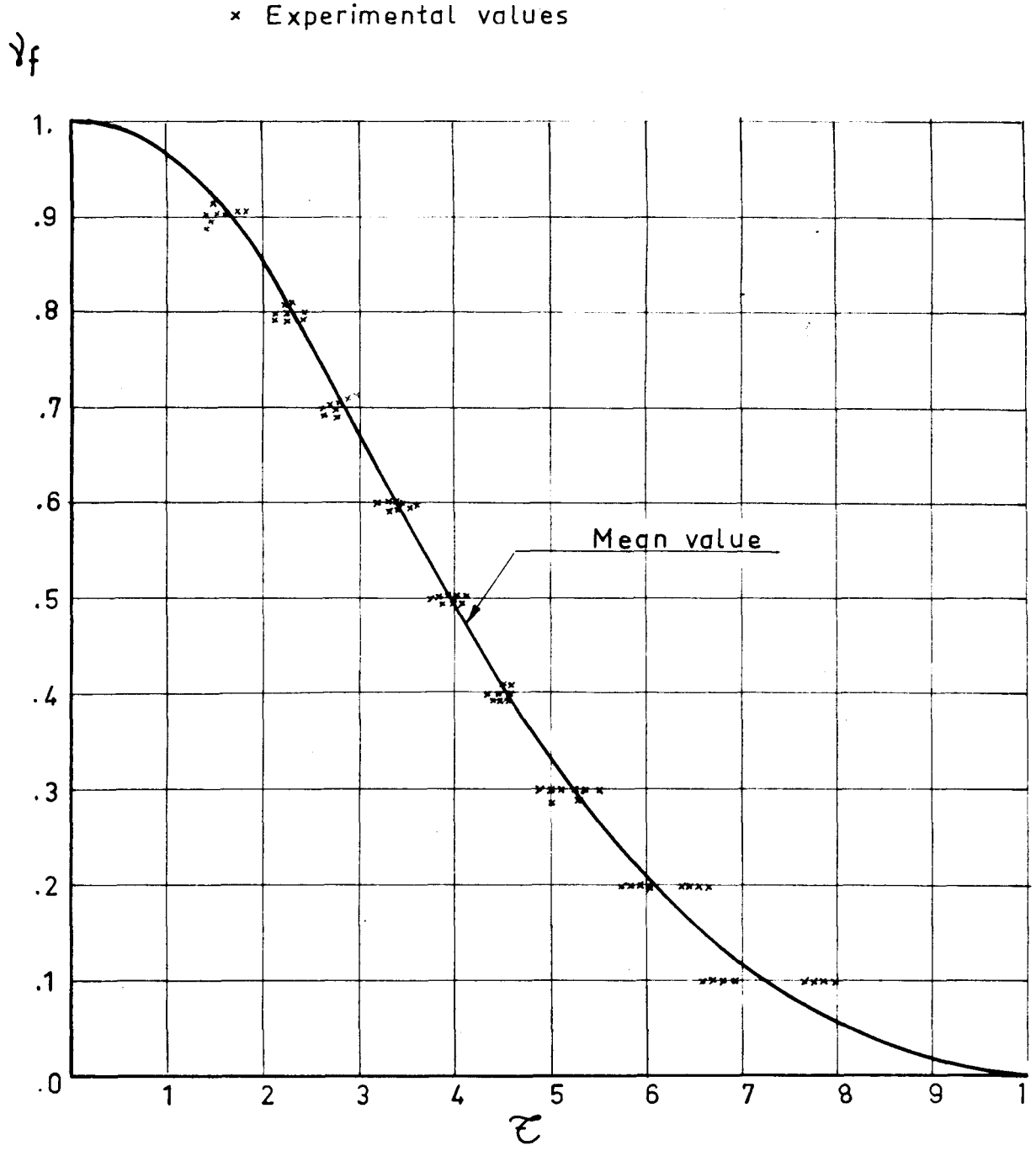

FIG. 42

FIREBRAND DIMENSIONLESS TERMINAL VELOCITY V.S. DIMENSIONLESS TIME

SPHERES

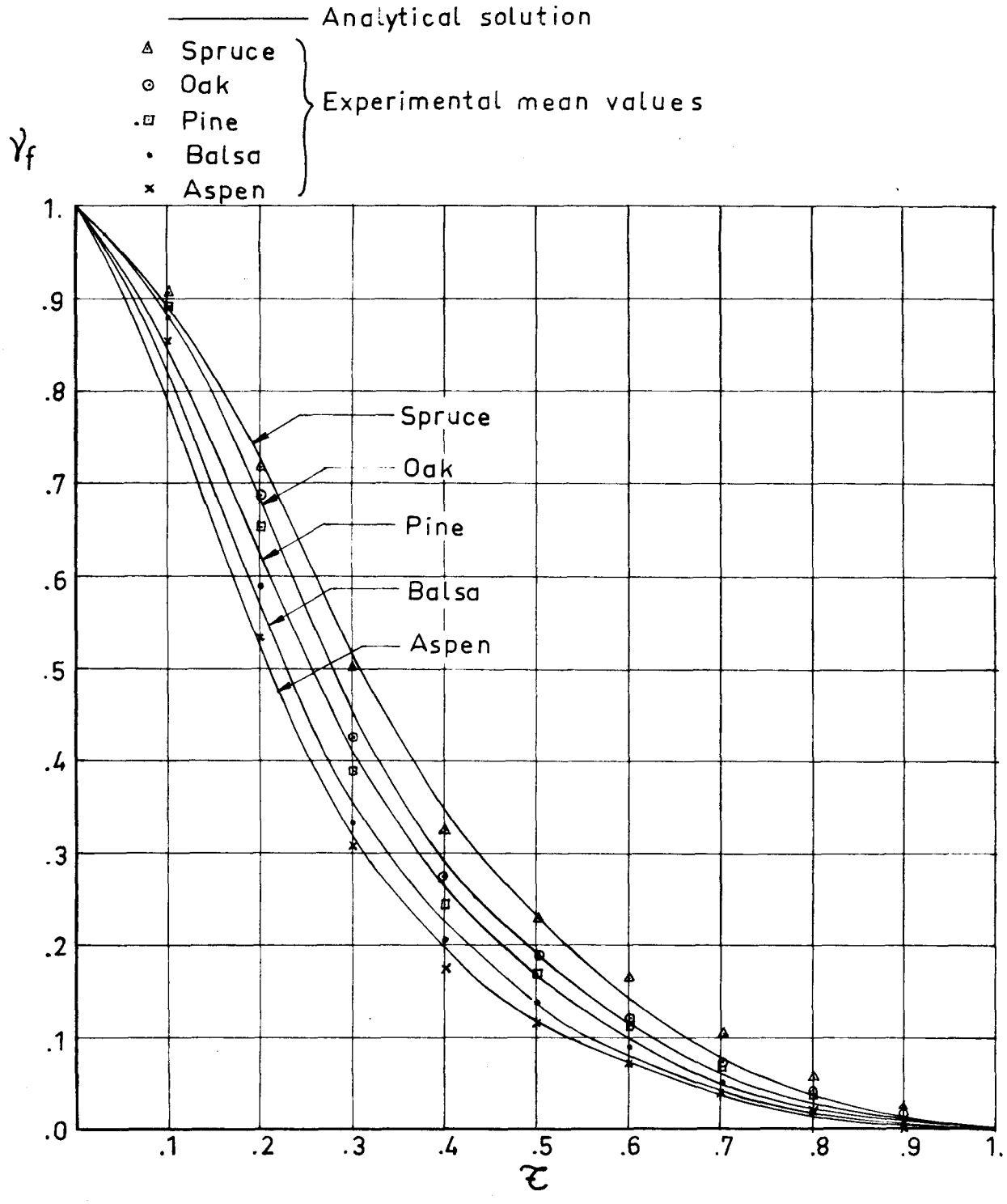

FIG. 43

FIREBRAND DIMENSIONLESS TERMINAL VELOCITY V.S. DIMENSIONLESS TIME

CYLINDERS

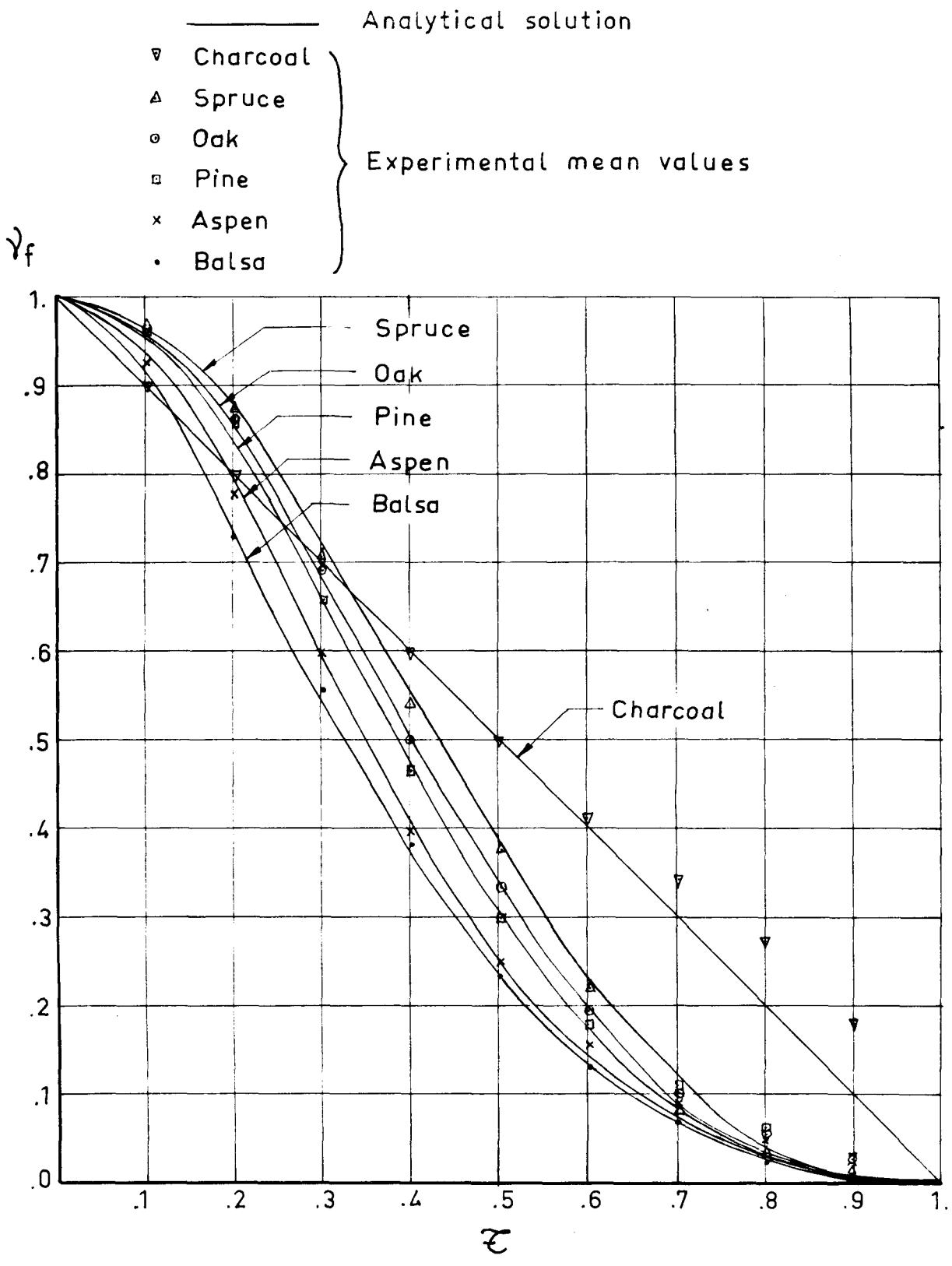

FIG. 44

FIREBRAND DIMENSIONLESS TERMINAL VELOCITY V.S. DIMENSIONLESS TIME

SQUARE PLATES

OAK

——— Analytical solution

• 32 × 32 × 16
⊙ 32 × 32 × 8
× 32 × 32 × 4
⊡ 32 × 32 × 2
} Experimental mean values

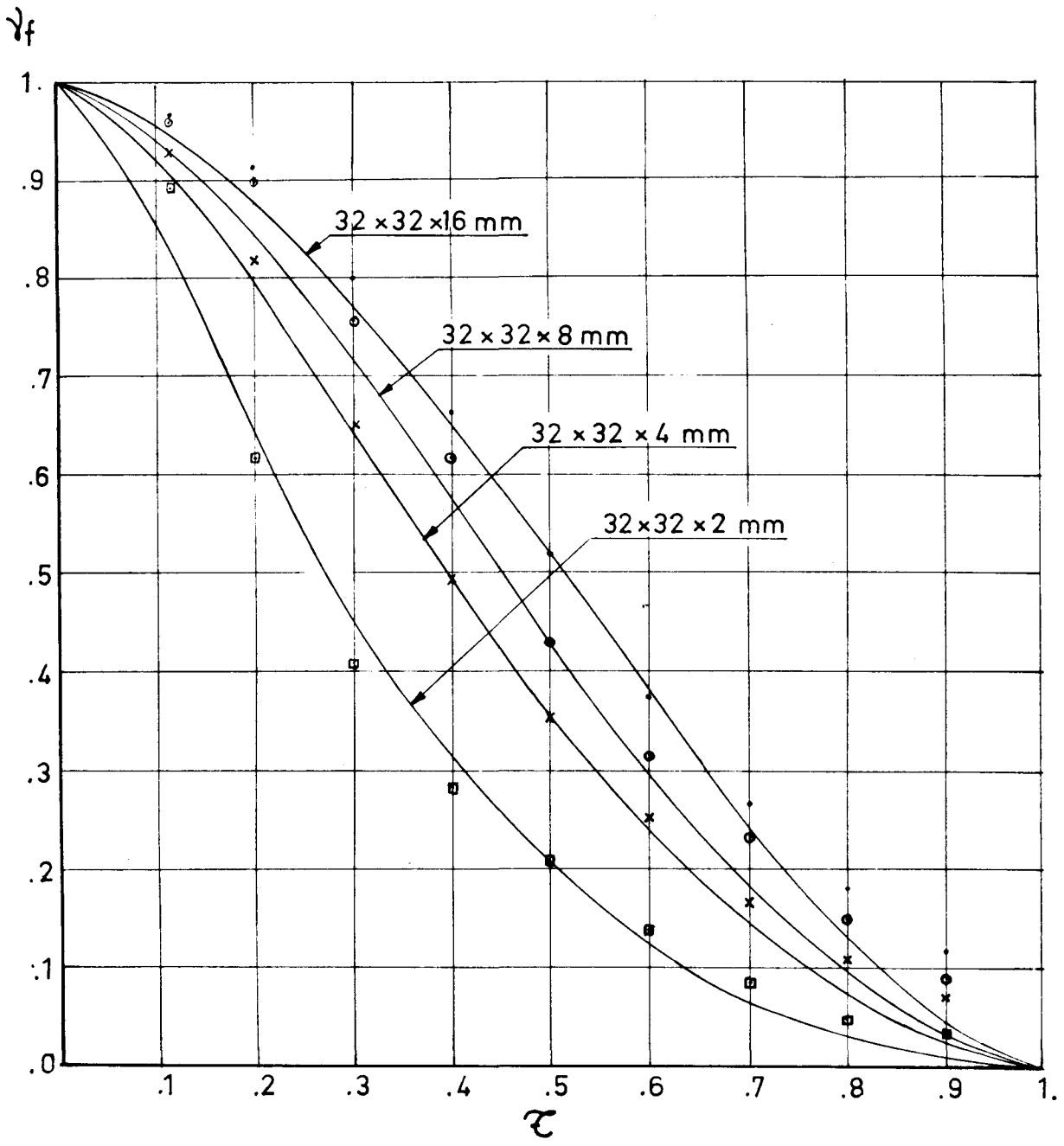

FIG. 45

FIREBRAND DIMENSIONLESS TERMINAL VELOCITY V.S. DIMENSIONLESS TIME

SQUARES PLATE

PINE

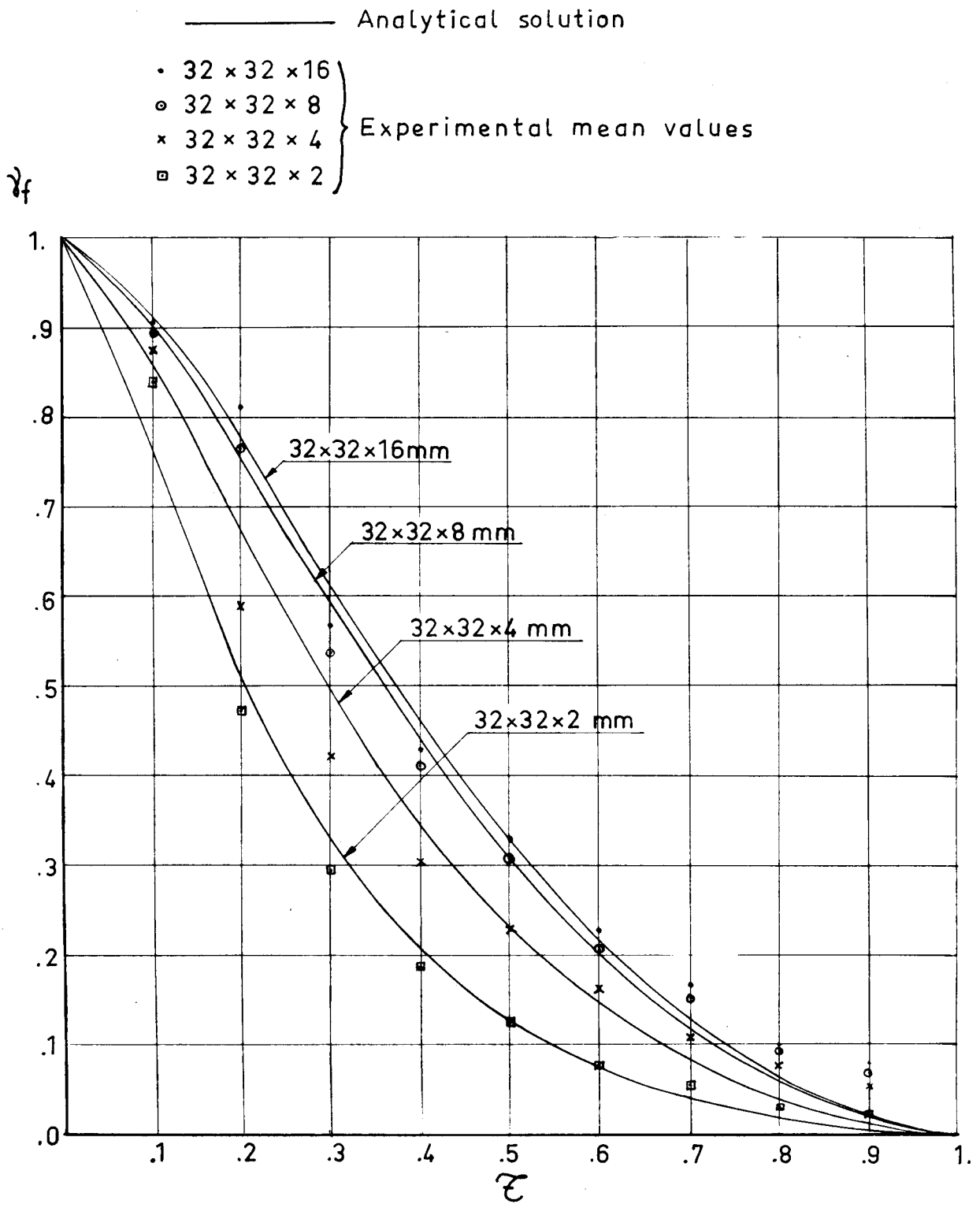

FIG. 46

FIREBRAND DIMENSIONLESS TERMINAL VELOCITY V.S. DIMENSIONLESS TIME

SQUARE PLATES

ASPEN

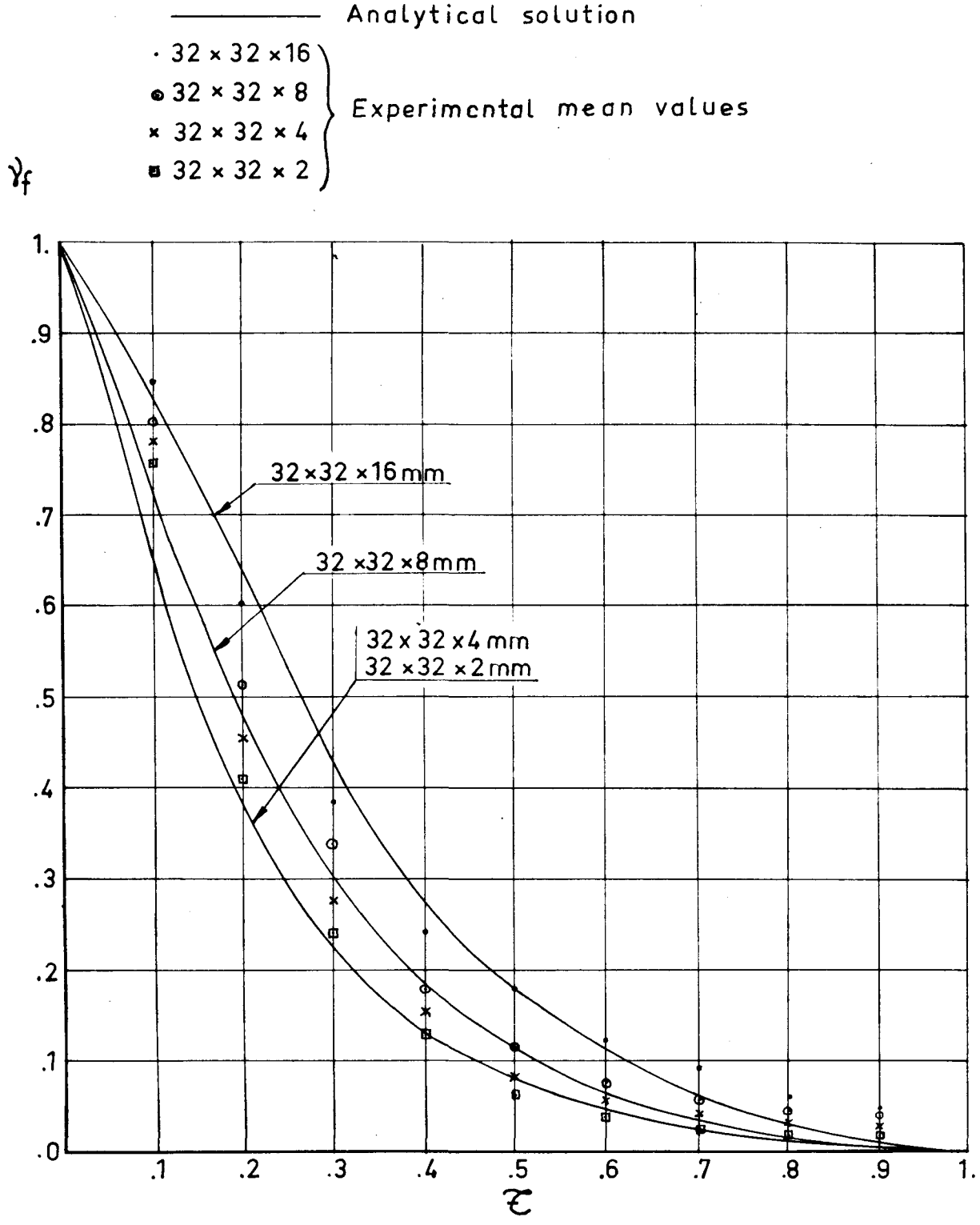

FIG. 47

FIREBRAND DIMENSIONLESS TERMINAL VELOCITY V.S. DIMENSIONLESS TIME

SQUARE PLATES

BALSA

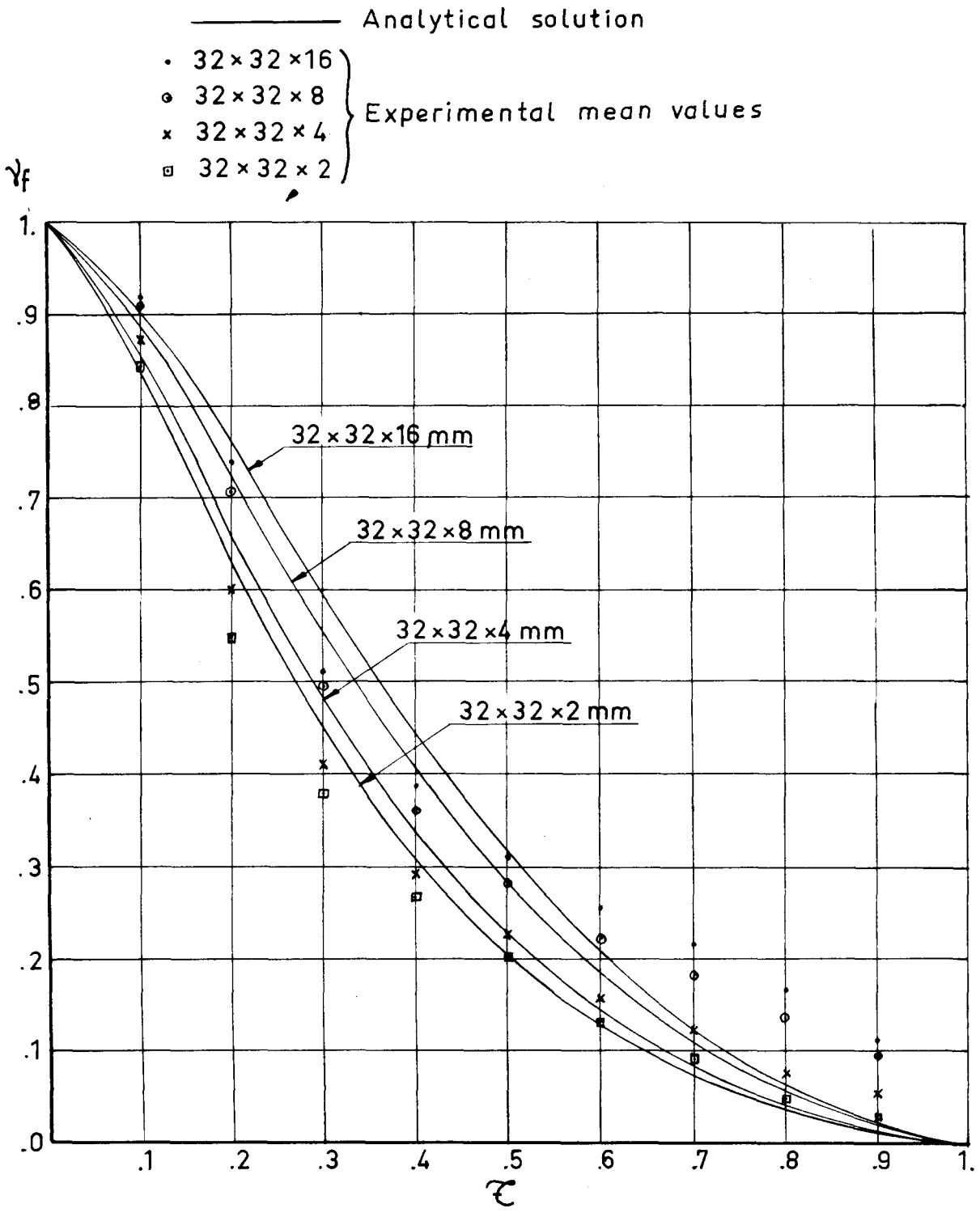

FIG. 48

BURN-OUT TIME V.S. WOOD DENSITY

SPHERES

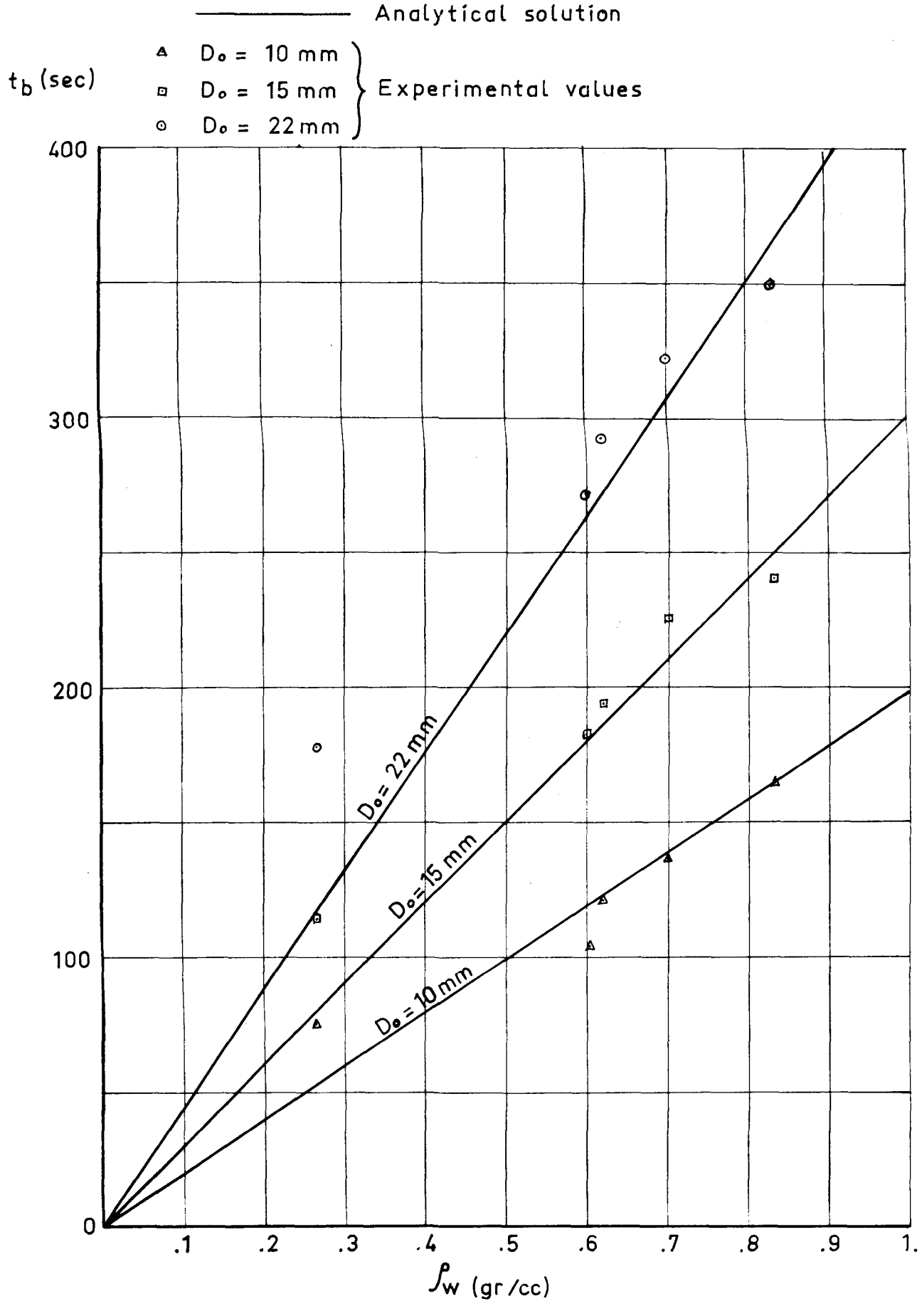

FIG. 49

BURN-OUT TIME V.S. WOOD DENSITY
CYLINDERS LENGTH/DIAMETER RATIO = 3

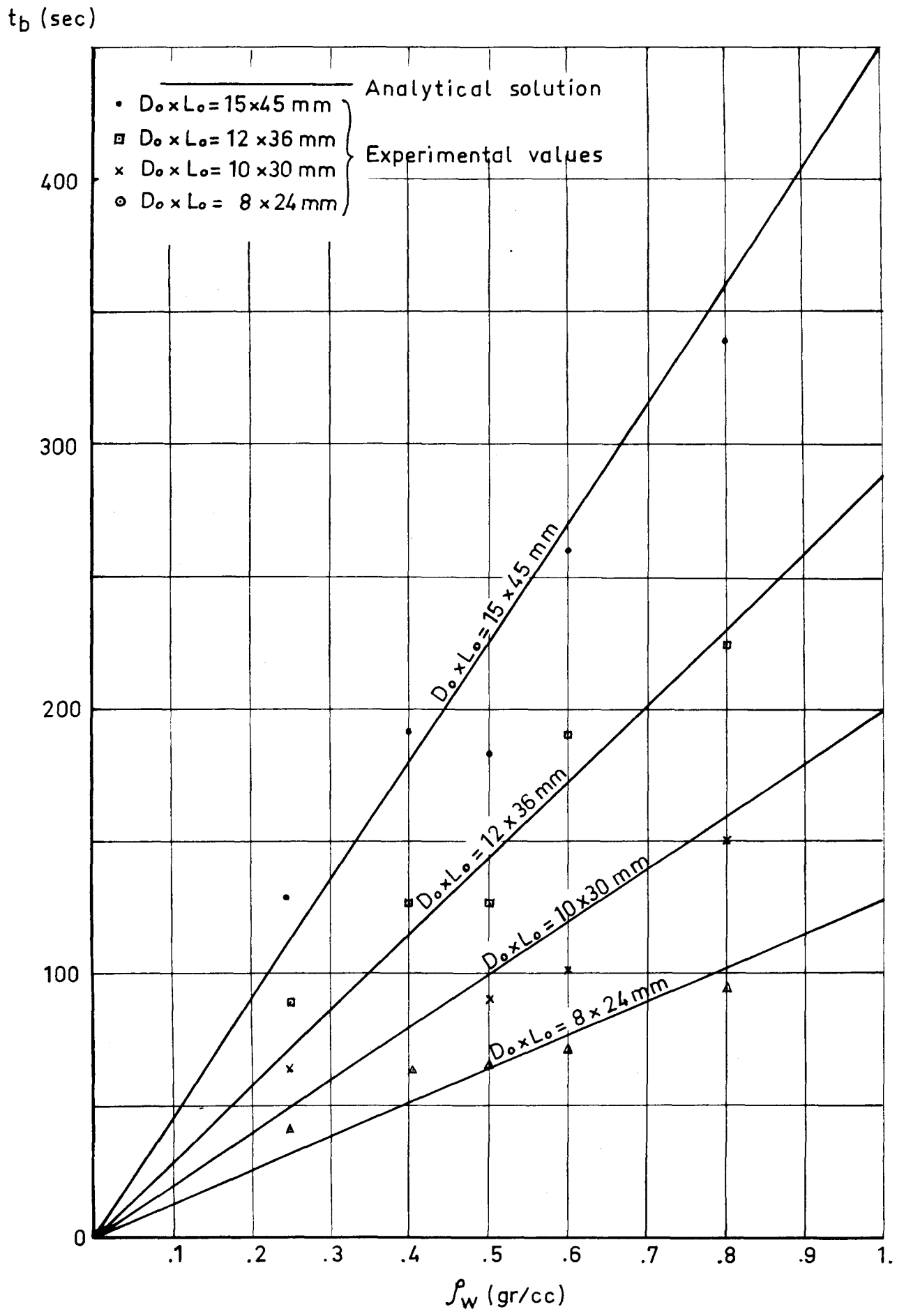

FIG. 50

BURN-OUT TIME V.S. WOOD DENSITY
SQUARE PLATES

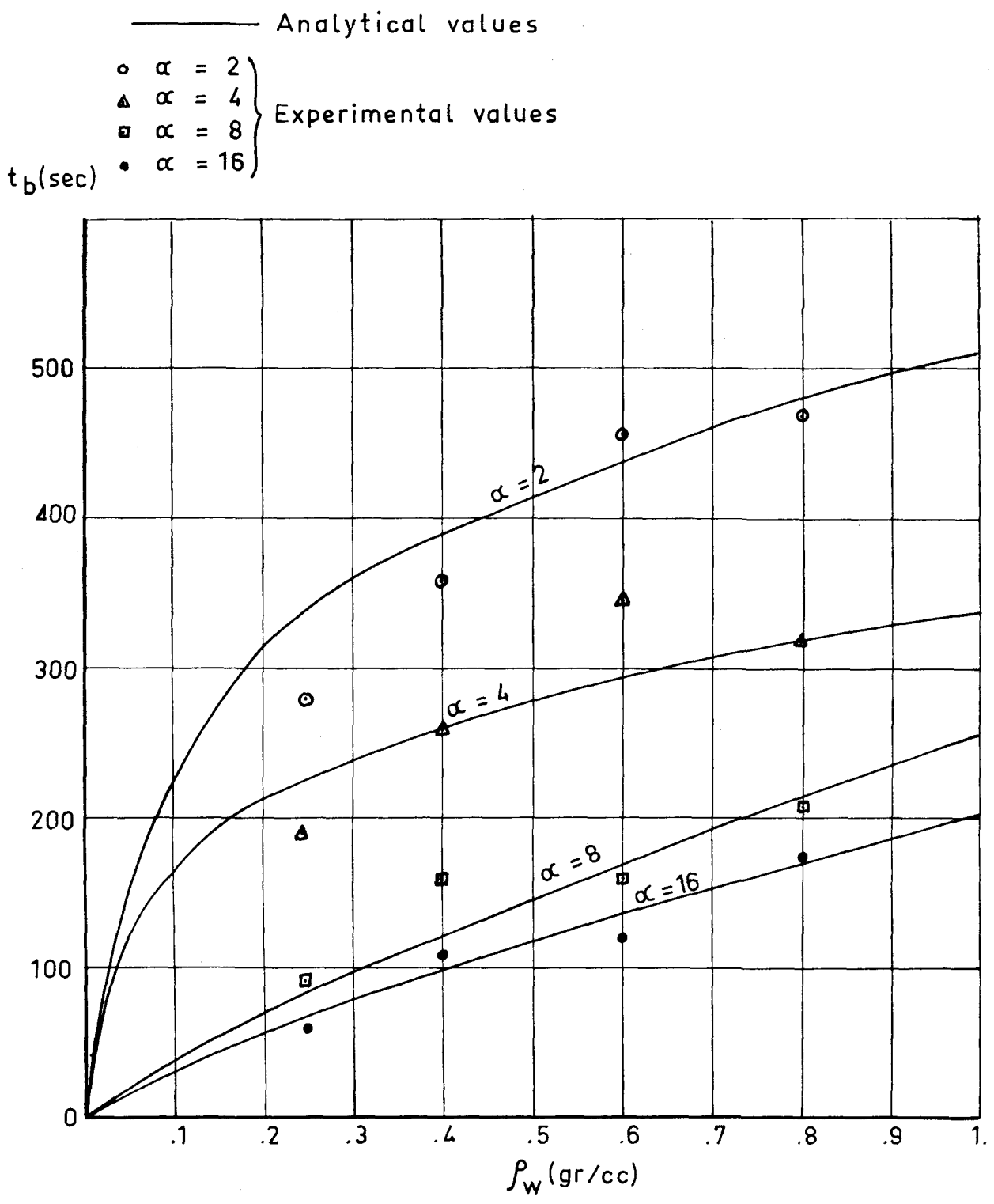

DIMENSIONLESS DISTANCE AT TERMINAL VELOCITY

FIG. 51

$$x = \int_0^{\tau} v_f \, d\tau$$

SPHERES

CYLINDERS

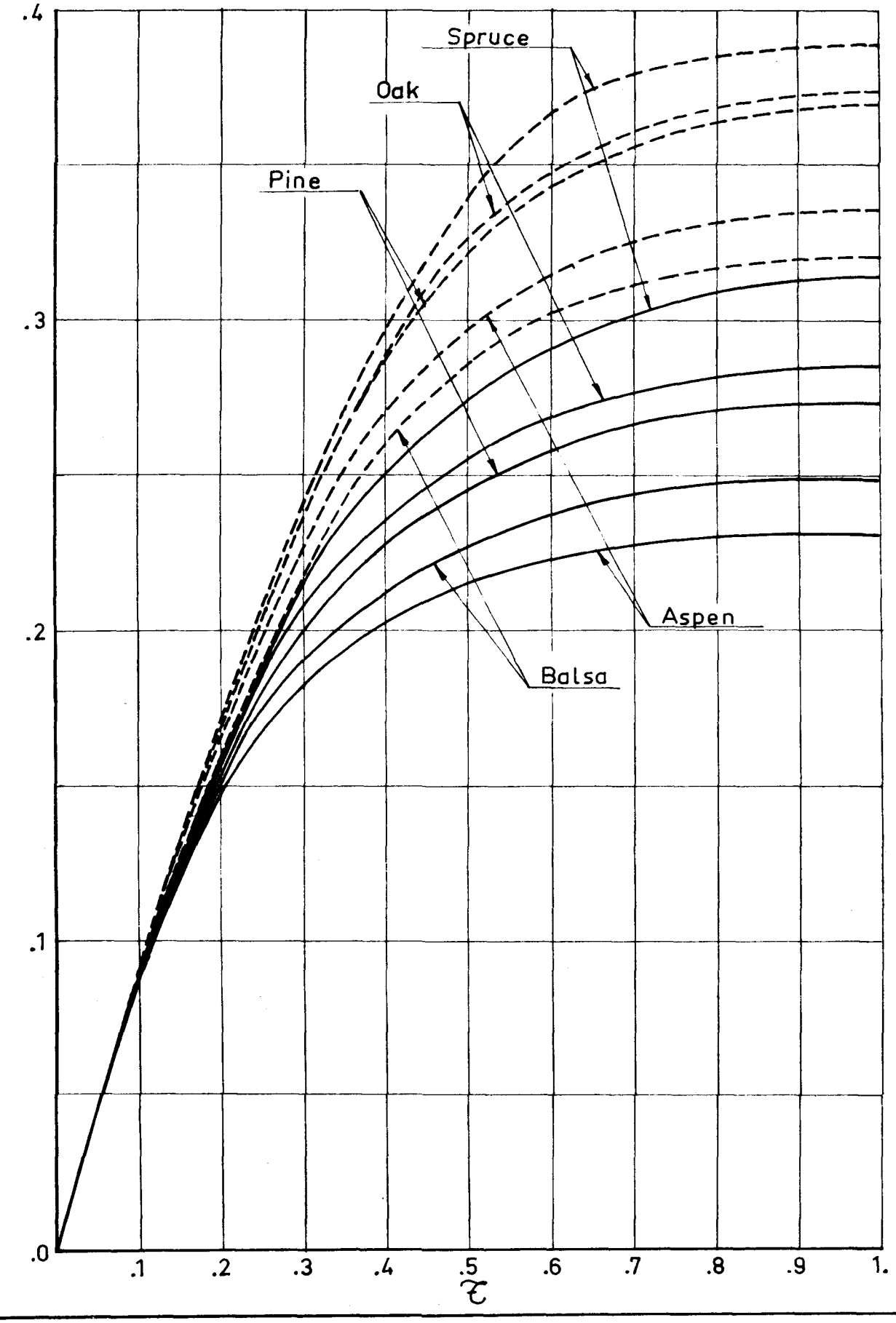

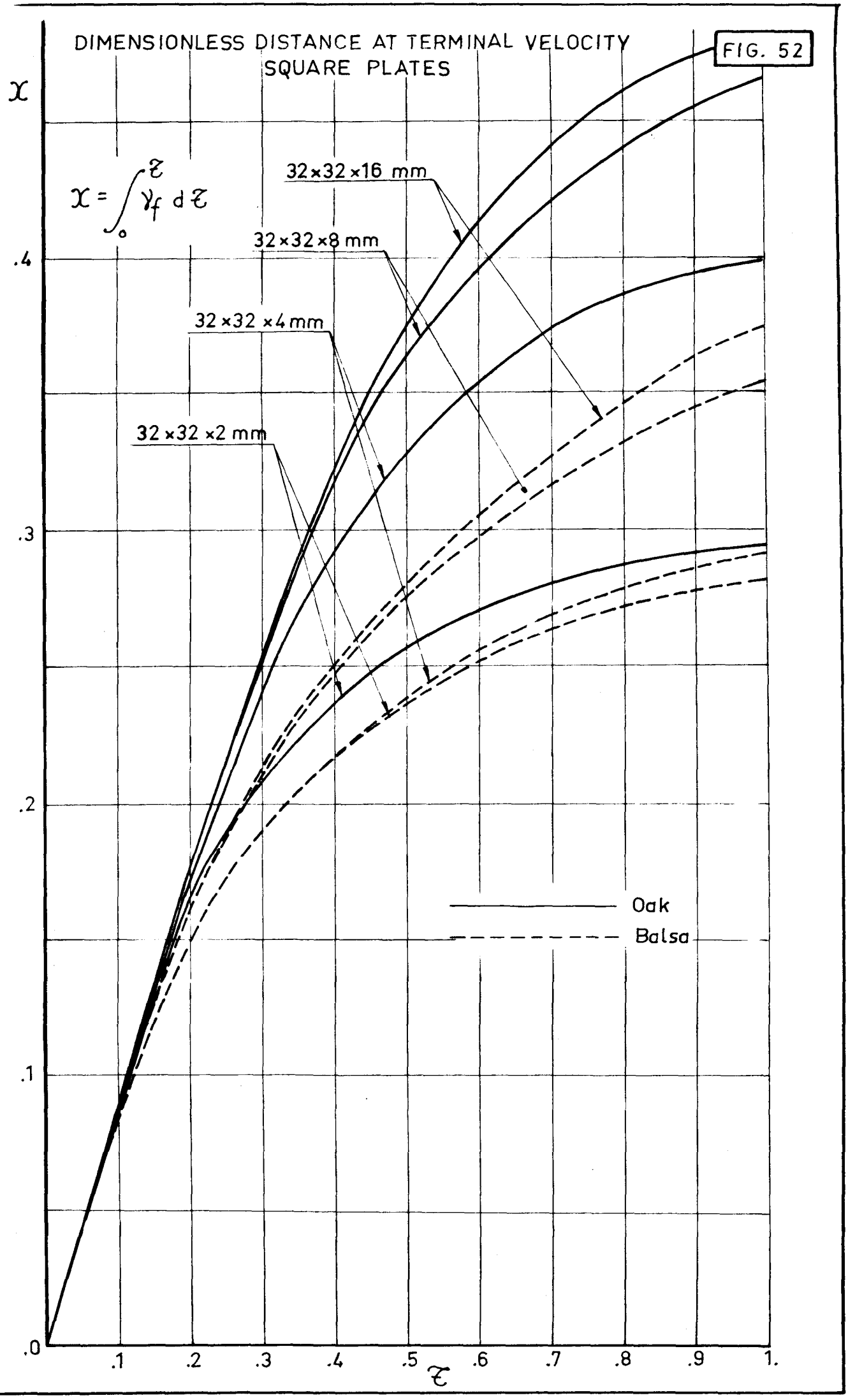
DIMENSIONLESS DISTANCE AT TERMINAL VELOCITY
SQUARE PLATES
FIG. 52
χ
$\chi = \int_0^{\zeta} \gamma_f \, d\zeta$
32×32×16 mm
32×32×8 mm
32×32×4 mm
32×32×2 mm
Oak
Balsa
.0
.1
.2
.3
.4
.5
.6
.7
.8
.9
1.
ζ

DIMENSIONLESS DISTANCE AT TERMINAL VELOCITY
SQUARE PLATES

FIG. 53

$$x = \int_0^{\tau} \gamma_f \, d\tau$$

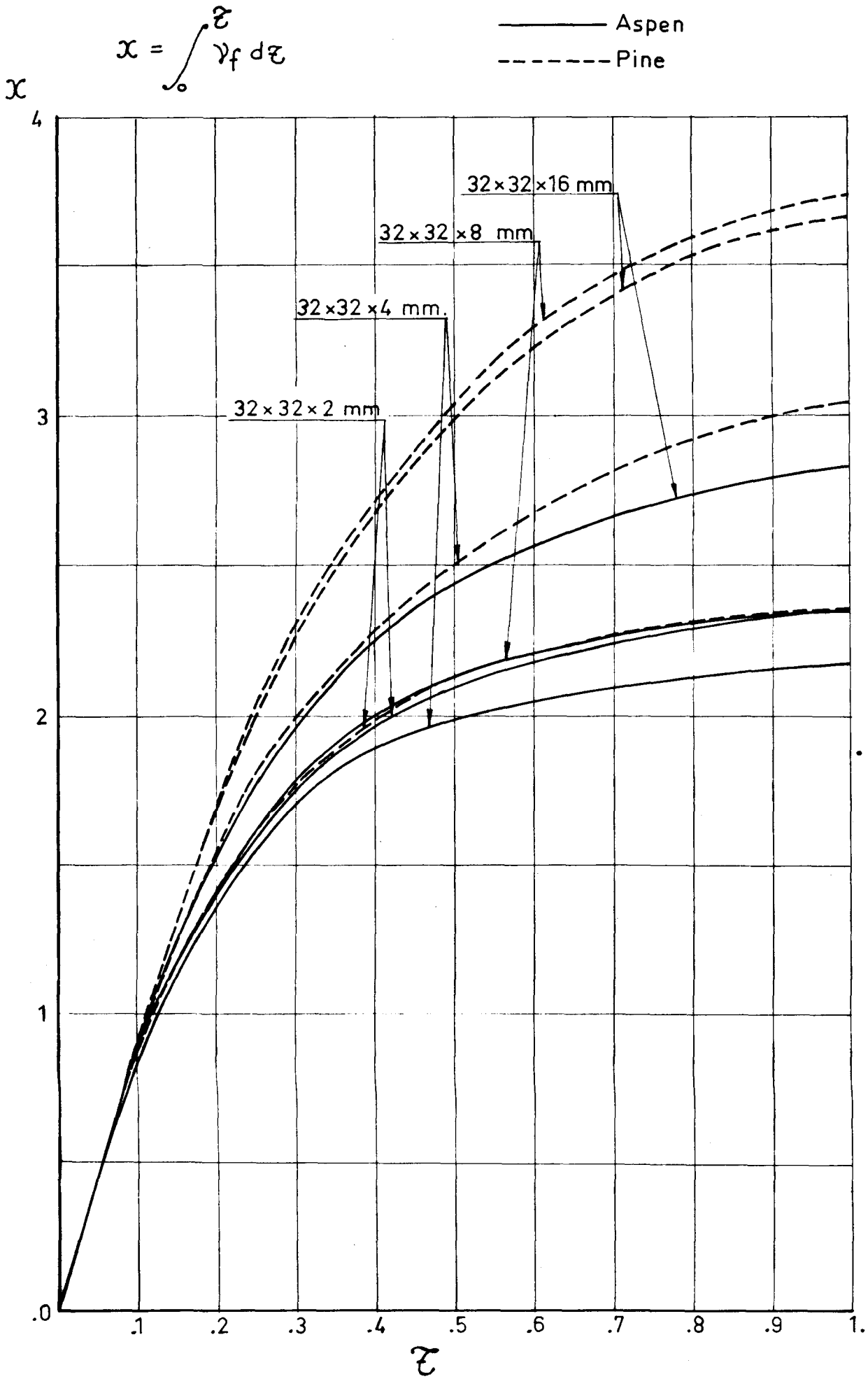

INCLINED CONVECTION COLUMN

15×45mm OAK CILINDERS

COMPARISON BETWEEN EXPERIMENTAL AND ANALYTICAL VALUES

FIG. 54

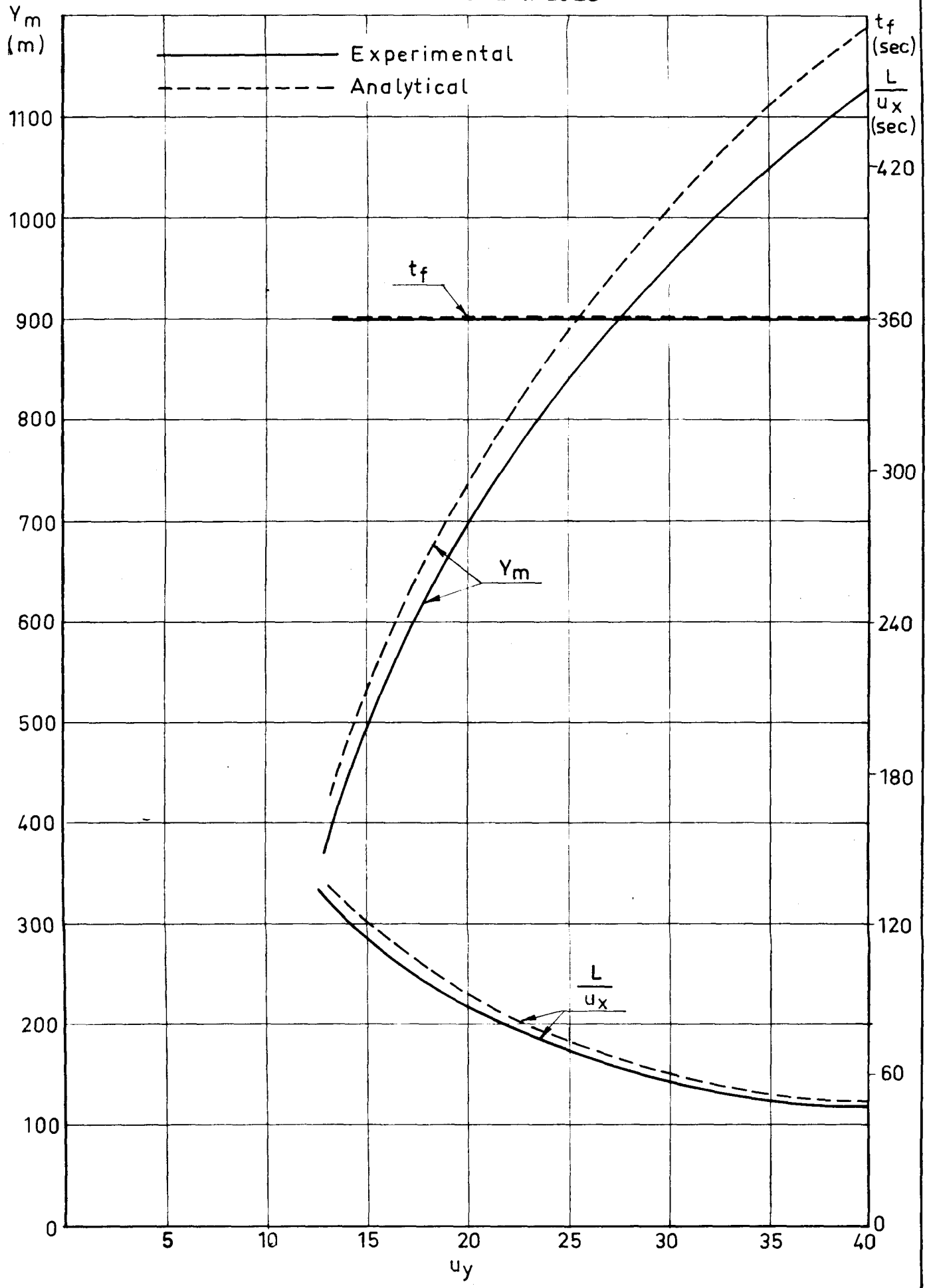

FIG. 55

MECHANICAL DEVICE FOR CALCULATING FIREBRAND TERMINAL VELOCITY

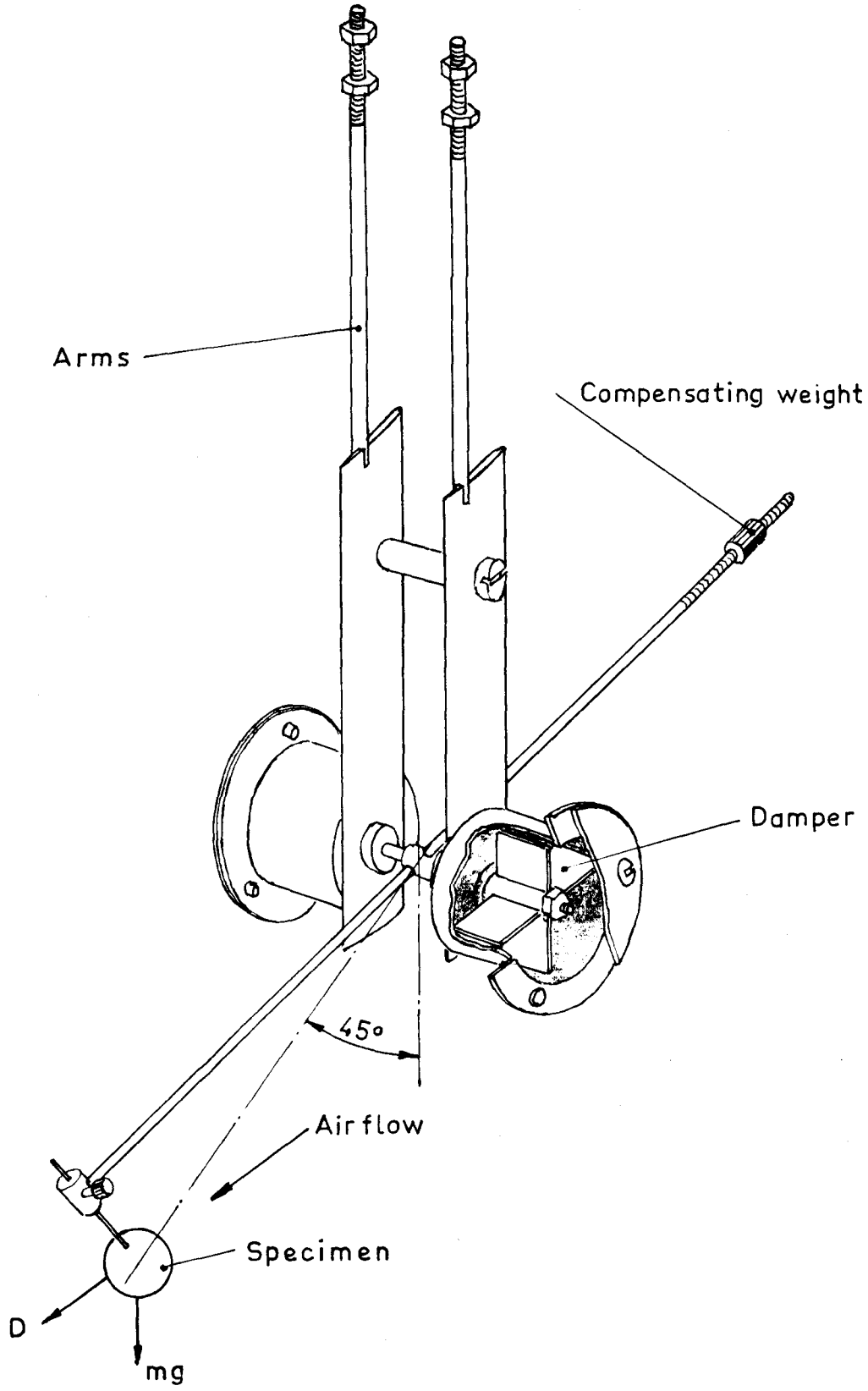

FIG. 56

DEVICE FOR THE ROTATION OF SPECIMENS

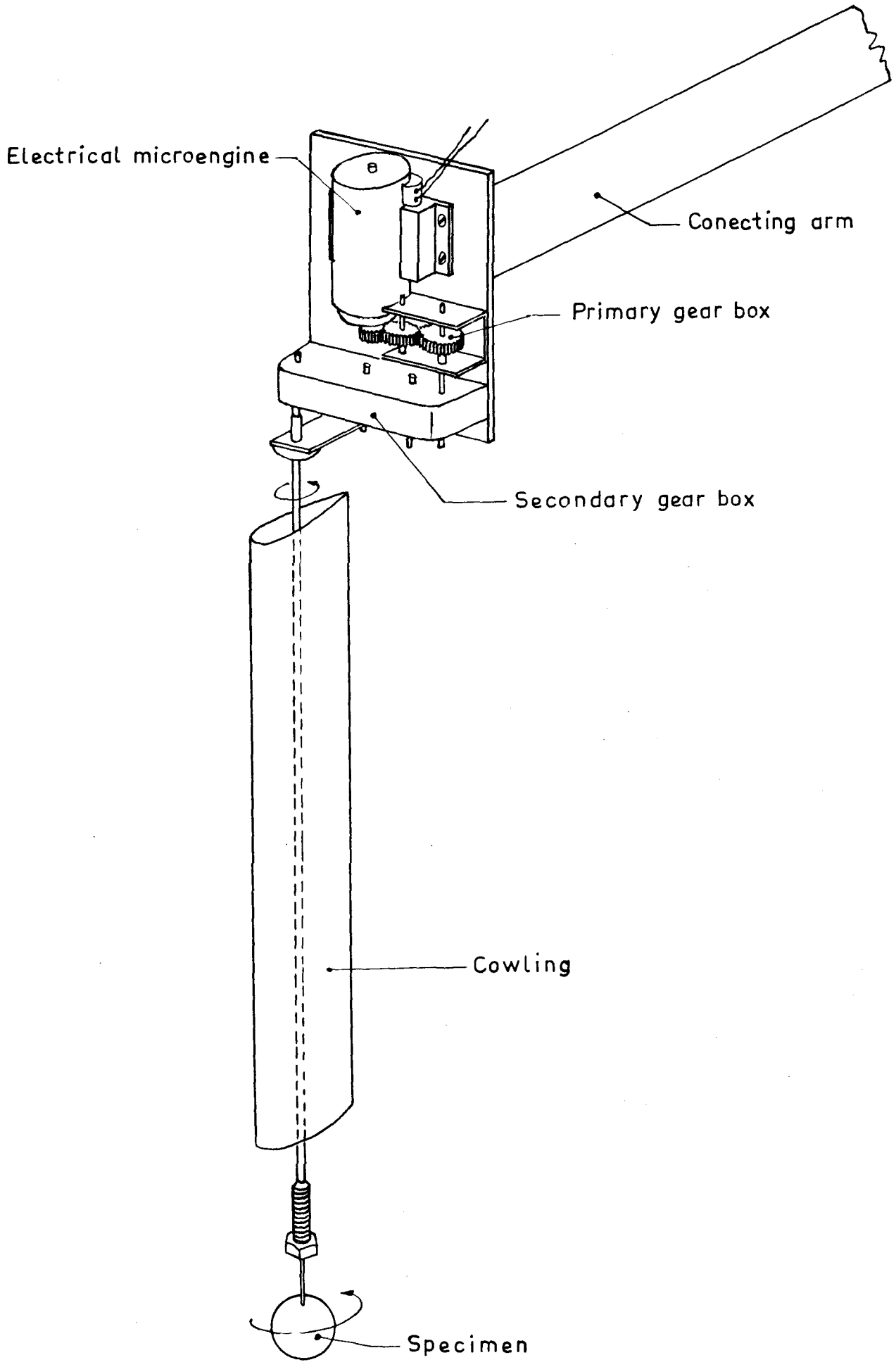

FIG. 57

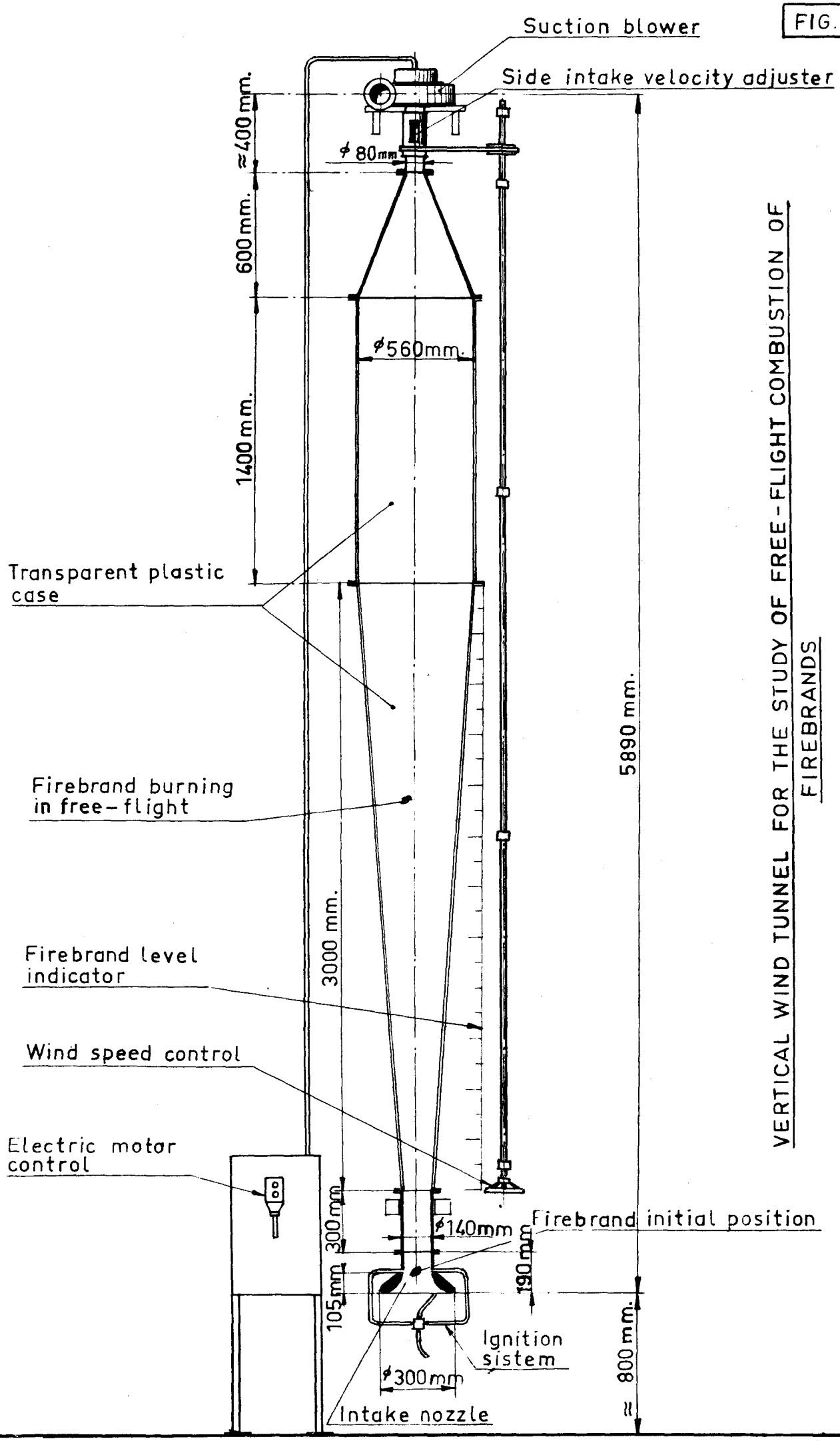

VERTICAL WIND TUNNEL FOR THE STUDY OF FREE-FLIGHT COMBUSTION OF FIREBRANDS

DIMENSIONLESS WEIGHT V.S. TIME

SPHERES $D_o = 22mm$

OAK

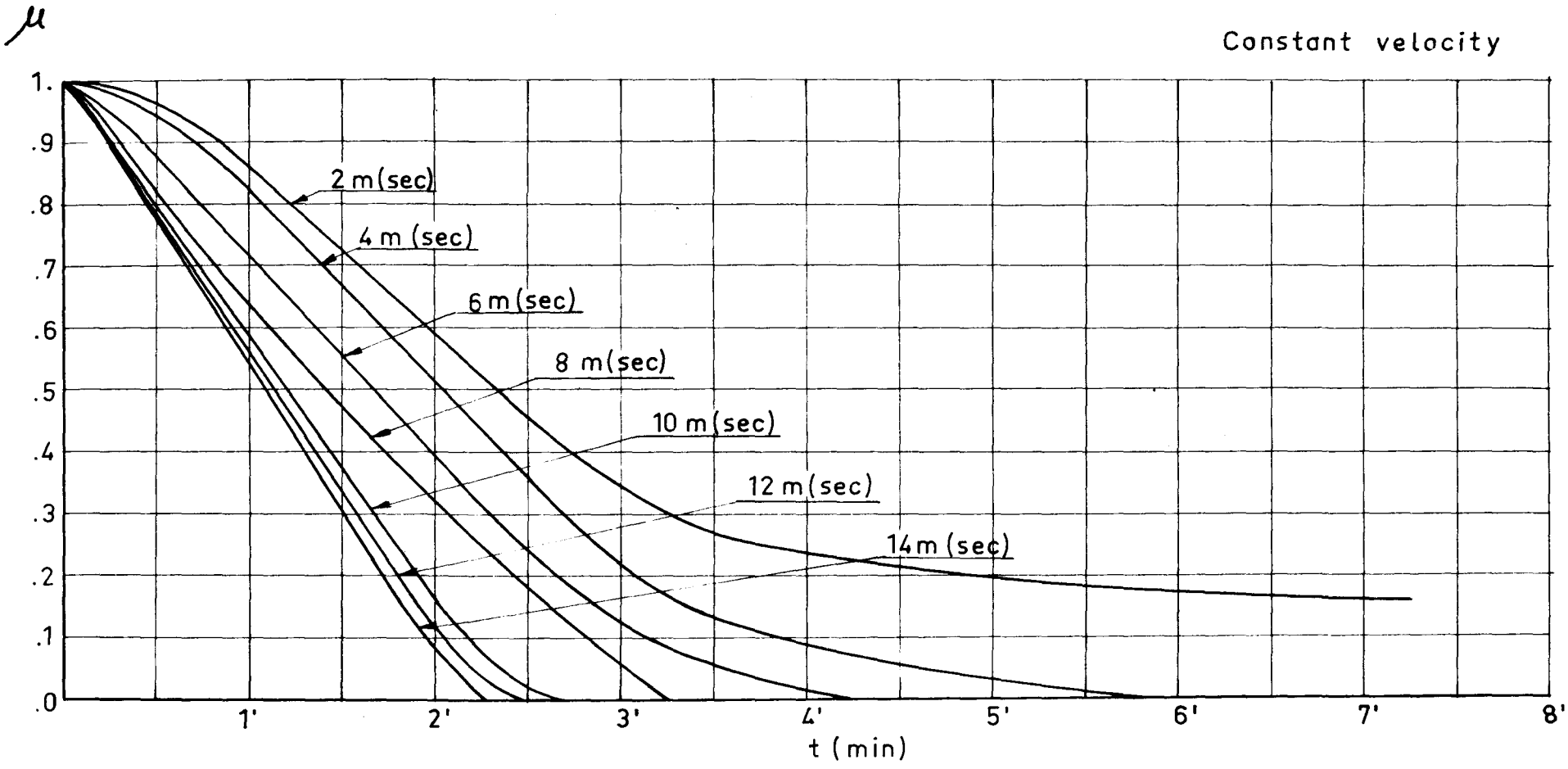

FIG. 58

DIMENSIONLESS SURFACE AREA V.S. TIME

SPHERES $D_o = 22mm$

OAK

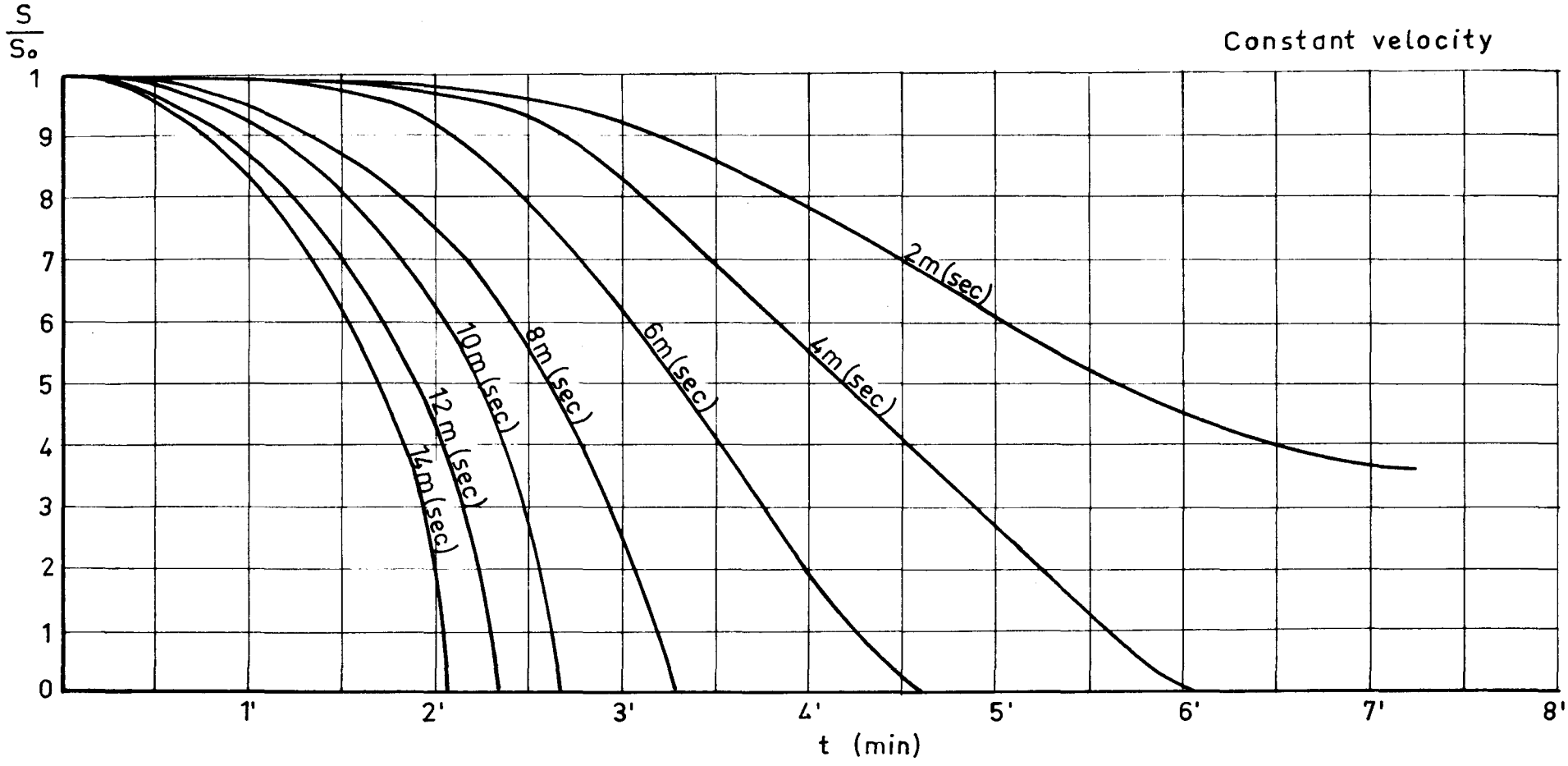

FIG. 59

DIMENSIONLESS VOLUME V.S. TIME

SPHERES D_o=22 mm

OAK

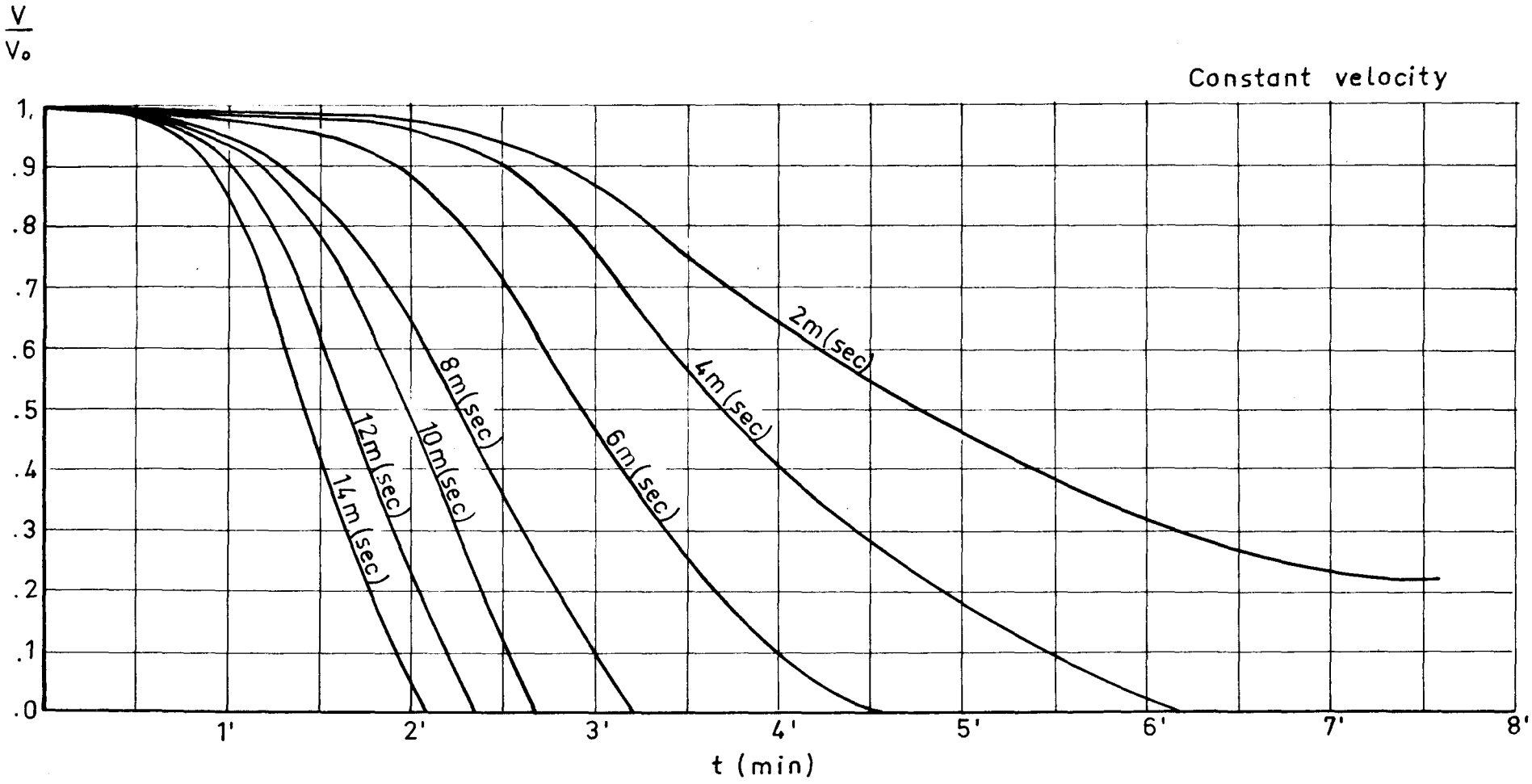

FIG. 60

FIG. 61

DIMENSIONLESS MASS V.S. DIMENSIONLESS TIME AT CONSTANT RELATIVE WIND VELOCITY

OAK

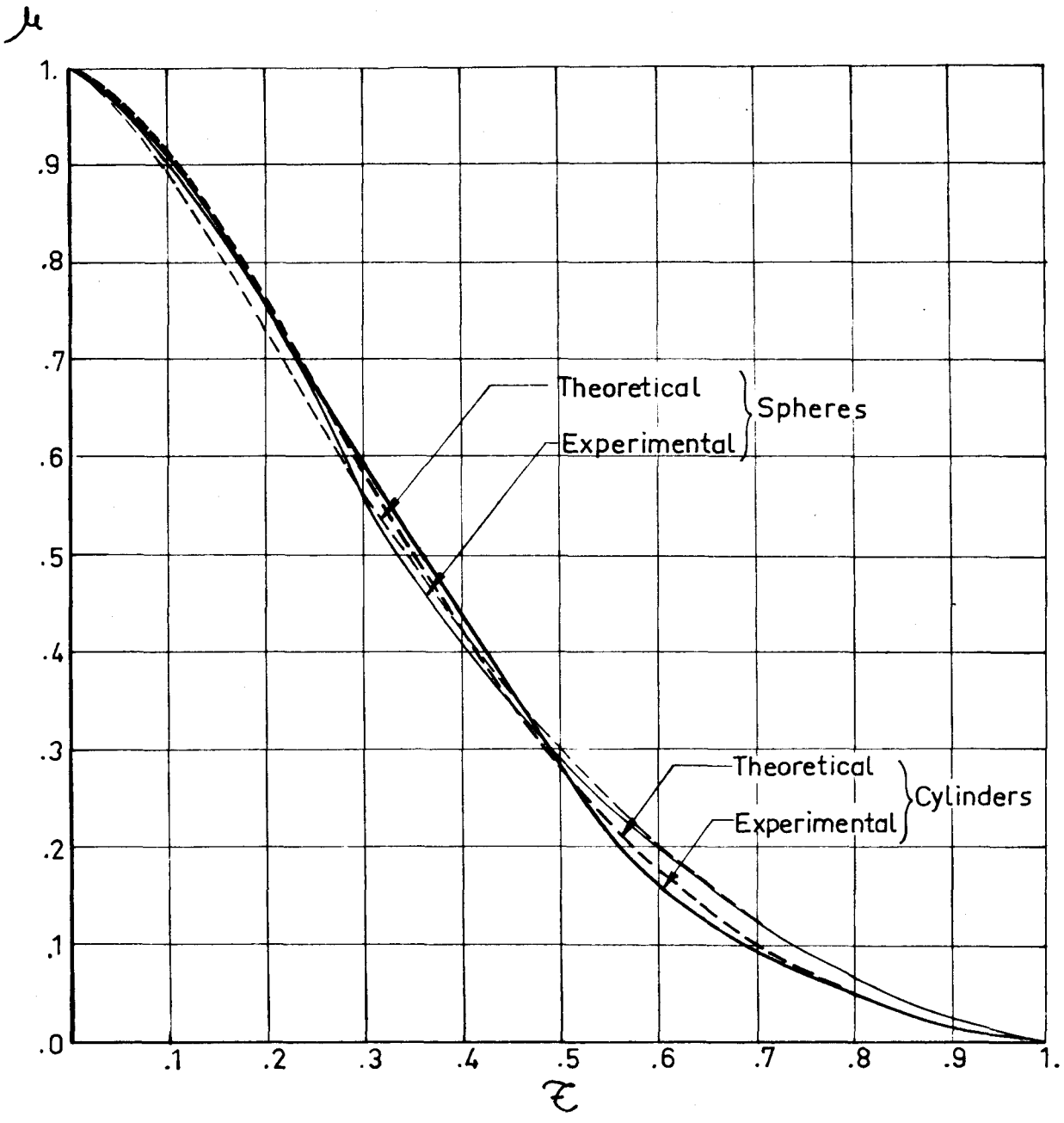

FIG. 62

DIMENSIONLESS SURFACE AREA V.S. DIMENSIONLESS TIME AT CONSTANT RELATIVE WIND VELOCITY

OAK

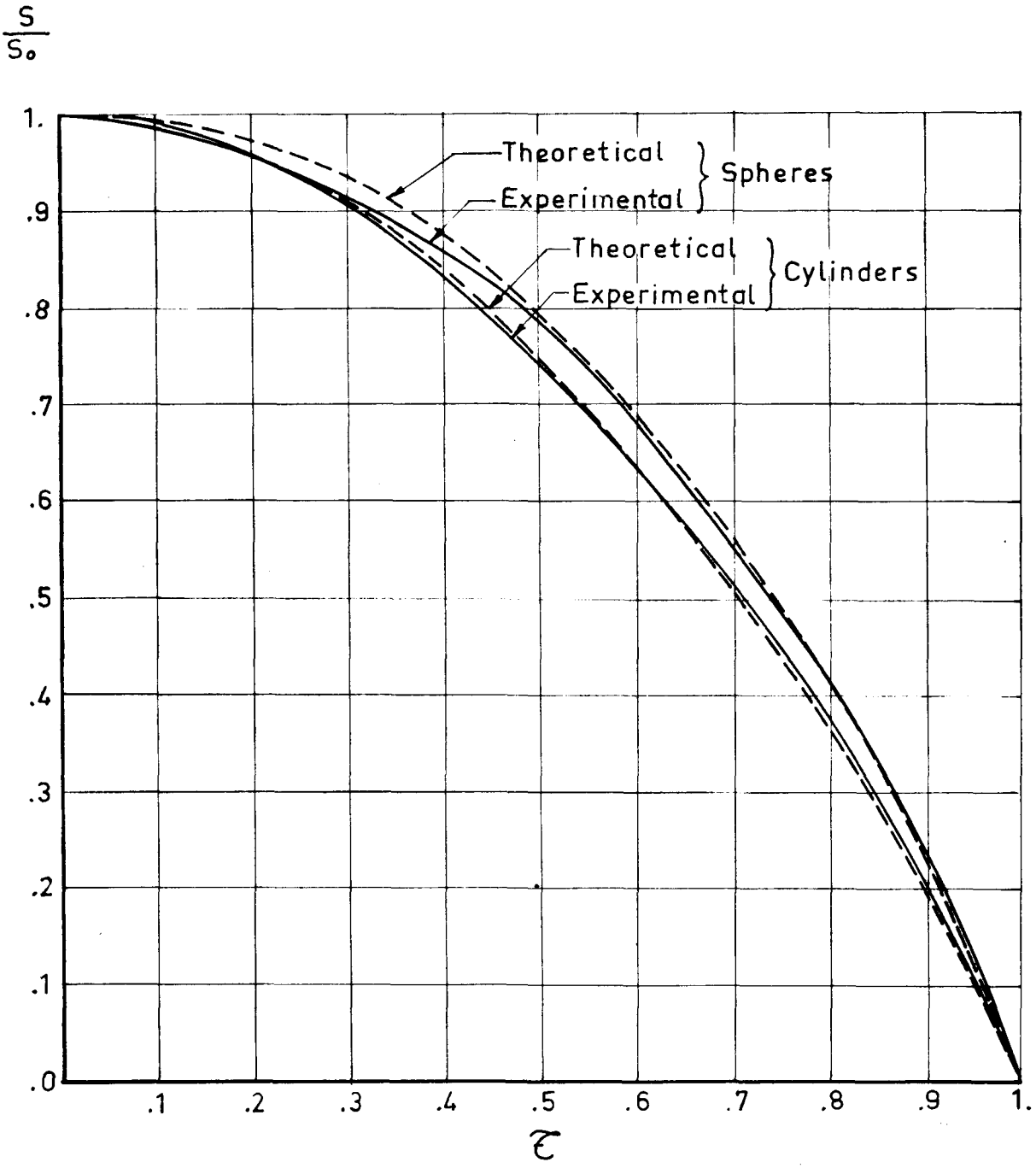

FIG. 63

DIMENSIONLESS VOLUME V.S. DIMENSIONLESS TIME AT CONSTANT RELATIVE WIND VELOCITY

OAK

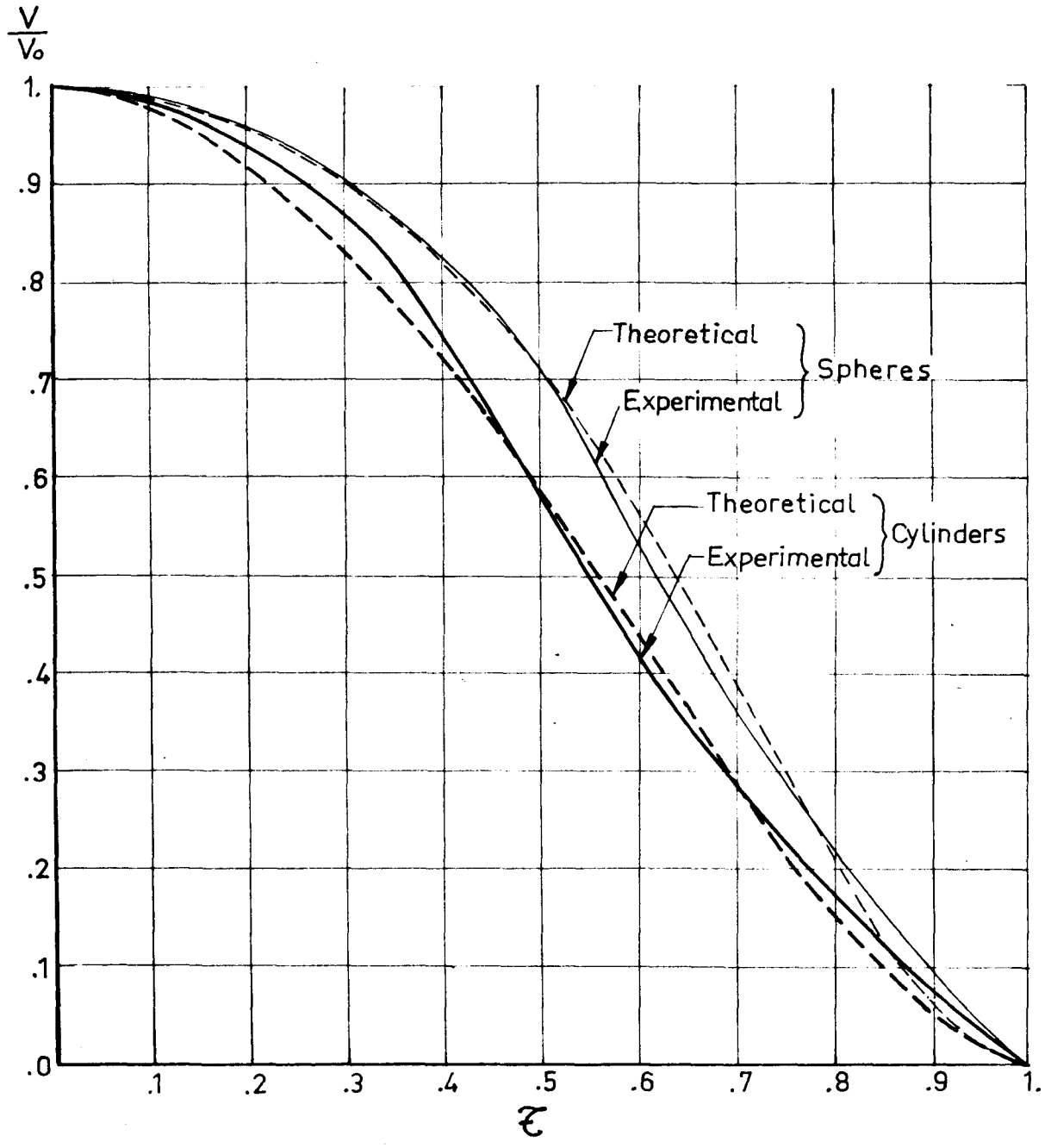

FIG. 64

DIMENSIONLESS WOOD DENSITY V.S. DIMENSIONLESS TIME AT CONSTANT RELATIVE WIND VELOCITY

OAK

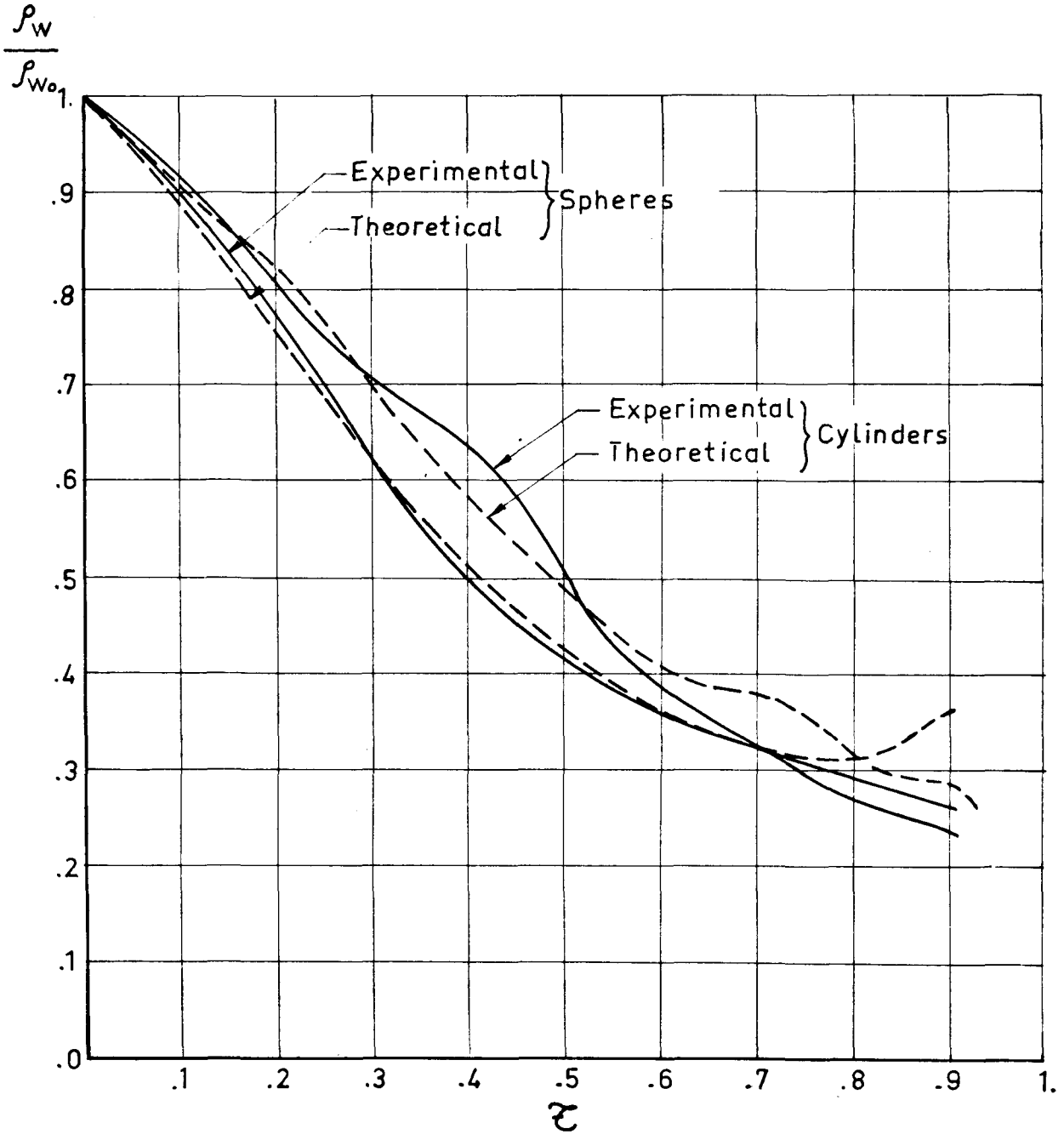

FIG. 65

DIMENSIONLESS CHARACTERISTIC RADIUS V.S. DIMENSIONLESS TIME AT CONSTANT RELATIVE WIND VELOCITY

OAK

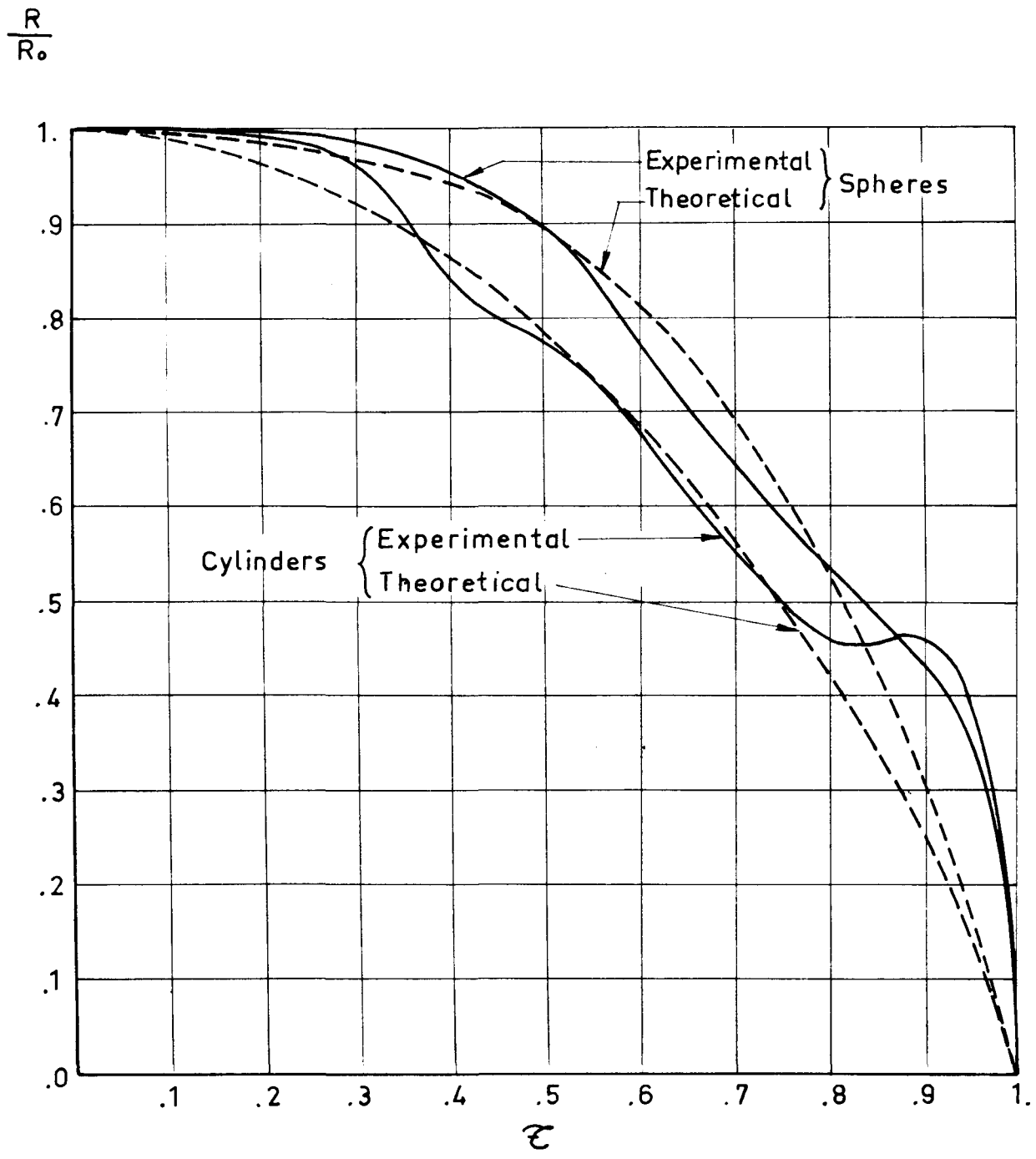

FIG. 66

BURN-OUT TIME V.S. RELATIVE WIND VELOCITY
OAK SPHERES AND CYLINDERS